Development Of A Real-Time Pedestrian Localisation System For A Warehouse Environment

Ryan Michaels Estep

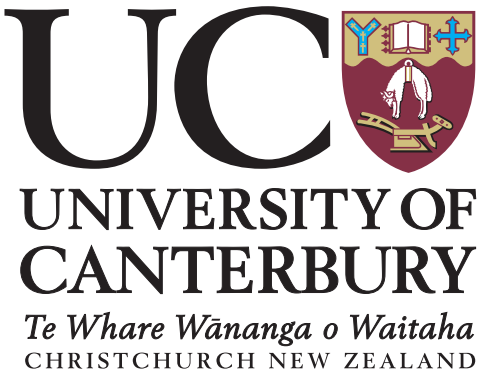

Wireless Research Centre and Spacial Engineering Research Centre

Department of Electrical Engineering

University of Canterbury

New Zealand

Supervisor: Dr Graeme Woodward

Co-supervisor: Dr Richard Green

Co-supervisor: Mr Kelvin Barnsdale

University of Canterbury, Christchurch, New Zealand

A thesis submitted in partial fulfillment of requirements for a Masters in Electrical Engineering.

Therefore, since we are surrounded by so great a cloud of witnesses, let us also lay aside every weight, and sin which clings so closely, and let us run with endurance the race that is set before us, [2] looking to Jesus, the founder and perfecter of our faith, who for the joy that was set before him endured the cross, despising the shame, and is seated at the right hand of the throne of God.

Hebrews 12:1-2 (ESV)

My prayer is that I will put aside all that impedes me, and run the race of life with all the endurance that comes from knowing the end goal. I am so thankful to have been given the opportunity to conduct this research.

Acknowledgments

I would like to express my sincere gratitude to Luke Waltz, Lisa Wong, Kashyap Chandrasekar, and Crown Equipment Corporation for supporting this thesis project both with financial support and dedicated time. The enthusiasm for this project, communicated via the fortnightly Skype meetings and the presentations given at RTC, were a real encouragement as to the importance of this research. A special thanks to Greg Sumner who originally investigated ultra-wide band radios in RTC; turns out your hunch was spot on.

My thanks goes out to my supervisor Dr Graeme Woodward. His patience and time were extremely valuable as I was wrestling with some of the more maths related problems. Graeme was always quick to respond to my queries, and gave me integral instruction and support for the academic elements of this thesis project.

Kelvin Barnsdale also deserves recognition for the hours he spent assisting me with the radio and signal integrity issues. His experienced instruction helped me a great deal in building and debugging the various hardware components used in this project.

Thank you Dr Richard Green for your support and encouragement of this thesis. You were always so enthusiastic about the project whenever it was discussed.

Thank you Kris Lancaster and Foodstuffs South Island Limited opening up your distribution centre for the testing conducted in this thesis. I really couldn't have completed this project without your generous support. The staff at Foodstuffs were accommodating when my testing took longer than projected, and when I needed space to mount my radios (see Figure 7.1).

Thank you Fred Samandari for keeping WRC and SERC running smoothly and keeping it a pleasant place to work. I'm very glad to have gotten to know you.

Thank you David Hunt, Kieran Morris, and Ben Lichfield; my colleagues with whom I shared the working space. A special thanks to Kieran, who gave up two days to assist me in testing the prototype hardware. You all were incredibly patient in allowing me to bounce ideas off you, and listening to me talk about Kalman filters way more than strictly necessary. Ben will have to be your sysadmin now!

Saving the best for last, I would like to thank my parents; Walt and Tina Estep. This has to be the biggest paper of mine you've ever proofread! Your aid in correcting my typos was invaluable, and a real encouragement when I was sick of reading my own writing. Your love and support is still palpable, even on the other side of the planet.

Abstract

This thesis documents the design, implementation, and testing of a real-time localisation system prototype that can operate in a warehouse environment. The performance in a warehouse of three radio technologies (Ultra-wide band time of flight measurement, 2.4GHz radio interferometry, and VHF signal strength mapping) were assessed. The ultra-wide band technology performed very well in the tests, and was used for the remainder of the thesis project. It is projected that 19 ultra-wide band radios can cover the tested 10,000m^2 warehouse section.

Two localisation algorithms were designed under simulation to accomplish the sensor fusion of the radio and inertial motion measurements. The implemented Unscented Kalman Filter achieved better performance than the sequential importance sampling particle filter. The Unscented Kalman Filter was also found to have a lower execution time, making it more feasible to implement on an embedded system.

The real-time localisation system prototype was constructed and then tested in a warehouse environment. The prototype achieved localisation within an average of 1.4 metres with 95% confidence under 4.0 metres. This fell outside the initial goal of 2.0 metres at 95% confidence, but the localisation system was still stably tracking the pedestrian with that precision. The electrical components would cost around 30 USD in full production for a system that will last a full 8 hour shift on a single charge.

Contents

List of Figures

List of Tables

Chapter 1

Introduction

Ubiquitous location information has become a mainstay for the modern 'location aware' technologies. In the consumer market, most smart phones and fitness trackers have access to a Global Navigation Satellite System (GNSS) for navigation and tracking purposes. In aviation, transportation, agriculture, and construction industries; cheap access to reliable GNSS has had a significant economic impact[1]. Despite this widespread adoption in outdoor environments, GNSS has not been used for indoor location sensing. This is due to satellite broadcast signals being too weak to be received reliably by commercial off-the-shelf receivers when the line-of-sight to the sky is blocked[2]. A need exists for a reliable and accurate system for providing location information for indoor environments.

1.1 Background

Right on the heels of civilian access to GPS (The United States' GNSS system) in 1994, research into providing a similar type of positioning system within buildings began. The earliest attempts in the early 2000's [3][4] are shockingly similar to the current state-of-the-art technology. They approach the location problem by combining both a radio frequency (RF) based method of measuring location and some sense of pedestrian motion (via predictive algorithms, or direct measurement with inertial sensors).

The method of combining data sources to measure a common state is called sensor fusion. Sensor fusion provides a statistical advantage while measuring the same physical states and different kinds of sensors can be used to track multiple physical states simultaneously[5]. In pedestrian localisation, the pedestrian's position can not be directly measured. The sensor fusion algorithm must map the sensors' measurements of physical characteristics into the higher-order global location. The industry standard methods of estimating this transformation in real-time are the kalman filter and particle filter, discussed in Section 5.1 and Section 5.2 respectively.

1.2 Problem Definition

The warehouse environment is particularly ill suited for RF based pedestrian localisation. Steel racking stretch floor to ceiling, packed full of pallets containing a variety of product types. The racking structure causes significant multipath effects to RF signals, resulting in fading signal strength and reduced accuracy of RF derived range measurements[6]. The racking's contents change during normal warehouse operations, adding a dynamic component to any attempt to model the long term multipath characteristics of the radio channel.

This environment also has a need for accurate but affordable real-time location of pedestrians. The same racks that contribute to multipath in RF signals also block visual line of sight to pedestrians inbetween the racking. In a 2004 paper on forklift safety[7], the authors look at multiple studies that show a significant portion of fatality and injuries involving warehouse mobile equipment are pedestrians struck by the machinery. As a safety measure, there is great value in locating the position of pedestrians to alert heavy machinery operators that may not be in line-of-sight.

This master thesis' goal is to design and build a prototype of a low-cost real-time pedestrian localisation system that can operate in a typical warehouse environment. For the localisation system to be useful, it must be accurate enough to locate a pedestrian within a single aisle. Each aisle in a warehouse is separated by racking that contains at least 2 pallets (approximately 2.4 metres deep), so the target system accuracy is 2.0 metres at a 95% (or 2 sigma) confidence. The system must not be prohibitively expensive to produce, so the target per-pedestrian volume-production[1] cost is 50 USD. Installing static infrastructure[2] must be minimised to reduce the expense in both labor cost and operational downtime.

1.2.1 Typical Warehouse Definition

Real world warehouses aim to store pallets in the available space as efficiently as possible, leading to as many different racking configurations as there are warehouses. To simplify this problem, this paper will use a portion of the Foodstuffs NZ Ltd. Hornby Distribution Centre (DC), whose floor plan is shown in Figure 1.1, as the typical warehouse model.

This section of the Hornby DC is selected as a typical representative of a warehouse because it has a rectangular area two faced rack design found in other literature[8]. Each aisle is 65.7 metres long, with a total of 10,776 square metres of floor-space for testing. This section of the DC is used for more long term storage so the traffic through the racks is lower and the contents of the racking changes less frequently.

[1] For the ease of costing materials 1000 units is the benchmark price-point.

[2] Static infrastructure includes lines for data and power, as well as the mounting and positioning of non-pedestrian mounted radios.

Figure 1.1: Foodstuff's Hornby Distribution Centre Existing Warehouse Layout

1.3 Contributions

To the authors best knowledge, this is the first work on RF based real-time pedestrian localisation specifically targeting a warehouse environment. There are no comprehensive studies of the operational limits of RF localisation technologies within warehouse racking (as conducted in Chapter 3). The field of indoor localisation and pedestrian navigation have made invaluable contributions to this work. The main contributions to the content of this thesis are as follows:

- Indoor localisation field surveys [9] and [10] for the overview on the state-of-the-art in RF localisation technologies and techniques.
- Röhrig's and Spieker's work on forklift localisation using Chirp Spread Spectrum [11] as the only available research on real-time RF localisation in a warehouse environment.
- DecaWave Ltd. UWB transceiver hardware[12], documentation, and software implementation of a two-way ranging algorithm.
- Julier's and Uhlmann's Unscented Kalman Filter [13][14] and the python implementation, pykalman [15], used for the real-time prototype.

1.4 Following Chapters

The remaining chapters of this thesis are organised as follows:

- Chapter 2 presents the information gathered in the literature review on the state-of-the-art of RF techniques and technologies in the field of indoor localisation.
- Chapter 3 presents the measured performance of three methods of obtaining location through radio measurements.
- Chapter 4 details the model of the radio and warehouse derived from the testing in Chapter 3.
- Chapter 5 present the theory and implementation details of two sensor fusion algorithms tested in the simulation.
- Chapter 6 gives details on the hardware and software used in the real-time localisation system prototype.
- Chapter 7 presents the performance of the prototype as observed in the warehouse.
- Chapter 8 discusses possible future work to improve the performance of the prototype and develop it into a commercially viable product.

Chapter 2

Technology Survey

In the field of indoor localisation there exists many RF technologies used to provide location information. This chapter provides an overview of the most applicable RF technologies currently researched in the field. The purpose of this survey is to identify RF technologies that have the capacity to provide location data in a warehouse localisation environment, which has significant multipath interference.

2.1 Localisation Techniques

This section gives an overview of the common methods of deriving location information from radio signals.

2.1.1 Time of Flight (ToF)

The Time of Flight (ToF) technique measures the radio signal's propagation time through air and calculates the distance based on the speed of light through air[9]. Trilateration from multiple radio measurements can then be used to calculate the position. This method relies on measuring the time when the signal is sent and received to nanosecond precision (a 1ns error translates to approximately 30cm of ranging error[1]). Synchronising the clocks across both the mobile target and infrastructure is complex and expensive; so most localisation methods utilise a variations of ToF that does not require all radios to be synchronised.

2.1.1.1 Time Difference of Flight (TDoF)

Time Difference of Flight (TDoF) uses infrastructure receiver radios with their clocks synchronised which record the time a poll message is received from the tracked target[10]. The relative difference between the

[1] c/n * 1ns = 30cm where c is the speed of light, and n is the index of reflection of air (1.0003)[16].

arrival times on two receivers can be used to calculate a hyperbolic curve of possible locations, and additional receivers can be used to resolve the position of the target[17]. The TDoF technique is efficient in use of the mobile targets power and the spectrum's bandwidth. One poll message from the target is all that is required to estimate the target's location. The accuracy of the system relies on all receivers' clocks to be synchronised to sub-nanosecond accuracy, increasing the cost and complexity of the infrastructure.

2.1.1.2 Round-Trip Time of Flight (RT-ToF)

RT-ToF avoids the ToF technique's requirement for time synchronisation by using the same hardware to measure the time of flight of the signal. A transmitter sends a signal which is reflected or re-transmitted with a known or measured delay by the target which is in turn received by the original transmitter[10]. The clock drift of the hardware, and any uncertainty of the delay on reflection/transmission is the main contributor to ranging error.

2.1.1.3 Double-Sided Two-Way Ranging (DS-TWR)

DS-TWR is the method used in IEEE 802.15.4a[18], and reduces the impact that crystal oscillator drift has on the ranging accuracy. The technique uses two rounds of RT-ToF measurements, halving the error introduced by clock drift[19]. This method increases accuracy with cheaper hardware, but requires double the time to complete the ranging operation.

2.1.2 Angle of Arrival (AoA)

The Angle of Arrival (AoA) technique uses an antenna array to observe the direction of an RF signal's propagation. A triangulation technique is used to calculate the target's position[9]. This method's accuracy is particularly vulnerable to multipath signals, which change the sensed angle of the signal and so require methods to identify the first path signal [20]. The multiple antennas required by AoA implementations also increase the hardware cost of the system.

2.1.3 Map Matching

The map matching method uses a map of known positions to the Received Signal Strength Indicator (RSSI) of any sensed RF signals. Once the map is created, the RSSI from all sources are measured in real-time, and the closest match to the map is used as the current position[9]. This method is typically used on existing sources of RF signals, such as WLAN; so requires little to no additional infrastructure.

The system's precision is dependant on how accurately the map reflects the current RSSI propagation of the environment. An extensive site survey is required to calculate an effective map, and the map must be re-calibrated when factors change the radio propagation characteristics of the environment. In a warehouse the stock stored within the racking change as part of normal operation; so any localisation system employing a map matching technique must not be effected by changes in the racking's content.

2.2 Indoor RF Localisation and Ranging Technologies

2.2.1 Indoor Global Navigation Satellite System (GNSS)

Direct use of GNSS for indoor localisation is impractical due to the signal being attenuated by the building[2]. Ground based GNSS transmitters, which operate like their satellites counterparts, have been used in military research to reach centimeter accuracy[21]. These 'pseduolites' are expensive, requiring an extremely stable clock[22]. The technique also suffers from closer pseduolites signals jamming signals from more remote pseduolites, called the the near-far problem[23].

Instead of replicating the satellites entirely, GNSS repeaters are available which receive the GNSS signals outside and re-transmit them within the building[2][22]. The repeater hardware is cheaper than the pseduolites, being a RF amplifier that does not need a stable clock. Infrastructure cost is significant for a repeater system, requiring a rooftop antenna to receive the original GNSS signals, and the delay in each line to the indoor repeaters must be measured and removed via calibration.

2.2.2 Frequency-Modulated Continuous-Wave (FMCW) Radar

FMCW radar continually transmits a frequency modulated saw-tooth signal, called a chirp, which is reflected off the target. Unlike traditional radar technology, the reflected signal is squared with the transmitted signal which creates a low frequency beat that can be be used to calculate the range to the target[24].

Indoor settings are a cluttered environment, so active tags are used to reliably distinguish pedestrian from untracked objects and the room. Active tags boost the reflected FMCW signal with a stable time delay[25], which gives the reflected signal a better effective range. In indoor tests the measurements have 8cm precision, but multipath conditions indoors negatively impact the effective range of the system to 24m in open air[26].

FMCW radar with active reflecting tags cannot reach the required range to cover a warehouse aisle, and is negatively affected by multipath interference[27]. A commercial TDoF implementation[28] operates indoors but requires all radios to be in range of the time synchronisation base-station, which is likely to be a failure mode in a large warehouse. Likewise the FMCW radar transceivers are expensive, and operate at 5.8-24 GHz which would have poor penetration through racking.

2.2.3 Ultra Wide-Band (UWB)

Ultra Wide-Band technology uses sub-nanosecond pulses more than 500MHz wide for communication. The time the pulses are received can be measured, and so ToF class of techniques are used to measure the distance traveled. The Federal Communication Commission (FCC) regulations allow UWB to operate indoors within 3.1 - 10.6 GHz without a license as long as the transmission power is under -41.3 dBm[29]. Regulations in New Zealand follow the more strict European Union regulations, requiring a Low Duty Cycle (LDC) for the 3.8-4.2GHz band[30]. UWB technology have multiple commercial off-the-shelf (COTS) implementations built for both communication and ranging applications [12][31].

UWB is particularly suited for indoor localisation due to its tolerance to multipath interference. UWB transceivers, using a Rake receiver, can combine the delayed signals that are the result of multipath interference to decrease the symbol error rate. In ranging applications, this same knowledge can be used to find the first component of decoded multipath signal[32].

Due to the short wavelength of unlicensed UWB frequency, signals do not propagate sufficiently through solid objects. While the signal is traveling through material, the propagation delay will cause other reflected multipath components (traveling through open air) to reach the receiver first[33]. It is possible to detect when the line of sight is blocked, but the distance can not be recovered from such observations[34].

2.2.4 Chirp Spread Spectrum (CSS)

CSS uses 'chirps' that are composed of sweeping sinusoidal waves about the 2.4 GHz ISM band[35]. CSS based ranging has shown ranges of up to 60m in Line of Sight (LoS) conditions[36], but like UWB, the technology has reduced accuracy when LoS is blocked. A fork-truck localisation system using the CSS is shown to achieve 2m accuracy[11].

COTS implementations of CSS based localisation is expensive and not readily available. There is only one commercial CSS ranging radio on the market produced by Nanotron Technologies using ToF[37]. Semtech Corporation describes a TDoA method of localisation in relations to their LoRa Alliance technologies[38], but no papers or hardware referencing are accessible at the time of this writing.

2.2.5 Radio Interferometric Based Positioning System(RIPS)

RIPS utilises 2 transceivers emitting precise frequencies close enough in wavelength to generate a low frequency interference signal. By measuring the phase difference of multiple transmitters over multiple frequencies, the target position can be calculated. The original design proposed a method using 2 time synchronised receivers and network of 8 transmitters to discern a 3d location[39]. An updated version of the same system

demonstrated a more practical application of multiple moving targets[40]. The system is reported to use 12 transmitters to cover a 72,000 m^2 outdoor area. A solution using a frequency sweep to determine ToF has been shown to increase the range of the system in simulation[41].

RIPS based localisation can operate using cheap RF hardware and a wide range of carrier frequencies, but requires computationally complex differential analysis of signal phase[39]. Atmel have developed a proprietary ranging technology that sweeps over the 2.4GHz ISM band using their AT86RF233 radio transceiver[42].

Dual-tone RIPS (DRIPS) is a modification of the original design where the targets emit dual-tone signals separated by less than the channel's coherence bandwidth[43][44]. The dual-tone signal is received by multiple anchor stations, which when squared together create low frequency tones whose phase contain enough information for TDoF localisation. The technique is shown in simulation to improve effective range dramatically and reduces system complexity. The system is far more inaccurate than RIPS due to frequency approximations made to remove time synchronisation between the radios.

RIPS gives inaccurate ranging in environments with multipath interference[45]. DRIPS is shown in simulation to mitigate the problem of multipath phase shift[44], but as presented the precision is on the order of 100m.

2.2.6 Near Field Electromagnetic Ranging (NFER)

The Q-Track Corporation has developed a localisation technology which uses near field effects of low frequency transmissions called NFER. The technology exploits the fact that two parameters of the magnetic field have a 90 degree phase offset at the antenna, and do not completely come into phase until a half-wavelength away. The phase difference of the two parameters directly correlate to the distance from the antenna[46].

NFER benefits from using long wavelengths, which are better able to penetrate through solid objects and more resistant to multipath. Q-Track's localisation system using a wavelength of 232m achieves 4m accuracy with a 70m indoor range[47].

Q-Track has patented the use of near field effects for ranging[48] and no other sources of research are attainable. Practical antenna size also limits the effective range; Q-Track is already operating their antenna close to the maximum theoretical gain relative to size[49].

2.2.7 Wireless Local Area Network (WLAN) Map Matching

WLAN map matching uses the RSSI of 2.4 GHz and 5 GHz WLAN access points (APs). The simplest implementations use an RSSI fading model to directly correlate measured RSSI to distance from the APs[50].

RSSI is impacted by constructive and destructive interference from multipath, so most WLAN based localisation use a map matching system discussed in Section 2.1.3. Modern warehouses require WLAN coverage for normal operation, so a localisation system based on this would require no additional infrastructure.

Stability of RSSI over distance and time are major factors for an accurate WLAN based localisation system. The measured RSSI is not stable throughout the day as temperature and humidity change. Pedestrian orientation also has an effect on the RSSI, causing the signal strength to drop 5 dBm to 10 dBm when the antenna is blocked by the pedestrian's body[51]. Long term environmental changes also degrade system reliability[52], requiring updates to the map to maintain system accuracy. The warehouse is particularly ill-suited for the WLAN map matching techniques; pallets with metal product and heavy machinery change positions in the warehouse during normal operation and have strong influence on RSSI measurements[53].

2.2.8 Very High Frequency (VHF) Map Matching

VHF radio is an alternative to WLAN for a map matching system that may mitigate some of the stability issues with WLAN RSSI. COTS personal range FM radio transmitters operate between 88.1 MHz and 107.9 MHz that are more stable over time than WLAN frequencies[54]. Regulatory requirements are not standardised for all countries regarding low power unlicensed VHF transmitting, but the effective transmission range is limited to 60 metres by FCC guidelines[55].

Using both VHF and WLAN map matching together show success at increasing system accuracy and stability. An implementation used VHF map matching from local FM radio towers to achieve room level accuracy[54]. Another implementation uses local low-power COTS FM transmitters with known locations and achieves accuracy of 0.85m with 95% certainty[56].

2.3 Technologies Considered for Warehouse Testing

Due to the absence of available literature on the surveyed localisation technologies performance in warehouse environments, the next step involves the selection of credible technologies as candidates for the prototype and to ascertain their practical performance in a warehouse. The decision matrix in Table 2.1 was constructed with the major criteria for a practical warehouse localisation system.

The criteria outlined as:

- Commercially Available: The basic technology must be available for mass production.
- Restricted Spectrum: The wireless spectrum utilised must be free to use (does not require spectrum leasing).

- Multipath Resistant: The warehouse is particularly likely to cause multipath interference. Any technology should give accurate ranges under multipath interference.
- Maximum Range: The longer the effective range of the technology, the lower the cost of static infrastructure. The technology should be able to range down a typical warehouse aisle of at least 80m.
- Best Case Accuracy: The accuracy of localisation must resolve to 2m to reach the objective.

Technology Type	Commercially Available	Restricted Spectrum	Multipath Resistant	Maximum Range	Best Case Accuracy
UWB	Yes	No	Yes	300m	0.1m[4]
CSS	Yes[1]	No	Yes	60m	2m
RIPS	Yes	No	Unknown	100m	1m[4]
NFER	Yes[1]	No	Yes	70m	4m
Indoor GNSS	Yes[1]	Yes	No	Unknown	1m
WLAN Map Matching	Yes	No	N/A[2]	N/A[3]	1m
VHF Map Matching	Yes	No	N/A[2]	60m	1m
FMCW Radar	Yes	No	No	10m	0.1m[4]

[1] Limited commercial availability.

[2] Map matching techniques use multipath interference, so accuracy is not directly affected by multipath.

[3] Warehouse is fully covered by WLAN signals.

[4] Using ranging accuracy, no published indoor localisation system accuracy.

Table 2.1: Decision Matrix of Surveyed RF Technologies

UWB, RIPS, and VHF Map Matching were selected as the technologies to fully test in the warehouse environment, detailed in Chapter 3.

UWB meet all the criteria for the real-time prototype. The technology is mature enough to have two commercially available transceivers. Its use of wide bandwidth provides the best possible chance of mitigating multipath effects. The frequency the UWB transceiver uses a small antenna that will be easier to integrate into a wearable product.

RIPS was chosen for its low cost, commercial availability, and the maximum range was second only to UWB. There is no literature on RIPS specifically characterising the multipath interference performance. It was unknown the degree of multipath interference that would be present in the warehouse environment.

VHF Map Matching was selected to see if the VHF signals would be less affected by changes in racking content. WLAN Map matching was not considered because the warehouse is too dynamic to support an

accurate and repeatable WLAN based map matching system.

CSS and NFER both also meet the criteria set for a practical localisation technology, but were not selected due to limited hardware availability. The CSS hardware required for testing from Nanotron (the sole supplier) was over 4000 USD. NFER similarly would have required partnering with Q-Track to have access to the intellectual property required to develop a warehouse localisation system. Indoor GNSS and FMCW were similarly not selected for further testing due to the price of obtaining the equipment.

Chapter 3

Real-World Testing

The purpose of the real-world testing is to ascertain the practical performance of the technologies identified in Chapter 2. The trials provide valuable data for the system model, documented in Chapter 4. The equipment used to test the three most promising technologies, identified in the previous chapter, is described in Section 3.1. The remaining sections document the measurements conducted in Ilam Fields by the University of Canterbury and within the Foodstuff's Hornby DC.

3.1 Tested Hardware

3.1.1 Radio Interferometric Based Positioning System (RIPS)

The hardware purchased for RIPS testing is the Atmel REB233SMAD Evaluation Kit[57] shown in Figure 3.1. The evaluation kit uses the AT86RF233 2.4 GHz ISM transceiver with a integrated in phase difference measurement unit[58]. Included with the evaluation kit is a proprietary software stack developed by Atmel called the RTB Eval App[59].

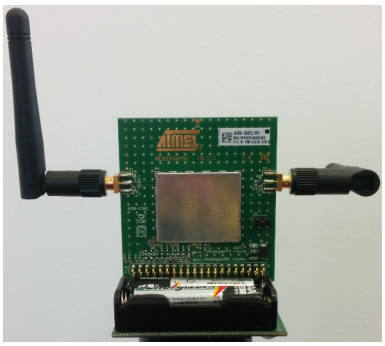

Figure 3.1: Atmel REB233SMAD Evaluation Kit

The RTB Eval App sends data with a standard IEEE802.15.4 protocol and then conducts ranging using the proprietary code. The ranging code sweeps over a user defined portion of the ISM band. During each ranging round, four separate sweeps are conducted using the four unique pairs of antennas. The four range measurements are then combined using a Distance Quality Factor (DQF) for a weighted mean. The weighed mean, weighed DQF, and each antenna pair's ranging and DQF are recorded on the PC via a supplied python application.

The RIPS radios have two different tuning parameters used in the tests: channel and step size. The radios operate on multiple IEEE 802.15.4 channels (11-26 which correspond to 2405MHz-2480MHz[58]). Using different channels can avoid interference from other radios operating in the 2.4GHz spectrum, shared by WLAN, and so indoor measurements were conducted using Channels 11 and 26. The other parameter sets the step size used by the Phase Measurement Unit(PMU). The proprietary ranging code steps through the entire 2.4GHz channel with the PMU measurement step size [59]. The shorter the step size, the more measurements are conducted.

3.1.2 Very High Frequency (VHF) Map Matching

The VHF transmitter was constructed as a 1/4 wavelength dipole antenna. The antenna was driven by a Silicon Labs Si4713 FM radio transmitter[60] on a Adafruit breakout board[61]. The transmitter was managed by a Freetronics Eleven[62] microcontroller using example code provided by Adafruit[63]. he transmitter box, shown in Figure 3.2, could be mounted both horizontally or vertically on a mounting pole to provide a horizontal and vertically polarised signal. The transmitter was configured to transmit a 88.1 MHz signal, the lowest allowable frequency not used by commercial FM radio.

Figure 3.2: Custom build VHF transmitter with 1/4 wavelength dipole antenna

The FM receiver hardware, shown in Figure 3.3, was constructed as a 1/4 wavelength dipole antenna. The antenna is vertically polarized and mounted close to the pedestrian inside a high-visibility vest. The receiver uses a Si4703 FM radio tuner[64] on a Sparkfun evaluation board. The FM tuner is managed by an Arduino Pro Mini microcontroller using a library supplied by Sparkfun[65] and the timestamped RSSI data was recorded on a PC.

(a) Front

(b) Back

Figure 3.3: Custom build VHF receiver with 1/4 wavelength dipole antenna

3.1.3 Ultra-Wide Band (UWB)

The DecaWave DW1000 UWB transceiver[66] on a pair of EVB1000 evaluation boards[67], shown in Figure 3.4, were used for hardware testing. The provided UWB antenna is an omni-directional antenna, but the gain still varies with regard to antenna rotation[68]. For consistent measurements, all readings were taken with the ground planes facing each other (with the exception of the orientation test in Section 3.4). The EVB1000 is supplied with a DecaRanging demo application which performs DS-TWR at various user-specified channels and configurations. During the trials, raw SPI communications are recorded from the PC DecaRanging application. After the tests a custom post-processing script is run over the SPI logs to generate the ToF, distance, approximated received signal level, and approximated first path power level.

Two parameters of the UWB transceivers were investigated as part of the testing. The first parameter is the UWB channel number, as documented in Table 3.1. While channel 4 has a lower centre frequency, channel 7 is preferred because it can be used in Europe and New Zealand without special licensing[30]. The second parameter are the three data rates (6.8Mbps, 850kbps, and 110kbps) of which faster speeds have a negative impact on the maximum transmission range[66]. It is valuable to keep the data rate as high as possible, as the higher data rates leave more airtime free, supporting more radios.

Channel Number	Centre Frequency (MHz)	Bandwidth (MHz)
4	3993.6	1331.2
7	6489.6	1081.6

Table 3.1: UWB Channels Used In Warehouse Testing

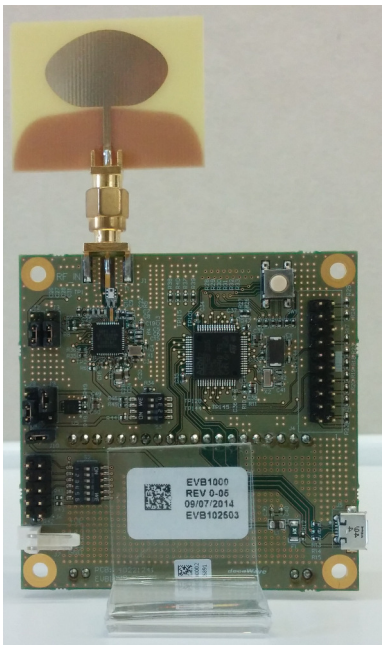

Figure 3.4: DecaWave's EVB1000 UWB transceiver development board

3.2 Testing Methodology and Notation

The sections below present the data gathered from many tests conducted to determine the performance of the three selected RF technologies. This section gives the reader an overview of how the data was processed and how the figures in the subsequent sections present the data.

3.2.1 Ranging Error Calculation

The RIPS and UWB technologies both measure the distance between the two radios. As the technologies must provide an accurate measurement over any arbitrary distance, a metric herein referred to as 'Ranging Error' is used to compare their performance. The ranging error is calculated in Equation 3.1

$$\epsilon = d_{gt} - d_r \tag{3.1}$$

where the ranging error ϵ is the difference between the ground truth measured distance d_{gt} and the distance from the ranging measurement d_r.

3.2.2 VHF Received Signal Strength Measurement

The VHF receiver has built in hardware for measuring the RSSI of the received signal. Unlike the ranging technologies, the RSSI cannot be directly converted into a distance, so the ranging error calculation presented in Section 3.2.1 is not applicable to this technology. For map matching to work with the VHF signals, the

tests are looking for invariance in the RSSI over different product in the racking. For this reason the figures reporting on the performance of the VHF radio show the RSSI gathered during testing.

3.2.3 Testing Results Figure Notation

All the tests presented in the subsequent sections involve recording multiple measurements at each location. The notation presented below uses the hourglass box plot to give the reader a visual reference of the mean, variance, and overall shape of the data. Figure 3.5 shows the raw ranging error of a typical UWB measurement with the generated box plot next to the data. The centre horizontal red line is the mean of the data. The blue horizontal lines of the box show where 50% of the data lies, and the whiskers show where 75% of the data lies. Any measurements that are observed beyond these bounds are plotted as semi-transparent red points. The notch about the mean line shows the 95% confidence interval about the mean. The wider the notch, the more the raw data is spread out around the mean.

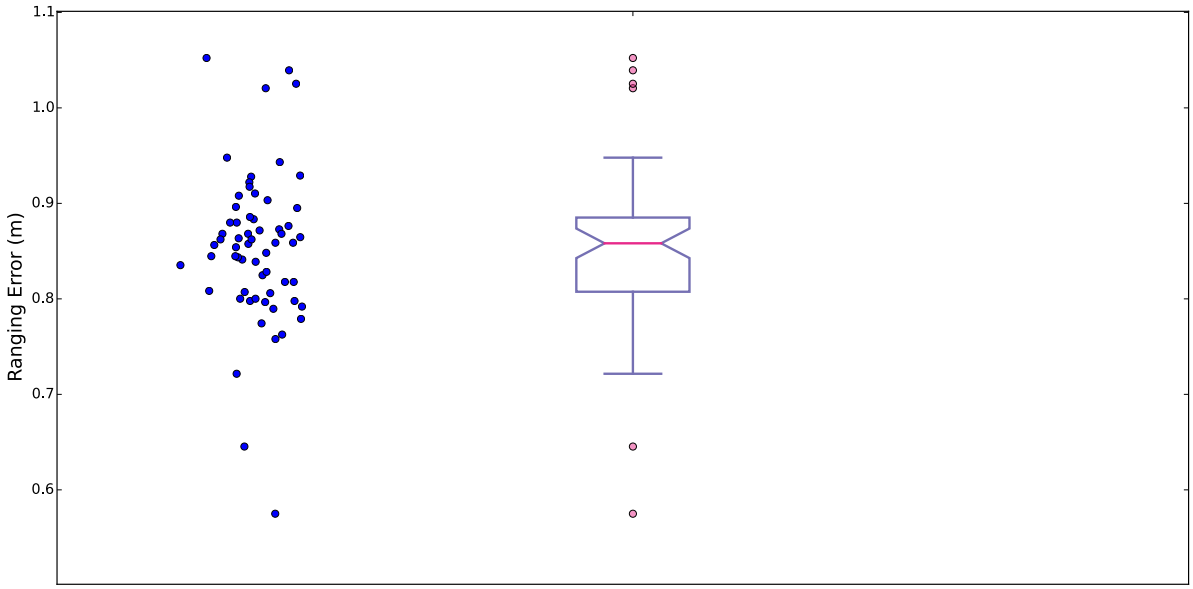

Figure 3.5: Raw UWB Ranging Error With Generated Box Plot

3.3 Open Field Test

The open field tests were conducted in Ilam Fields next to the University of Canterbury. The equipment is setup as shown in Figure 3.6. Ground truth was measured with a Leupold RX-800i laser rangfinder[69] aimed at the wooden board used as a target. The stationary radio was placed 20 metres from the street, and the other radio was moved down the length of the field.

The UWB results are shown in Figure 3.7. The DecaWave spec sheet claims 300m maximum range[12], but

after 200 metres the target board was too small for the laser rangefinder to measure. The data rate of the UWB communication had a clear impact on the maximum range. The 6.2 Mbps configuration was only able to communicate to 40m. This rules out the 6.2 Mbps data rate as a viable option, and is not considered in the remaining tests. The 850 kbps data rate was able to achieve communication the full 200m range; longer than any line of sight distance in the warehouse.

The maximum range of the Atmel RIPS was 75m using a 2MHz step size. Shown in Figure 3.8 are the results up to 50m. The precision of even the smallest distance step was greater than 2m, and at maximum range the measurements were incredibility imprecise. The 0.5 MHz step size was not able to conduct ranging after 50m, and the 2MHz measurements did not improve in precision.

In the open field test, the RSSI of the VHF signal decreases quickly over distance, as shown in Figure 3.9. The horizontally polarised signal showed slightly higher RSSI than the vertically polarised signal.

3.4 Antenna Orientation

The antenna orientation test was conducted in the same field as the open field test discussed in Section 3.3. Ground truth was measured with a 30m tape measure laid out over the length of the testing area. At each distance interval, ranging was taken at approximately 45 degree increments in the azimuth.

The UWB measurements shown in Figure 3.10a appears relatively unaffected by antenna orientation. The precision of the UWB measurements, shown in Figure 3.10a, is under 20cm, which is the same precision observed in the open field tests. The 270° data at the 1m reading was corrupted and unrecoverable.

The RIPS measurements shown in Figure 3.10b show no predictable bias based on antenna orientation. The variation measured is mostly below 0.4m which the earlier open field tests show is below the radio's ranging precision. During the 20m ranging trials, the radios had difficulty communicating, and far larger errors were observed and compared to those in 10m or 30m. The effect was not observed in the open field test.

The orientation of the antenna and pedestrian does not have a predictable effect on the RSSI of the VHF signal, shown in Figure 3.10c. At the 180° measurement, the receiver is facing away from the transmitter (signal travelling through the pedestrian), and there is no appreciable RSSI drop except in the 1m observation. The RSSI measurement changes over the rotation by $10 - 15$ dBµV without any apparent pattern relating to orientation, as observed in the open field test.

Figure 3.6: VHF Signal Strength Setup In The Open Field Test

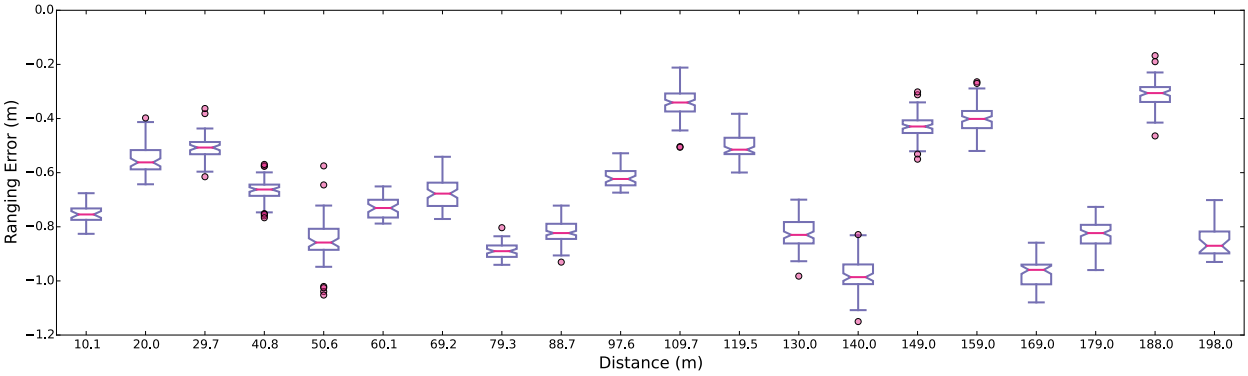

(a) Channel 7 at 850kbps

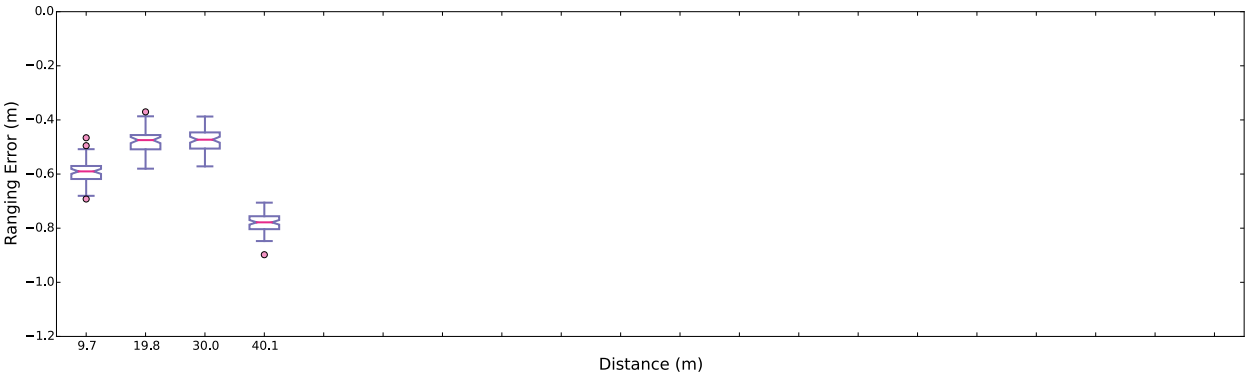

(b) Channel 7 at 6.2MHz

Figure 3.7: UWB ranging error in open field test

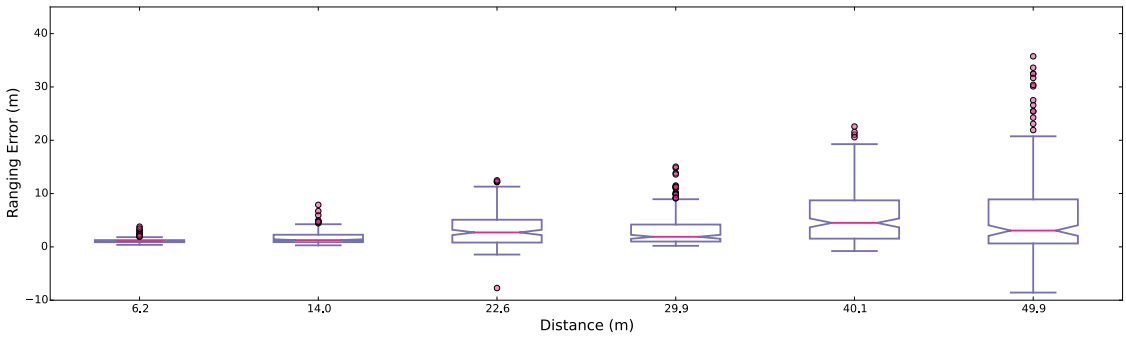

(a) Channel 26, Step Size 0.5 MHz

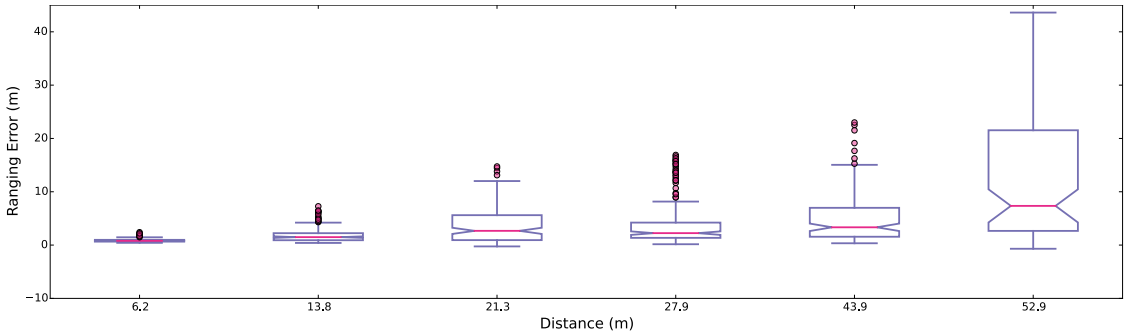

(b) Channel 26, Step Size 2 MHz

Figure 3.8: RIPS ranging error in the open field test

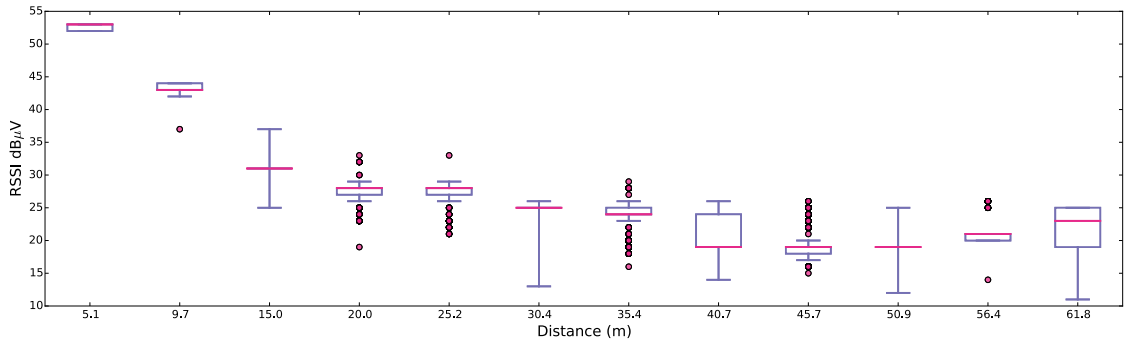

(a) Horizontal Polarization

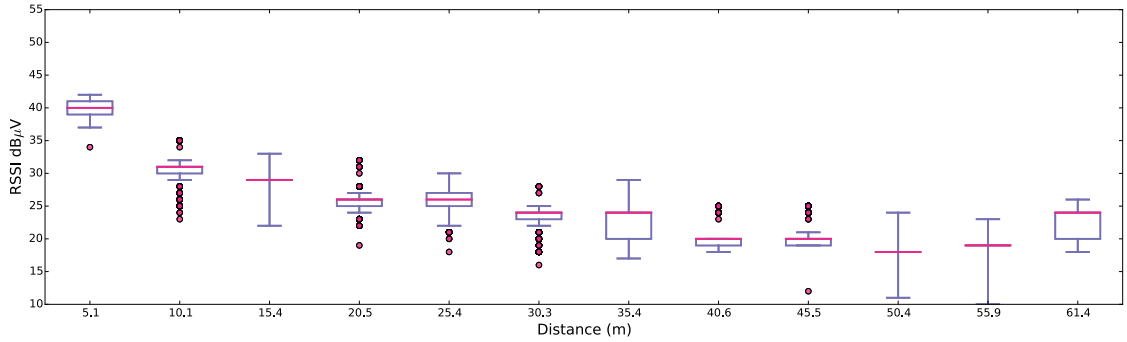

(b) Vertical Polarization

Figure 3.9: VHF 88.1 MHz in the Open Field Test

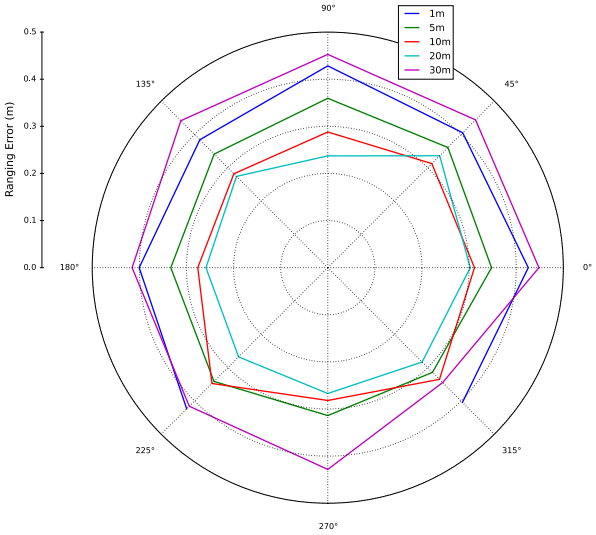

(a) UWB Antenna Orientation Results

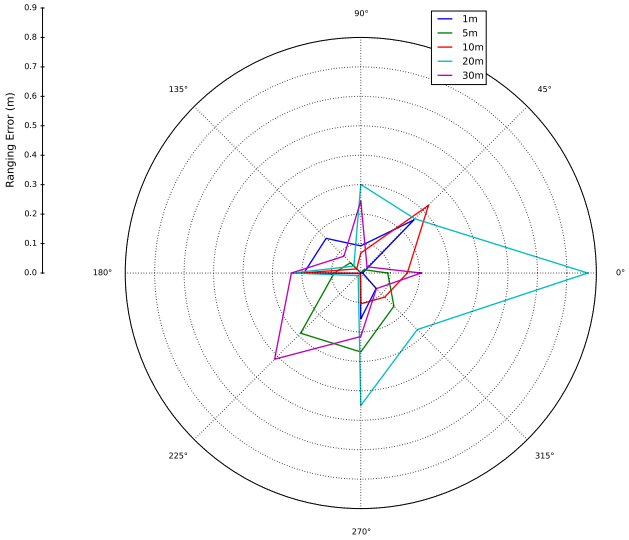

(b) RIPS Antenna Orientation Results

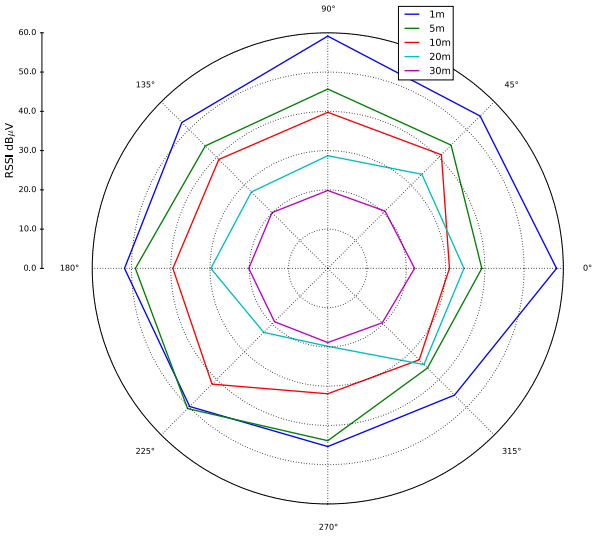

(c) VHF Pedestrian Orientation Results

Figure 3.10: Antenna Orientation Test Results

3.5 Pedestrian Interaction

The pedestrian interaction test's purpose is to observe the effect of closely mounting the RIPS and UWB to a pedestrian. The VHF's response to pedestrian interaction was observed along with orientation in Figure 3.10c. The radios were mounted close to the centre of the pedestrian with a plastic bracket. Ranging measurements were taken facing front (radios had clear line of site) and back (signals were forced to travel through the pedestrian) up to 30m in a clear open field. Ground truth was established using a 30m tape measure as in the orientation test in Section 3.4.

The UWB signal was significantly effected by the pedestrian's body. When the the line of sight was blocked by the pedestrian's body in Figure 3.11b, the system lost communication before 7m. The signal was not significantly affected by the pedestrian's body when it wasn't blocking the signal's path.

The RIPS ranging performed similarly to UWB when blocked by the pedestrian. As shown in Figure 3.12b, the maximum achievable range was 7m, 1m further than UWB was able to achieve. The ranging accuracy was similar to the open field test when the pedestrian's body did not block the signal's path, shown in Figure 3.12b.

For the VHF signal, the pedestrian interaction showed no appreciable affect on the RSSI in Figure 3.10c. For this technology, this test had to be combined with the orientation test because the radio was worn by a pedestrian on all tests to eliminate the effects of coupling with the pedestrian's body.

3.6 Open Warehouse Aisle

The open aisle test was conducted at the Foodstuff's Hornby Distribution Centre. The radios were set up 40cm from the edge of the aisle (80cm for the FM radio), and ground truth was taken by lining up the measurements with a rack leg. A majority of the testing was conducted in a section of the warehouse with racks 66m long, and so this is the maximum length measured in this test. The purpose of the test is to measure the best case performance that can be expected in the warehouse environment.

UWB ranging was able to accurately measure the full length of the 66m aisle. Channel 7, shown in Figure 3.13b, had similar precision and bias seen in the open field test described in Section 3.3. Figure 3.13b leaves out some outlying measurements at the 40m distance which give ranges 20-40m shorter than ground truth. The channel 4 ranging, shown in Figure 3.13a, have lower precision in the same distances which the outliers are observed in channel 7. The outliers are observed throughout the testing, and are discussed further in Section 3.11.

The RIPS radios were unable to range effectively down the full length of the aisle, shown in Figure 3.14. Channel 11 failed to communicate past 60m and channel 26 suffered many ranging failures after that distance.

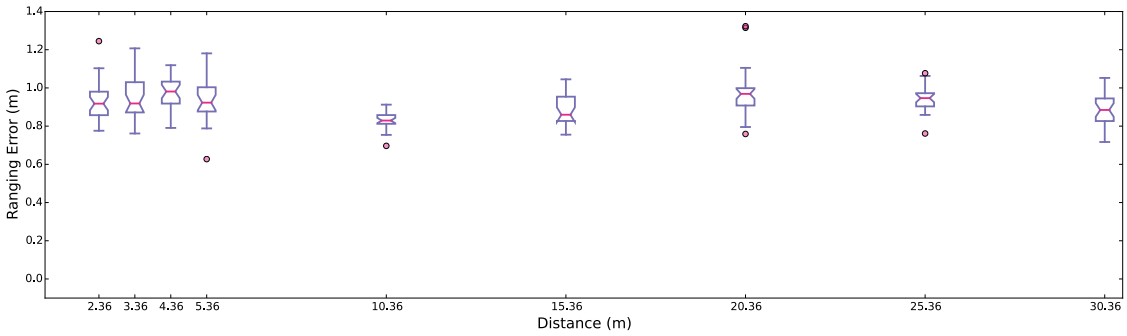

(a) Unblocked

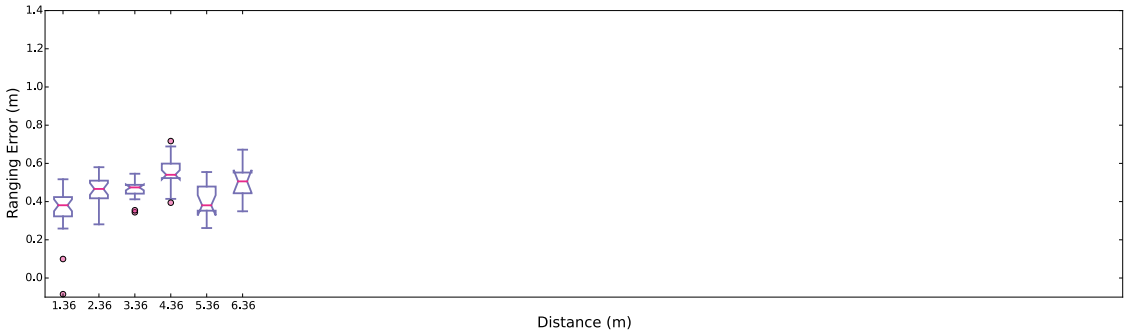

(b) Blocked

Figure 3.11: UWB Pedestrian Interaction Ranging Error

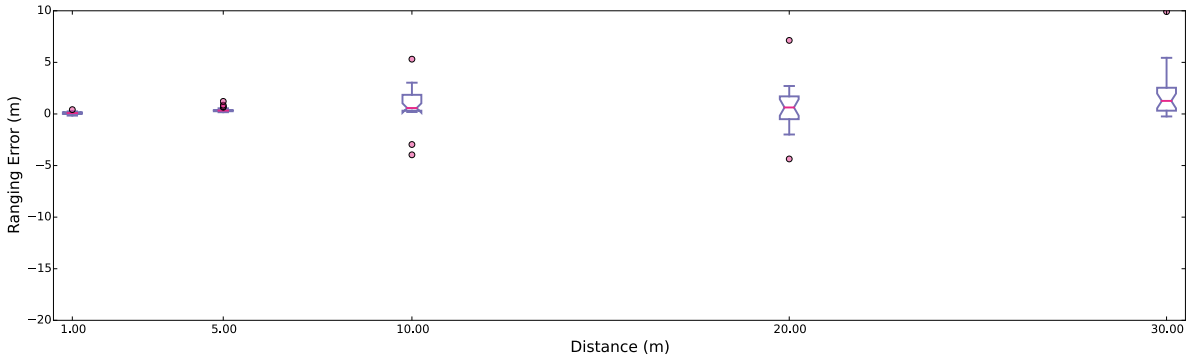

(a) Unblocked

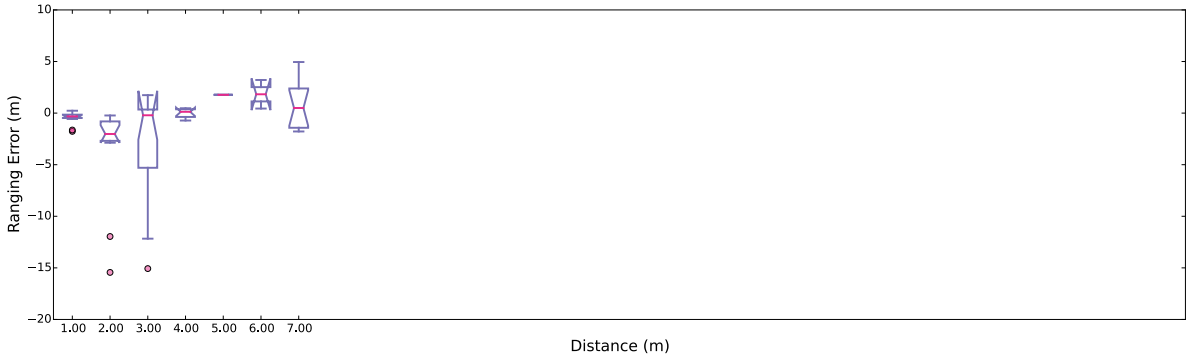

(b) Blocked

Figure 3.12: RIPS Pedestrian Interaction Ranging Error

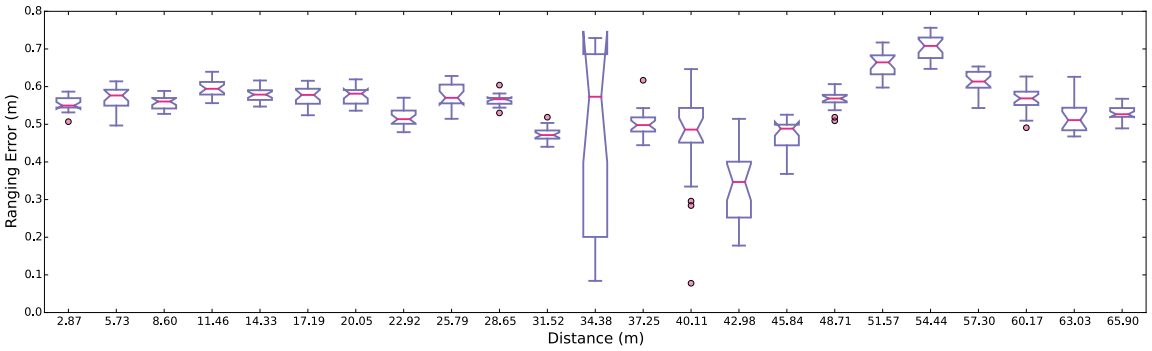

(a) Channel 4

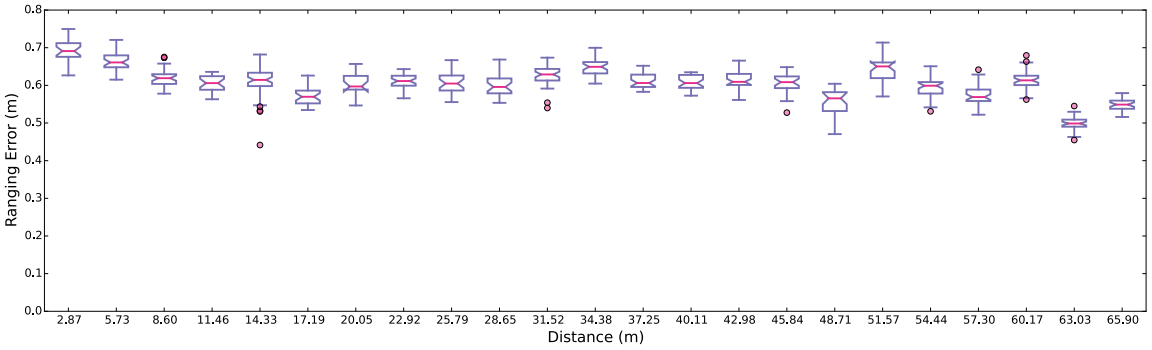

(b) Channel 7

Figure 3.13: UWB Open Aisle Ranging Error

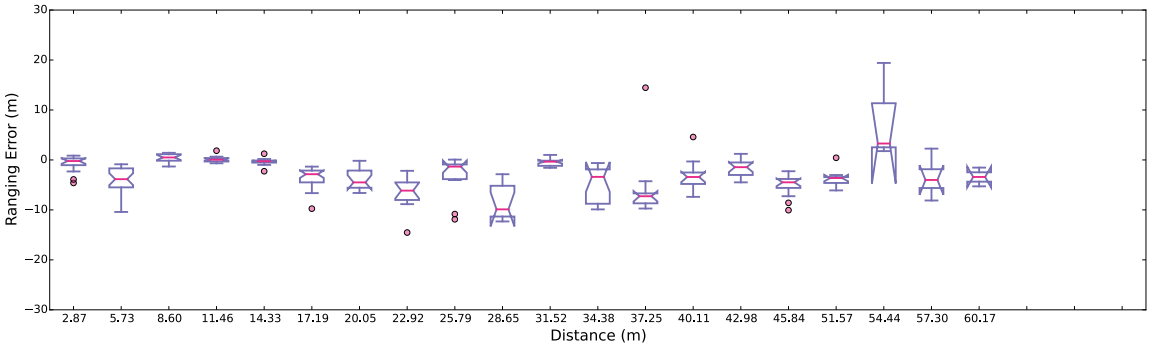

(a) Channel 11

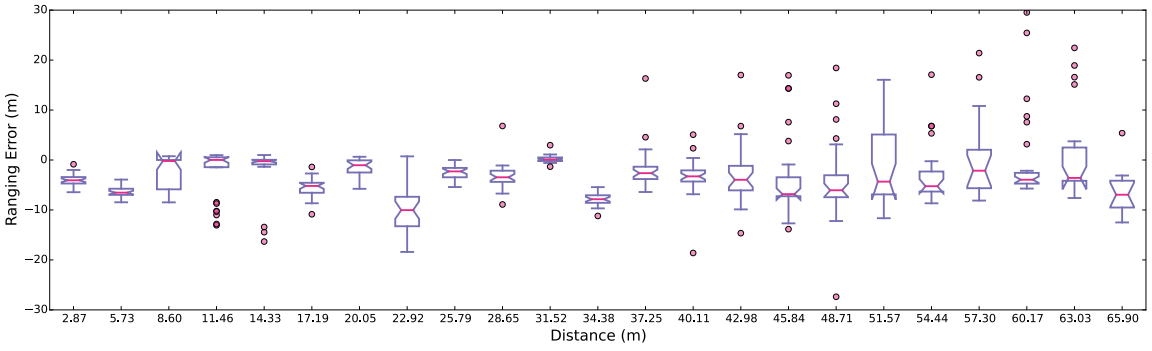

(b) Channel 26

Figure 3.14: RIPS Open Aisle Ranging Error

Other than max range there appears to be little difference between the two channels.

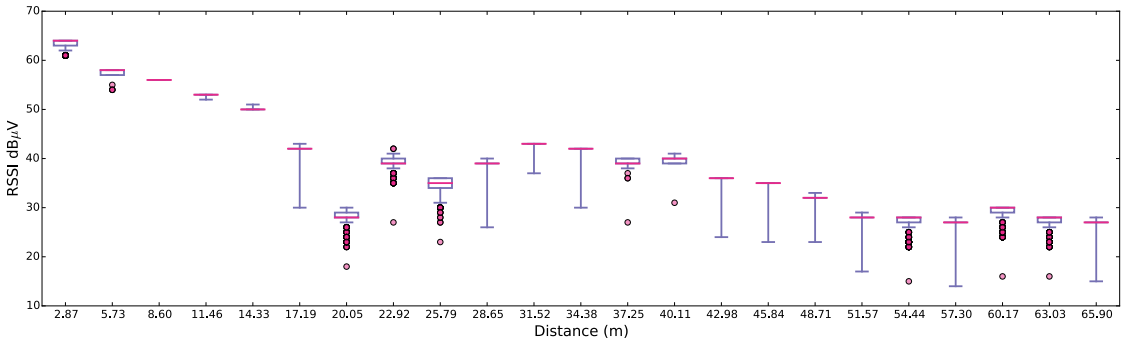

(a) Horizontal

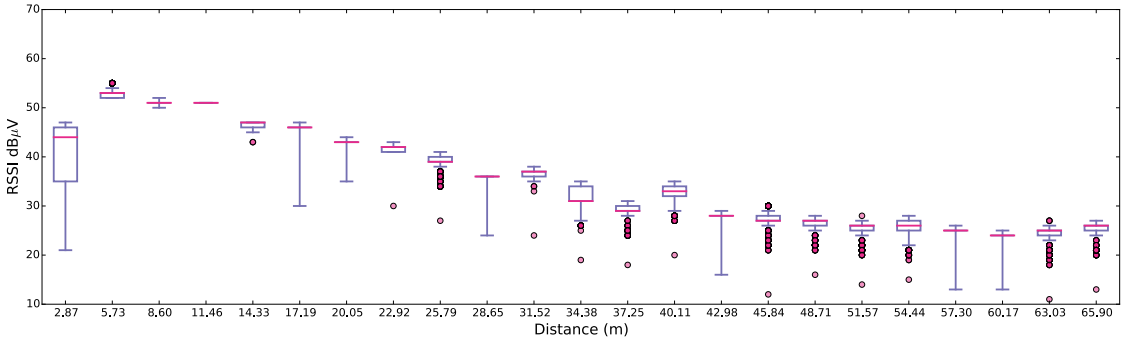

(b) Vertical

Figure 3.15: VHF Open Aisle RSSI

Figure 3.15 shows that the VHF RSSI is affected by the racking. As with the open field test, the horizontal polarisation shows a slightly higher RSSI, but the horizontal polarisation also shows more erratic fading than the vertical polarised signal. Both polarisation's are quite weak by 50m, where the signal would be indistinguishable.

3.7 No Line Of Sight (NLoS) Ranging Performance

The NLoS tests were conducted in the Foodstuff's DC, in the same location as the open aisle tests in Section 3.6. Ground truth is measured using a combination of the Leupold laser rangefinder used in Section 3.3 and a measuring tape. The purpose of this series of tests is to determine how the ranging is affected by the racking and to determine if different classes of products will change the ranging performance.

3.7.1 Ultra Wide-Band

Shown in Figure 3.16, the ranging precision of UWB remained around 20cm while ranging through empty racking. The accuracy of the measurements deteriorated quicker than the open aisle measurements, but it

was still under the 2m target. The maximum ranging distance was around 40m, but after 27m the radio was transmitting through a metal grate that was part of the racking structure. After another metal grate at 43m the received packets were too corrupted to be decoded. This leads to the conclusion that UWB ranging is not significantly affected by the presence of racking which is not in the line of sight path.

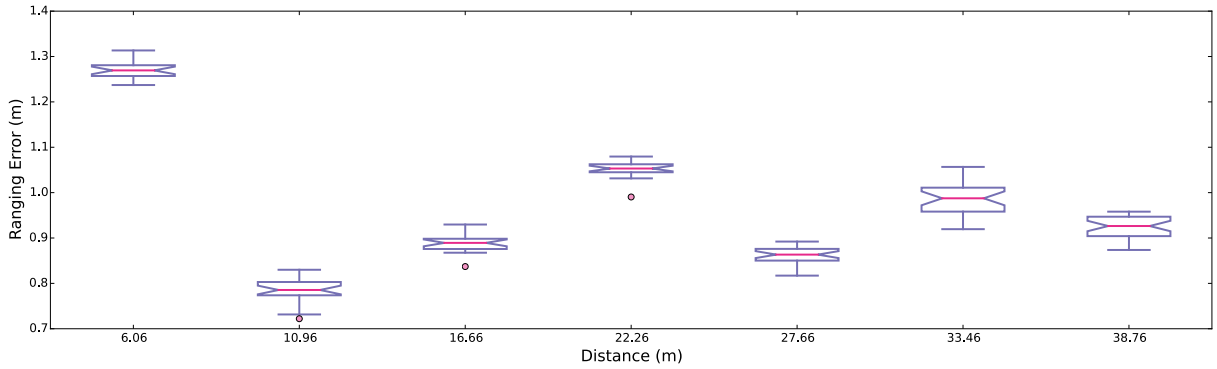

Figure 3.16: UWB Channel 4 Ranging Error Through Empty Racking

The NLoS ranging tests were conducted using both channel 4 and 7. Channel 4 is lower in frequency but is only viable for localisation in the United States due to spectrum licensing restrictions. Figure 3.17 shows that the channel 4 has a longer effective range in NLoS ranging, but channel 7 is as accurate as channel 4. The increased range afforded by channel 4 comes at reduced accuracy, especially in the metal product racking, where ranging is 2m greater than the ground truth.

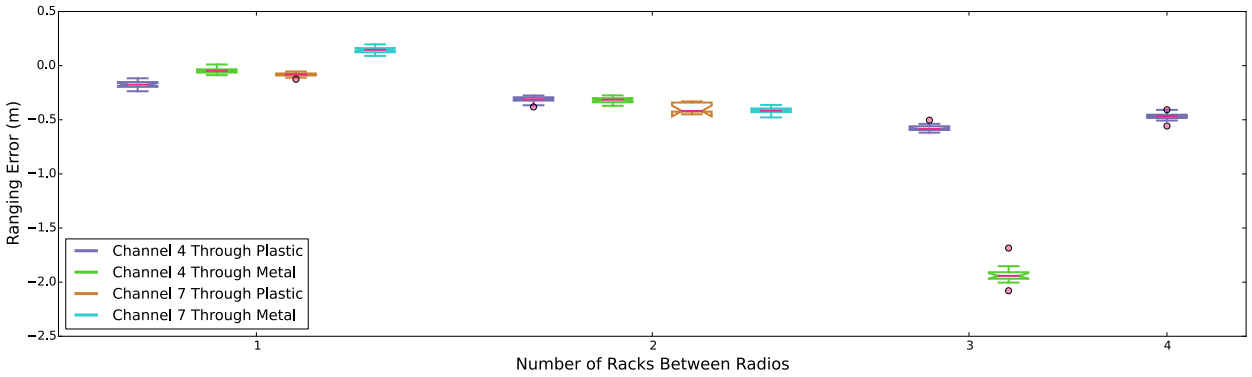

Figure 3.17: UWB Racking Interaction Performance

3.7.2 Atmel RIPS

The Atmel ranging system was significantly affected by the racking only ranging in clear line of sight through four racks (around 25m). The final two measurements (at 20m and 25m distance) had very few successful range measurements, with most signals being corrupted. Figure 3.18 shows the accuracy and precision of the measurements are in the same order of those observed in the open aisle test in Section 3.6, far too inaccurate for a 2m localisation system.

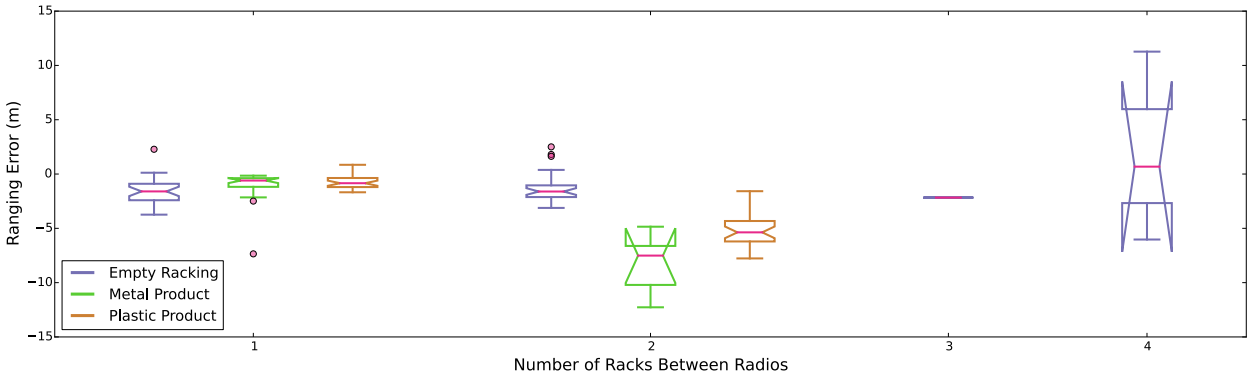

Figure 3.18: RIPS Racking Interaction Performance

3.8 VHF Racking Interaction Tests

The VHF racking interaction tests were conducted to measure how racking containing different classes of product change the RSSI. The first set of racking had almost no product on the bottom levels, the second rack contained mostly plastic and paper products, with some electronics at the end of the aisle, and the third aisle contained beer kegs and other bottles and cans. The transmitter was positioned near the wall pointed down the centre of the racking with the antenna oriented horizontally. Measurements were taken at every rack leg down each side of the rack.

The RSSI measured from each side of the rack shows in Figure 3.19 that the can/liquid filled racking affects the RSSI reading more than the empty or plastic product racking. The plastic product and empty racking show similar, but not identical, characteristics.

3.9 Discussion

In the tests conducted, UWB technology has proved to be an accurate ranging sensor for the warehouse environment. The accuracy and precision of the ranging is not negatively affected by racking and product. Obstacles decrease the maximum effective range of the system, so the radios must be strategically placed (discussed more in Section 3.10) to effectively cover the warehouse space. Antenna placement on the pedestrian is also a concern, as the antenna must not be blocked by the tracked pedestrian.

VHF RSSI is still affected by product in the racking, which does not solve the major issue of WLAN map matching in the warehouse. The VHF signals are blocked by the metal product, which would cause unpredictable changes to the RSSI map in a normally functioning warehouse. The range of the VHF radios is on par or worse than the UWB radios, and would require similar infrastructure commitment to cover the warehouse.

Atmel's phase analysis ranging is highly inaccurate with multipath interference found in the warehouse

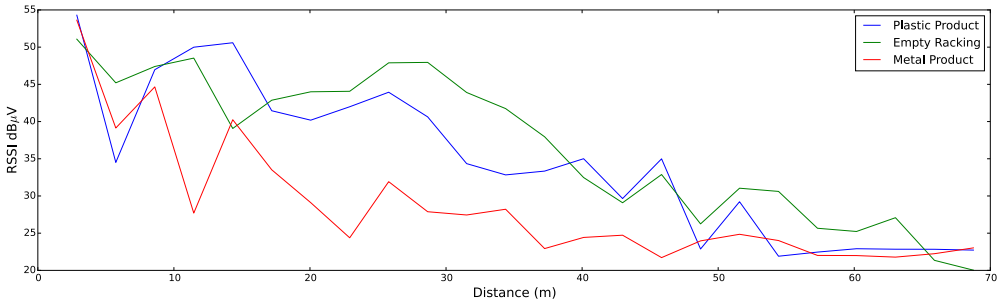

(a) Left Aisle

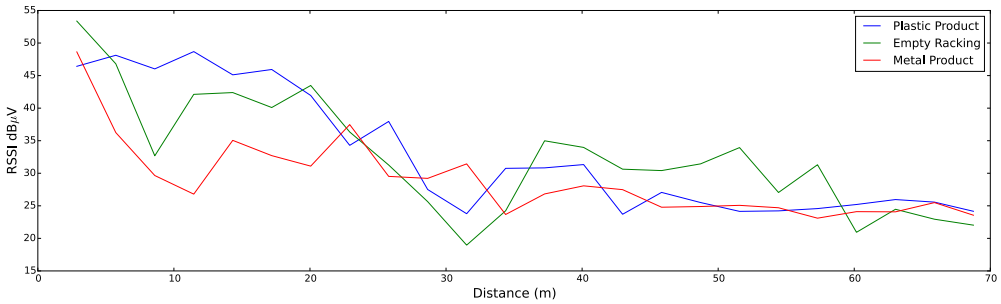

(b) Right Aisle

Figure 3.19: VHF Racking Intersection Average RSSI

environment. Even with the best case scenario with line of site down an aisle, the measured accuracy and precision would not lead to a system with 2m accuracy. The technology had abysmal range when passing through racking making it hard to judge if the ranging was affected by product in the racking. Therefore, UWB was selected as the RF technology used in the rest of this investigation.

3.10 Effective UWB Signal Coverage Tests

Once UWB was chosen as the technology to be used in the prototype, the next question is the number and placement of radios required to cover the warehouse. Due to building safety restrictions, the radios could not be easily mounted on the ceiling or within the racking. This meant the radios must be positioned outside the racking. The coverage tests were conducted to determine if the UWB radios could cover multiple aisles. The tests were conducted within two racking structures inside the Foodstuff's Hornby DC, the old warehouse with a set of racking 66m long, and in the new warehouse with two split racks forming a 90m long aisle.

3.10.1 In Line With Racking Placement

The in-line placement positions the radio to cover two aisles, while having line of sight down no aisle. The first test was conducted in the old warehouse, where the radio is placed as close to the wall but between two aisles. Measurements were taken down both aisles, and signal strengths for both Channel 4 and 7 are

recorded in Figure 3.20. Only one measurement was taken at the centre of each aisle, and so the generated figures show an expanded x axis. The blue point represents the position of the radio and the grey boxes plot the position of the racking. Both channels show similar signal strengths, with Channel 4 having a slightly higher signal strength at the far end of the aisle.

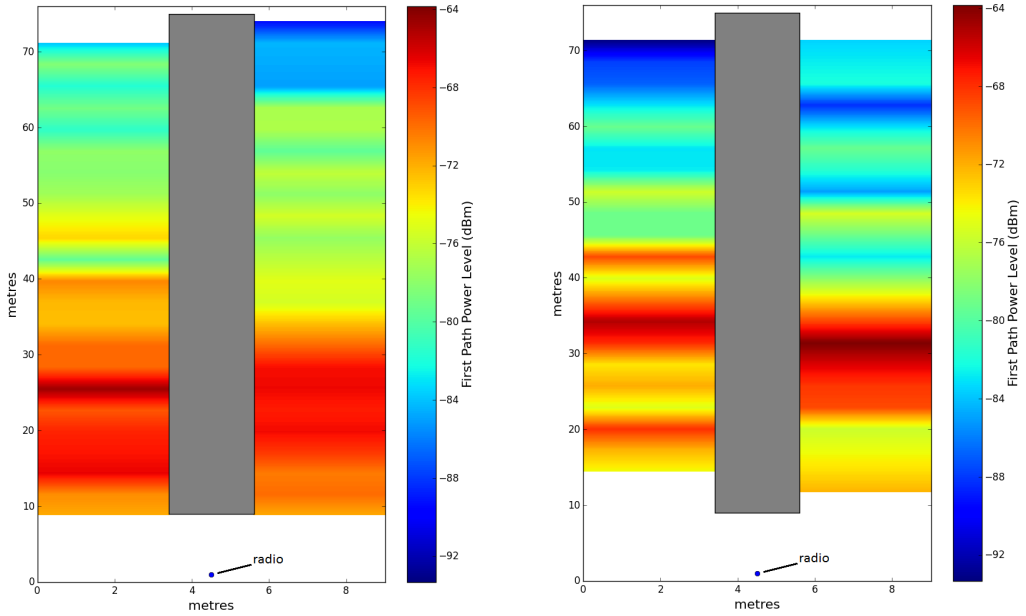

(a) Channel 4 (b) Channel 7

Figure 3.20: UWB Signal Strength with In Line Radio Placement in the Old Warehouse

3.10.2 Single Aisle Coverage

The single aisle coverage test was conducted in the new section of the warehouse, placing a radio in the centre line of the aisle. The signal for channel 7, shown in Figure 3.21, is detected down the centre aisle. In the adjacent aisles, the signal is detected up to around 30m down each aisle.

3.11 UWB Outliers

In most of the measurements conducted in the warehouse on channel 7, some ranging measured a lower time of flight than possible given the distance separating the radios. Figure 3.22 was compiled to show the best example of the outliers (the grey boxes were added to show where the racking is in relation to the distance axis). The data was gathered as the clear line of sight portion of Figure 3.21, but it was also observed in Figure 3.13b. The racking surrounding this aisle primarily held canned goods in the first set of racking, and wine bottles in the second set. The outlier frequency increased when entering the second set of racking, which points to a possible environmental cause.

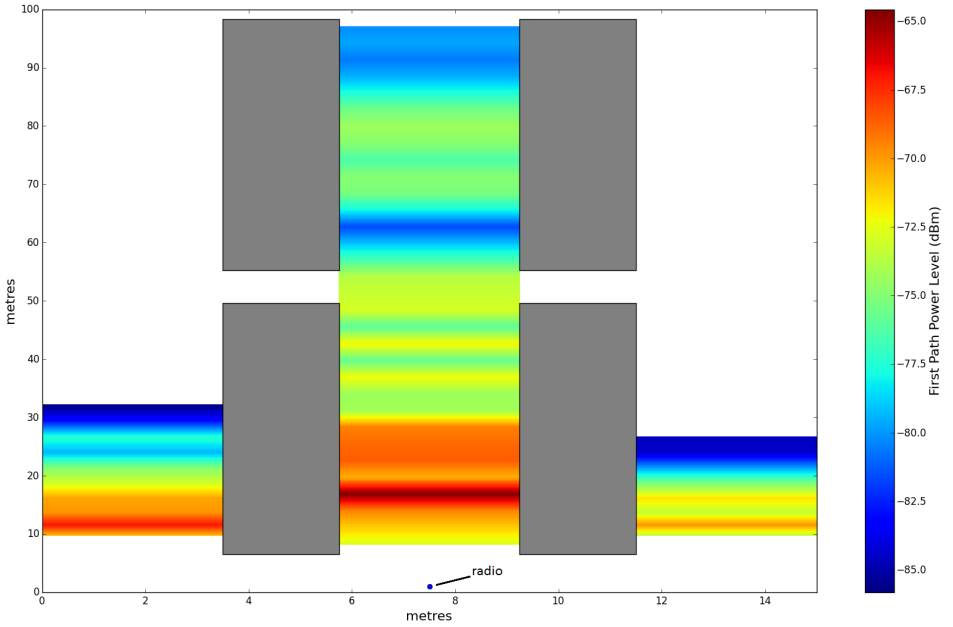

Figure 3.21: Channel 7 Single Aisle Signal Coverage in the New Warehouse

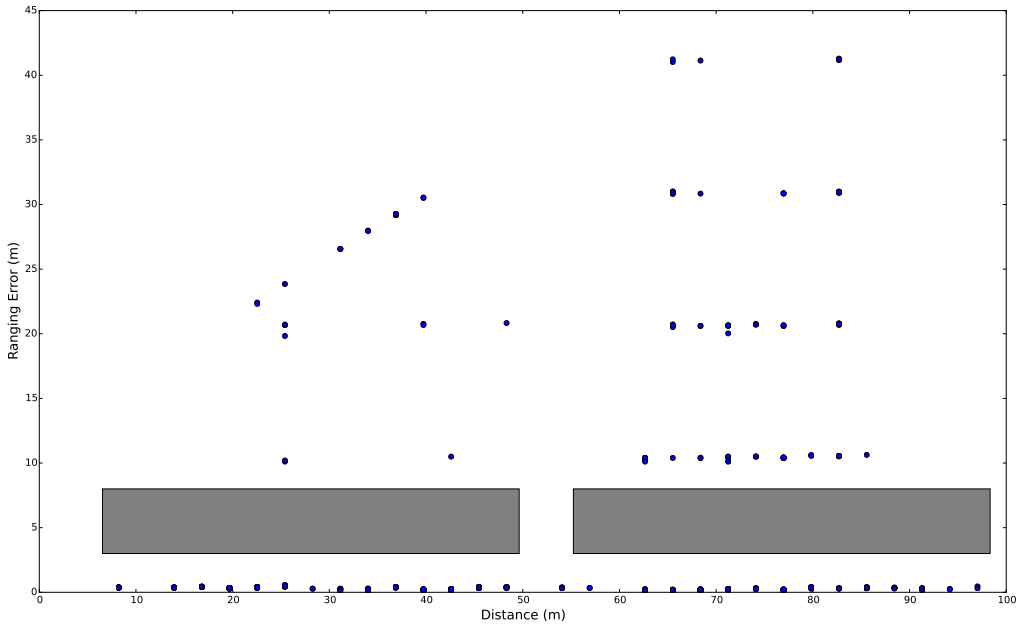

Figure 3.22: UWB Measurements Observed in a Single Aisle of the New Warehouse

The testing conducted in this thesis did not determine the cause of the outlying measurements, why channel 7 measurements are more susceptible to the error, or how the measurements are recording distances closer than ground truth. The pattern of 10 metre groupings in the second set of racking also remains unexplained. Any error attributed to multipath should have a longer time of flight. The channel is also clear from other UWB signals; in this ranging scheme the UWB frames are sent at 150ms intervals and no other UWB radios were on at the same time. While the outliers waste channel resources, they should be easy to filter out within the localisation system. The measurements are far outside the normal error bounds of UWB ranging.

3.12 Conclusion

The measurements clearly show that out of the three technologies tested, UWB based ranging will be the most accurate and reliable method for measuring distance. The UWB signal strength survey shows a single radio can cover the entire length of the longest aisle in the Foodstuff's Hornby DC. The next step to developing the real-time localisation system is to create a model of the warehouse using the data already gathered.

Chapter 4

System Simulation

The sensor fusion algorithms presented in Section 5.1 and Section 5.2 require a set of models to transform the information observed by the sensors into location data. Algorithm development necessitates a simulation to analyse multiple implementations of the algorithms on an even playing field. In Section 4.1, the models derived from the measurements conducted in Chapter 3 are presented. Section 4.2 and Section 4.3 describe the models used to simulate inertial motion and the racking structure. Section 4.4 describes the performance metrics used to compare the effectiveness of the localisation algorithms under test. Concluding the chapter is a demonstration of the simulated environment by showing the performance while dead-reckoning.

4.1 Radio Model

4.1.1 Radio Communication Distance

The effective range of the UWB communication was modeled using Equation 4.1

$$attenuation(d_{LoS}, d_{nLoS}) = max(1 - \frac{1}{290} * d_{LoS} + \frac{1}{13.846} * d_{nLoS}, 0) \tag{4.1}$$

where d_{LoS} and d_{nLoS} are the distance the signal travels through open air and racking respectively. The equation results in a floating point value between 1 (full strength), and 0 (no signal). The LoS constant was derived from the DecaWave's reported maximum signal range, and the nLoS constant was derived from the signal strength measurements recorded in Figure 3.17. The simulated map shown in Figure 4.1 shows coverage range of 30-35m down adjacent aisle. This is only 5-10m off of the signal strength observed in Figure 3.21.

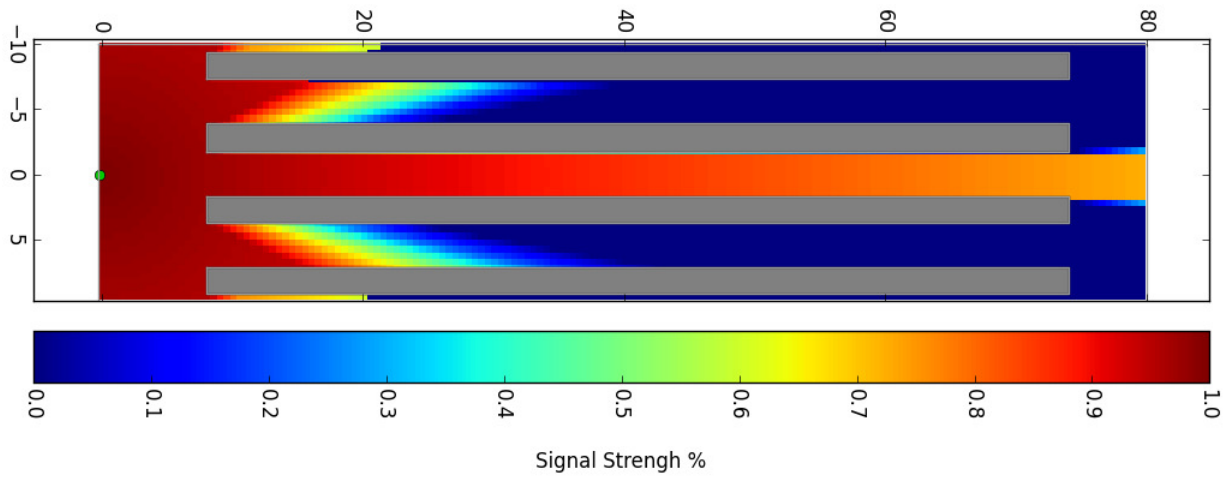

Figure 4.1: Simulated UWB Propagation Distance

4.1.2 Radio Ranging Error Model

The UWB observed ranging measurements have both a constant bias and random error component. The constant bias is set to zero in the model because it can be compensated via calibration of the antenna delay[66]. The random error component of the ranging is modeled using a Gaussian distribution with a standard deviation twice the magnitude observed in the warehouse observations (to account for unforeseen environmental factors).

4.2 Inertial Motion Model

Inertial motion provides the other information for the sensor fusion. The prototype was designed to use an accelerometer to count steps and a gyroscope to track orientation.

4.2.1 Step Counting Error

The step counting algorithm has not been implemented, and the error characteristics were not well understood at the time of creating the simulation. The simulation adds uniformly distributed error to the simulated velocity measurement at each step using an error estimated from literature on tracking pedestrians via inertial motion alone[70].

4.2.2 Orientation Tracking Error

The gyroscope's noise can be modelled as two components, a white noise and an unstable bias[71]. The white noise is simple to simulate as a Gaussian error introduced at each simulation step. The standard deviation is obtained from the target gyroscope's (MPU-6000) data sheet under the value of Rate Noise Spectral Density[72]. The unstable bias is modelled as random walk based on the bias stability. The MPU-6000 data sheet does not quote the bias stability. The closest available datasheet is a temperature controlled gyroscope ADIS16334, which quotes a 25 degree per hour stability[73]. Temperature controlled gyroscopes have a lower bias stability than non temperature controlled gyroscopes, so the simulation uses an order of magnitude more unstable gyroscope at 100 degrees per hour.

4.3 Warehouse Model

The warehouse model is constructed to replicate the old warehouse section of the Foodstuff's Hornby DC, the target testing site for the real-time prototype. The racking positions were obtained from site schematics provided by Foodstuff's. Figure 4.2 shows the graphical representation of the warehouse displayed by the simulation. The grey boxes represent racking, with the grey outline showing the outer walls of the warehouse. The green points represent UWB radios positioned 3 metres off the warehouse floor.

Radios are positioned at the end each of the 19 aisles as in the UWB signal strength survey conducted in Section 3.10.2. The radios are positioned on alternating sides of the aisle to provide a more uniform coverage outside the racking. Figure 4.3 shows the anticipated coverage of the warehouse with the given configuration of radio placement using Equation 4.1. The tracked target is in range to 3 radios at the edges of the aisles and outside the racking, and in sight of at least a single radio at all times while in the racking.

4.4 Performance Metrics

There are two performance metrics used to rate the algorithms. The metrics are based on the position error of the localisation algorithm, calculated in Equation 4.2 as the Euclidean distance between the estimated position and the ground truth position

$$\epsilon(P^{gt}, P^{alg}) = \sqrt{(x^{gt} - x^{alg})^2 + (y^{gt} - y^{alg})^2} \tag{4.2}$$

where P^{gt} and P^{alg} are (x, y) tuples giving the reported position of ground truth and localisation algorithm respectively. In simulation the ground truth position is trivially known.

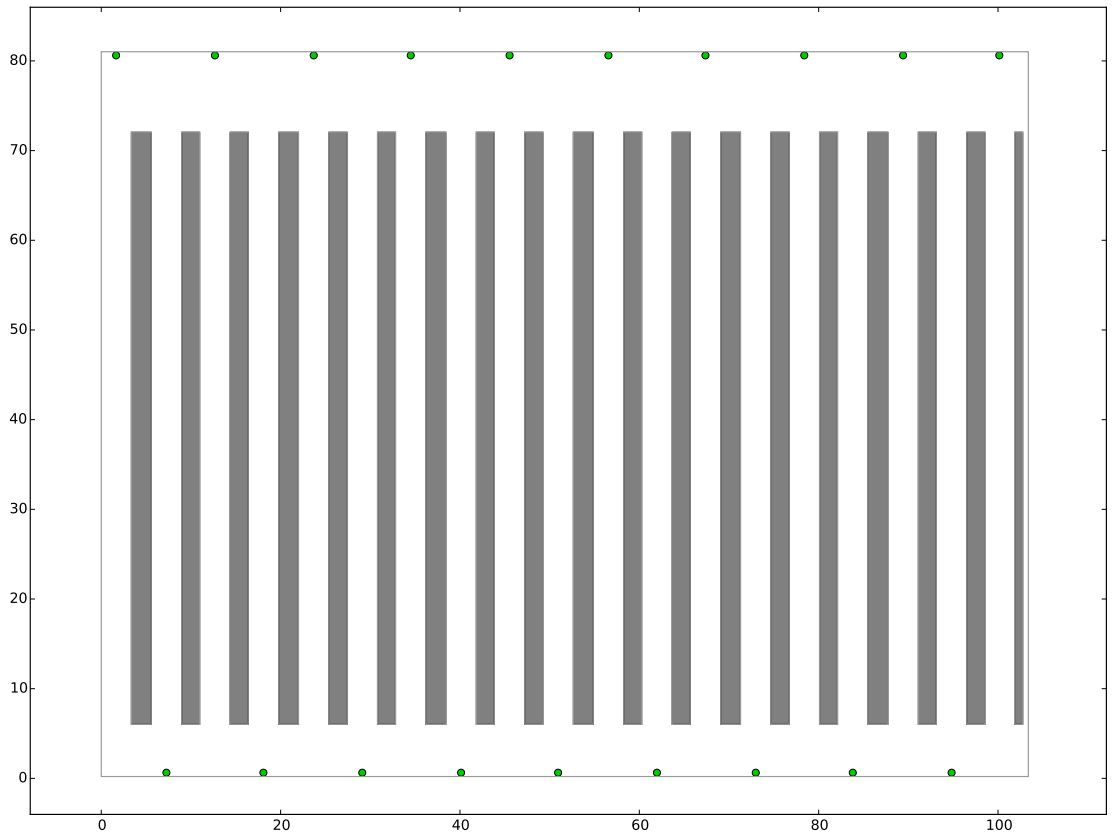

Figure 4.2: Infrastructure Positions in the Simulated Warehouse

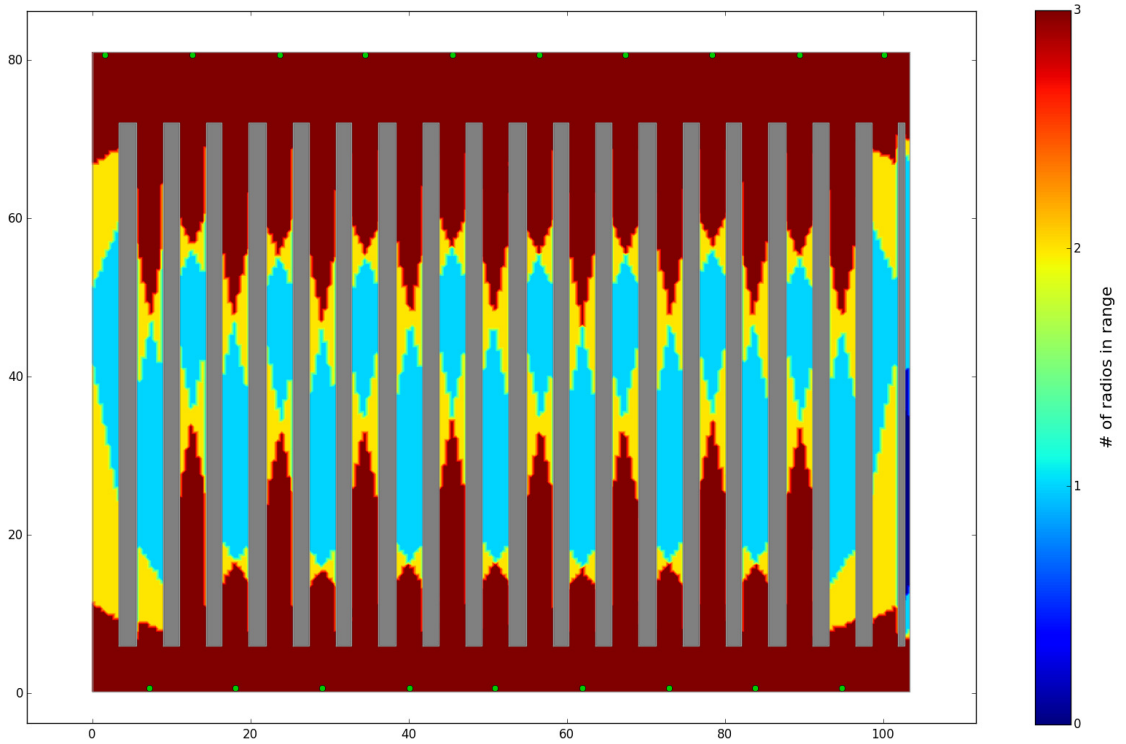

Figure 4.3: Simulated UWB Radio Coverage

4.4.1 Accuracy

Accuracy is a measure of how well the localisation algorithm tracks to the actual position of the pedestrian. Accuracy is the arithmetic mean of the localisation error, calculated in Equation 4.2, for all simulation steps. This is calculated by Equation 4.3

$$\mu(n, P^{gt}_{1:n}, P^{alg}_{1:n}) = \frac{1}{n} * \sum_{i=1}^{n} \epsilon(P^{gt}_i, P^{alg}_i) \tag{4.3}$$

where n is the number of steps performed by the simulation, $P^{gt}_{1:n}$ and $P^{alg}_{1:n}$ are arrays of n (x, y) tuples giving the reported position of ground truth and localisation algorithm respectively.

4.4.2 Precision

Precision is the measure of how consistent the localisation algorithm is when tracking the pedestrian. This is calculated by the root-mean-square deviation of the error as calculated in Equation 4.4.

$$\sigma(n, P^{gt}_{1:n}, P^{alg}_{1:n}) = \pm\sqrt{\frac{1}{n} * \sum_{i=1}^{n} (\epsilon(P^{gt}_i, P^{alg}_i))^2} \tag{4.4}$$

This thesis commonly expresses the precision by giving the error at 95% confidence, which is calculated in Equation 4.5 by assuming Gaussian distributed errors.

$$2\sigma(n, P^{gt}_{1:n}, P^{alg}_{1:n}) + \mu(n, P^{gt}_{1:n}, P^{alg}_{1:n}) \tag{4.5}$$

4.5 Dead Reckoning Example

The dead reckoning algorithm was implemented to test the simulation environment. The example also gives a benchmark to compare against the other localisation algorithms.

4.5.1 Simulation Model

The algorithm uses the simulated inertial motion sensors to recursively calculate the position via Equation 4.6

$$\theta_k = \theta_{k-1} + \Delta\theta_k \tag{4.6a}$$

$$x_k = x_{k-1} + v_k * \Delta t_k * cos(\theta_k) \tag{4.6b}$$

$$y_k = y_{k-1} + v_k * \Delta t_k * sin(\theta_k) \tag{4.6c}$$

where $\Delta\theta_k$ is the change in angle observed during the simulation step k via the gyroscope, v_k is the velocity measured via the simulated accelerometer based pedometry, and Δt_k is the time elapsed in the simulation step. θ_{k-1}, x_{k-1}, and y_{k-1} are the orientation and position information from the previous step.

4.5.2 Performance

Without references from the radio ranging, the dead reckoning's recursive algorithm cannot correct the error introduced in the gyroscope and pedometry information. This is observed in an example of the simulation, shown in Figure 4.4. The dead reckoning path is shown as the blue plot, while the ground truth path plotted in pink. The dead reckoning path illiterates how small errors in orientation will accumulate to have a major impact on the localisation accuracy.

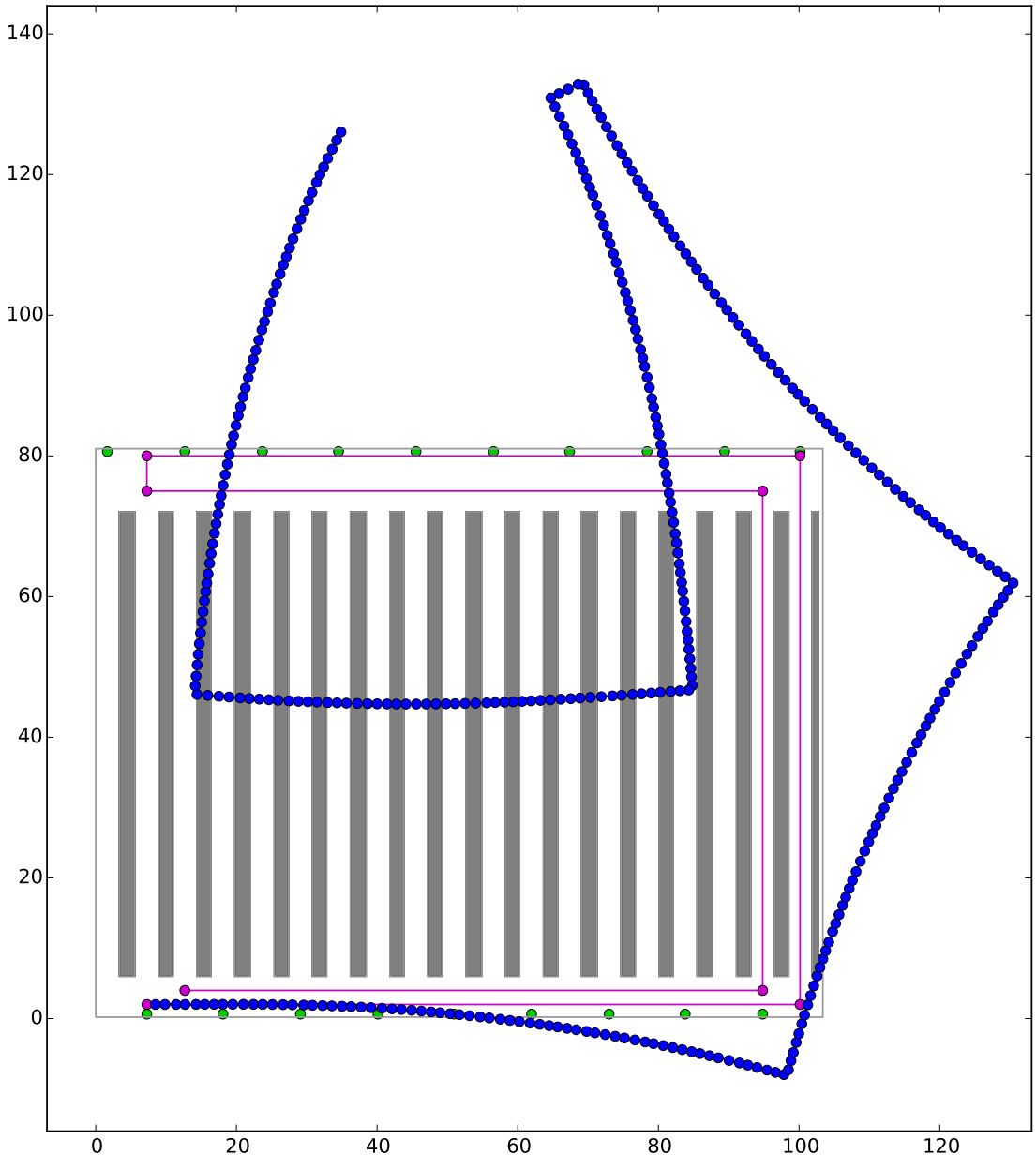

Figure 4.4: Simulated Inertial Motion based Dead Reckoning

Chapter 5

Sensor Fusion Algorithms

The next step in designing the prototype localisation system was to design a sensor fusion algorithm that correctly estimated the pedestrian's current position from radio ranging and inertial motion measurements. Two such algorithms were implemented; a particle filter described in Section 5.1 and an Unscented Kalman Filter described in Section 5.2. Each filter was tested in the simulation described in the previous chapter to select a single implementation for the localisation prototype.

Both algorithms are recursive filters that track the pedestrian in 2 spatial dimensions as well as the pedestrian's orientation and current velocity. As the typical warehouse does not include multiple levels, the pedestrian's height above the warehouse floor was not tracked. Collectively these tracked parameters are referred to as the pedestrian's state. The filters update the estimated position once a second, herein referred to as a simulation step, each time a new set of radio ranging information is gathered. The goal of each algorithm is to efficiently determine an accurate estimate of the pedestrian's true position from the noisy measurements.

5.1 Particle Filter

The particle filter was developed in 1993 as a solution to the nonlinear Bayesian filtering problem[74][75]. The filter uses many weighted sample points to represent any posterior distribution, and the sample points can be propagated through any non-linear, non-Gaussian model. This gives the particle filter a great degree of flexibility to accurately model systems that are hard to model with the Kalman Filter (discussed more in Section 5.2). The particle filter inherently models multimodal systems, as each particle represents a predicted state of the overall system.

5.1.1 Theory of Operation

The Sequential Importance Sampling (SIS) particle filter operates using N_s weighted sample points in state space (herein referred to as particles) $\{x_k^i, w_k^i\}_{i=1}^{N_s}$ where $\{x_k^i, i = 1, \dots N_s\}$ are the set of particles at the current time k, and $\{w_k^i, i = 1, \dots N_s\}$ are the associated weights[76]. If the weights are normalised such that $\sum_{i=0}^{N_s} w_k^i = 1$, then the weighted sample points can be used to approximate the current state x_k via Equation 5.1.

$$x_k \approx \sum_{i=0}^{N_s} w_k^i x_k^i \tag{5.1}$$

During real-time operation, the algorithm accomplishes the $\{x_{k-1}^i\}_{i=0}^{N_s} \rightarrow \{x_k^i\}_{i=0}^{N_s}$ transformation via Equation 5.2

$$\{x_k^i\}_{i=0}^{N_s} = f_k(x_{k-1}^i, z_k)\}_{i=0}^{N_s} \tag{5.2}$$

where the function $f_k()$ is a model that predicts the state x_k based on its previous state x_{k-1} and observations z_k. The weight of the new particles is calculated via Equation 5.3

$$\{w_k^i\}_{i=0}^{N_s} \propto \{w_{k-1}^i p(z_k|x_k^i)\}_{i=0}^{N_s} \tag{5.3}$$

where $p(z_k|x_k^i)$ is the posterior probability of the particles with reference to the current observations z_k. With the particle's state and weight calculated for time k, x_k can be computed using Equation 5.1.

An inevitable issue in the SIS particle filter is a phenomenon called the degeneracy problem[76]. This occurs after multiple recursive calls of the filter, all the weight will trend towards one particle with the rest having a negligible weight. The number of effective particles, N_{eff}, can be approximated by Equation 5.4.

$$N_{eff} \approx \frac{1}{\sum_{i=0}^{N_s}(w_k^i)^2} \tag{5.4}$$

This metric can be used to trigger a resampling of the particles. The resampling algorithms remove particles with negligible weights, and redistribute them around the particles with large weights. The weights of all the particles are then normalised to $1/N_s$.

5.1.2 Implementation

The implementation of the SIS particle filter was written in python using the concepts described in Section 5.1.1. The particles are initially seeded randomly around a Gaussian estimation of the starting position with equal weighting. During each measurement step, the particles' new predicted positions are updated using inertial motion dead reckoning as shown in Equation 4.6.

The posterior of the new particles are calculated from the available radio measurements gathered during each step. Equation 5.5 shows the posterior calculated for each radio measurement

$$p(z_k|x_k^i) = \frac{1}{\sqrt{2\pi}} * e^{-\frac{z_p^i - z_k}{2}} \tag{5.5}$$

where z_p^i is the predicted ranging measurement of the particle x_x^i. The posterior from all radio measurements were summed together, and then Equation 5.3 is used to calculate the particle's new weight. Finally, all the particles' weights are normalised such that the sum of all the weights are equal to 1.0.

5.1.2.1 Resampling Algorithm

Resampling is triggered when the number of effective particles, calculated via Equation 5.4, drops below $\frac{N_s}{2}$. Each particle is split into N_{copies} particles based on Equation 5.6 where w_k^i is the weight of the individual particle.

$$N_{copies} = \lfloor w_k^i * N_s \rfloor \tag{5.6}$$

Any particle with an N_{copies} value of 0, will be removed from the filter. When N_{copies} is greater than 1, any additional duplicates have uniform noise added to the orientation. This made duplicates of the parent follow different paths than the parent particle, and models the unstable bias of the gyroscope discussed in Section 4.2.2. All particles are assigned a weight of $\frac{1}{N_s}$.

In practice, more particles are deleted than copied with this resampling algorithm. To keep the particle population count constant, any additional particles required are randomly placed around the new average localised position, as calculated in Equation 5.1.

5.1.2.2 Racking Intersection Algorithm

Racking intersection information is easily reflected in the particle filter algorithm. Any particle that is within a rack has its weight set to 0. This leads to N_{eff} declining more quickly and triggers the resampling algorithm described in Section 5.1.2.1, removing the intersecting particles from the filter.

5.1.3 Simulation Performance

The particle filter's tracked the pedestrian with far better accuracy and precision than the dead-reckoning algorithm. Figure 5.1 shows the path of a typical simulation run, with the blue points showing the entire localisation path. The red points show individual particles at a second within the simulation, while the purple point shows the pedestrian's true position at that time.

The particle filter tracks exceptionally well within the racking, owing to the racking intersection algorithms. The filter's accuracy decreases as the particles spread out without the constraints of the racking. Figure 5.2 shows the accuracy for 10 simulated runs of the particle filter, a 95% accuracy of about 5.06 metres.

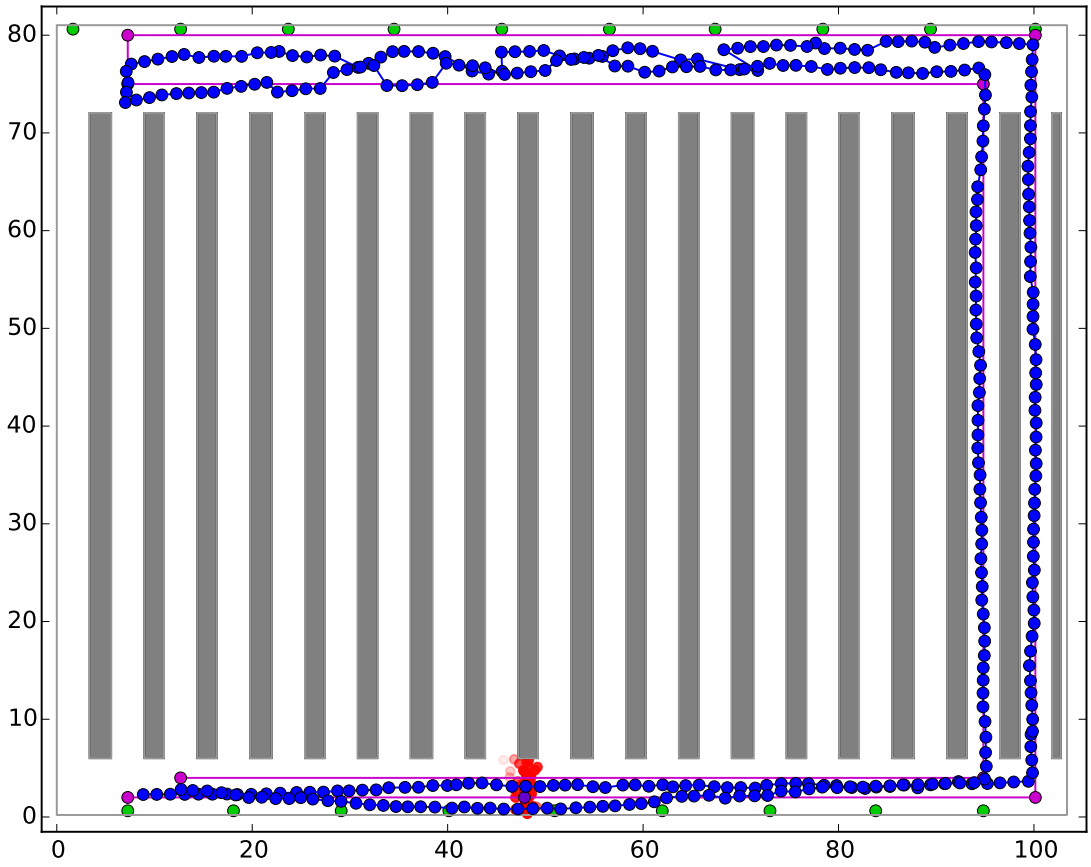

Figure 5.1: Simulated Particle Filter Pedestrian Tracking

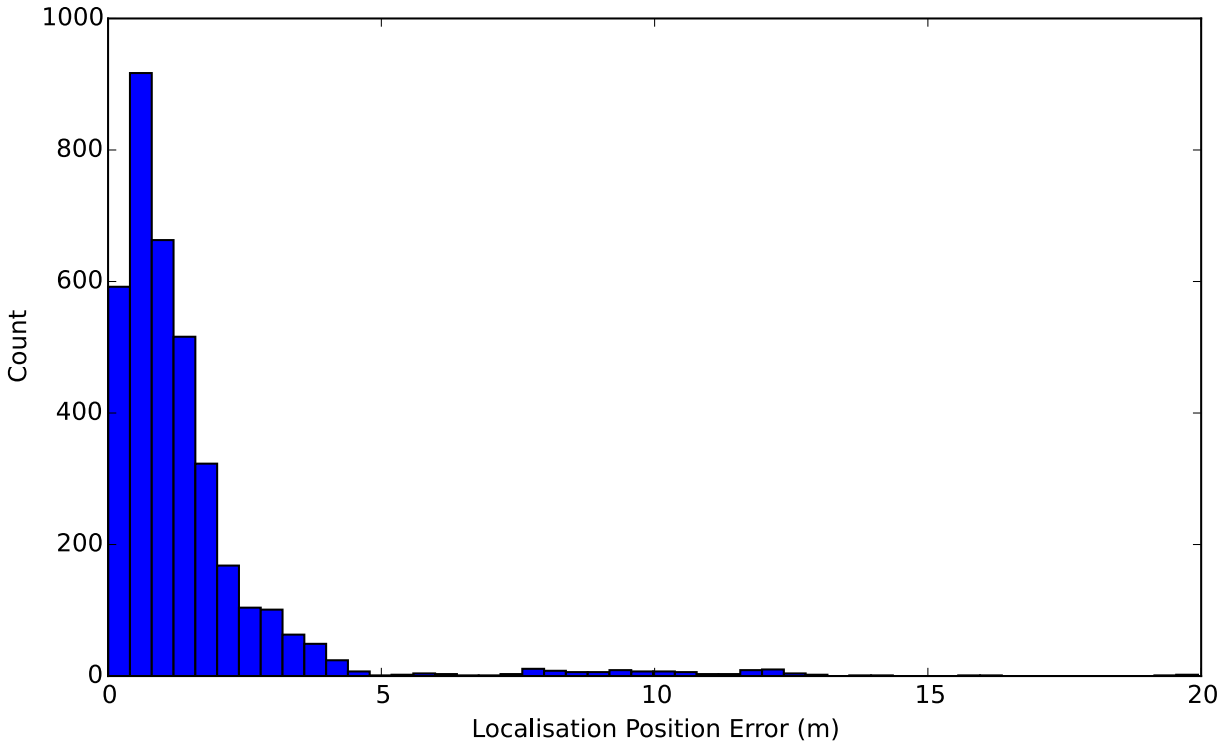

Figure 5.2: Simulated Particle Filter Performance Over 10 Runs

5.1.4 Limitations In The Weighting Algorithm

The leading cause of localisation error in the particle filter was the particle weighting algorithm, described in Equation 5.5, which did not accurately model the radio ranging accuracy. Figure 5.3 is used to illustrate the problem. The filter's prediction on this update is shown as a purple point, almost 2 metres away from the actual position (the pink point). Particles in region A and B have nearly identical weight (shown as the transparency of the red particles), even though region A has 3 radio ranges within close proximity to the particles (shown as the pink arcs). The problem was not fully analyzed due to the performance of the Unscented Kalman Filter; which proved in Section 5.2 to be simpler to implement, faster, and more accurate.

5.2 Unscented Kalman Filter (UKF)

The Unscented Kalman Filter (UKF) is an extension of the Kalman Filter (KF) for application in nonlinear systems. The KF is a recursive filter developed in 1960 by R. E. Kalman[77]. As a recursive filter it has the major computational benefit of not requiring data from previous iterations. However; the filter tracks all states as Gaussian random variables and the variables must be propagated through linear functions[78]. Assuming linearity is not realistic in most real world situations, extensive effort has been applied to use the KF algorithms in nonlinear systems.

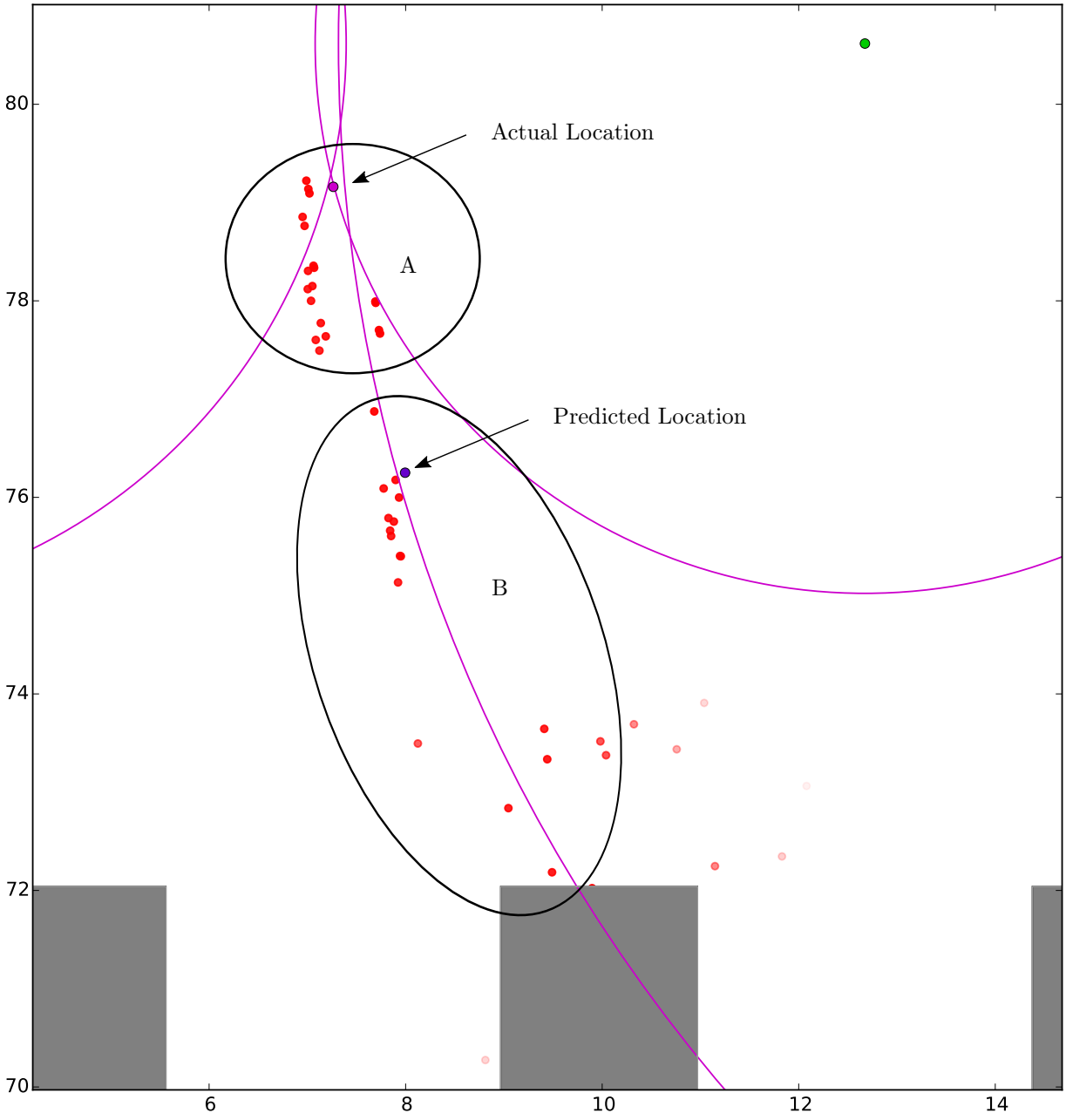

Figure 5.3: Particle Filter Weighting Algorithm Example

The de facto nonlinear adaptation is the Extended Kalman Filter (EKF), developed soon after the KF. The EKF linearises the nonlinear system about the mean using Jacobian matrices. The EKF's linearisation introduces error into the filtering; causing instability in particularly nonlinear systems, and computing Jacobian matrices can be difficult for certain applications. The UKF, developed by Simon J. Julier and Jeffery K. Uhlmann[13] in 1997, allows true nonlinear propagation functions without the requirement of calculating Jacobian matrices. This method has the further benefit of more accurately approximating the nonlinearity of the system[14].

5.2.1 Kalman Filter Theory of Operation

The Kalman filter is a recursive estimator that is typically split into a prediction and update phase. The filter tracks the current state x_k as a Gaussian random variable with a covariance of P_k.

The prediction phase uses Equation 5.7 and Equation 5.8 to predict the next state and covariance where F_k is a n by n matrix that predicts x_k based on the previous state x_{k-1}.

$$x_{k|k-1} = F_k x_{k-1} + B_k u_k \tag{5.7}$$

$$P_{k|k-1} = F_k P_{k-1} F_k^T + Q_k \tag{5.8}$$

The $B_k u_k$ and Q_k terms are used to apply control or unknown inputs to the prediction phase.

In the update phase, a set of m observations (called z_k with corresponding covariance of R_k) are combined with the prediction to reach the estimated state. The first part of the update phase is calculating the 'innovation' state and covariance, noted in Equation 5.9 and Equation 5.10 as y_k and S_k respectively.

$$y_k = z_k - H_k x_{k|k-1} \tag{5.9}$$

$$S_k = H_k P_{k|k-1} H_k^T + R_k \tag{5.10}$$

The innovation state and covariance describe how different the actual observations at time k are from their predicted values. The m by n matrix H_k is used to translate the predicted state and covariance into the observation space. Next the optimal Kalman gain is calculated in Equation 5.11.

$$K_k = P_{k|k-1} H_k^T S_k^{-1} \tag{5.11}$$

The Kalman gain is the optimal minimum mean-squared error linear estimation of x_k assuming the models F_k and H_k are accurate. The Kalman gain is then used to calculate the current state and covariance in Equation 5.12 and Equation 5.13.

$$x_k = x_{k|k-1} + K_k y_k \tag{5.12}$$

$$P_k = (I - K_k H_k) P_{k|k-1} \tag{5.13}$$

5.2.2 Unscented Transform (UT) Theory of Operation

The Unscented Transform is a method for transforming Gaussian random variables through nonlinear functions by means of approximating the Gaussian distribution[13]. The Gaussian random variable x with a mean of $\bar{x}$ and covariance of P_x is transformed into a set of weighted points $\{x^i, w^i\}_{i=0}^{2n+1}$, herein referred to as sigma points. The minimum number of sigma points is $2n+1$ where n is the dimension of the Gaussian random variable x.

The sigma points' values are calculated in Equation 5.14

$$x^i = \bar{x} \qquad i = 0 \tag{5.14a}$$

$$x^i = \bar{x} + (\sqrt{(n+\lambda)P_x})_i \qquad i = 1, \ldots, n \tag{5.14b}$$

$$x^i = \bar{x} - (\sqrt{(n+\lambda)P_x})_{i-n} \qquad i = n+1, \ldots, 2n \tag{5.14c}$$

and the weight w^i is the tuple $\{w^i_{mean}, w^i_{cov}\}$ with values for mean and covariance, calculated in Equation 5.15.

$$w^i_{mean} = \lambda/(n+\lambda) \qquad i = 0 \tag{5.15a}$$

$$w^i_{cov} = \lambda/(n+\lambda) + (1 - \alpha^2 + \beta) \qquad i = 0 \tag{5.15b}$$

$$w^i_{mean} = w^i_{cov} = \frac{1}{2(n+\lambda)} \qquad i = 1, \ldots, 2n \tag{5.15c}$$

The λ term is a scaling parameter calculated in Equation 5.16

$$\lambda = \alpha^2(n+\kappa) - n \tag{5.16}$$

where α determines the spread of the sigma points about $\bar{x}$, κ is usually set to 0, and β incorporates knowledge of the distribution of x (where $\beta = 2$ is optimal for Gaussian distributions).

The sigma points' values can then be propagated through any nonlinear function, called $G()$ in Equation 5.17, resulting in new set of sigma point values $\{y^i\}$.

$$\{y^i\} = \{G(x^i)\}_{i=0}^{2n} \tag{5.17}$$

Then the new Gaussian random variable's mean is calculated by the weighted average of the transformed points in Equation 5.18.

$$\bar{y} \approx \sum_{i=0}^{2n} w^i_{mean} y^i \tag{5.18}$$

The new covariance is calculated using the weighted outer product of the points as in Equation 5.19.

$$P_y \approx \sum_{i=0}^{2n} w^i_{cov} \{y^i - \bar{y}\}\{y^i - \bar{y}\}^T \tag{5.19}$$

5.2.3 Unscented Kalman Filter (UKF) Theory of Operation

The UKF simply applies the UT in the KF equations to replace the F_k and H_k matrices with nonlinear functions $f_k()$ and $h_k()$. The prediction phase is completely replaced with the unscented transform, shown in Equation 5.20

$$x_{k|k-1}, P_{k|k-1} = UT(x_{k-1}, P_{k-1}, f_k) \tag{5.20}$$

where the function $UT()$ is the complete unscented transform described in Equations 5.14-5.19. The $f_k()$ function, like the F_k matrix it replaces, describes the predicted state of each particle at time k, given the sigma particle at $k-1$. Control inputs $B_k u_k$ and Q_k of Equation 5.7 and Equation 5.8 are also used by $f_k()$ but are left out for the sake of brevity.

The update phase of the KF is also revised to make use of the UT's nonlinear support for the observations. The innovation mean and covariance step is replaced by another application of the UT in Equation 5.21.

$$y_k, P_z = UT(x_{k|k-1}, P_{k|k-1}, h_k) \tag{5.21}$$

The prediction mean and covariance is propagated through the observation function $h_k()$, which translates the sigma point into the observation space. When Equation 5.20 has been used to predict $x_{k|k-1}$ and $P_{k|k-1}$, the sigma points generated by the prediction can be directly used in this step.

After collocating the covariance P_z, the cross-covariance matrix P_{xz} is calculated using the sigma points from Equation 5.20 and Equation 5.21 and the observations z_k in Equation 5.22.

$$P_{xz} = \sum_{i=0}^{2n} w_{cov}^i \{x^i - x_{k|k-1}\}\{y^i - z_k\}^T \tag{5.22}$$

This cross-covariance matrix is used in Equation 5.23 with innovation covariance to calculate the Kalman gain.

$$K = P_z P_{xz}^{-1} \tag{5.23}$$

After the Kalman gain is calculated, the term is applied to the predicted mean and covariance, shown in Equation 5.24 and Equation 5.25, to reach the filtered estimate.

$$x_k = x_{k|k-1} + K(z_k - y_k) \tag{5.24}$$

$$P_k = P_{k|k-1} - K P_z K^T \tag{5.25}$$

5.2.4 Implementation

The UKF implemented for tracking the pedestrian uses four states; the position in the x and y axis, velocity, and orientation. A majority of the UKF equations were implemented using the python pykalman library[15].

5.2.4.1 Transition Model

The transition model, $f_k()$ in Equation 5.20, is implemented as a constant velocity dead reckoning model. The basic equations for constant velocity dead reckoning are described in Equation 4.6. The velocity is assumed constant from the previous state, and the $\Delta\theta_k$ is provided as a control input observed by the gyroscope.

5.2.4.2 Observation Models

The UKF uses two different observation models for $h_k()$ depending on the number of radio observations. The first model, shown in Equation 5.26, predicts the raging measurement using the distance formula to the anchor radio with a known position $R^i = \{R^i_x, R^i_y, R^i_z\}$, where i is the number of radio observations in the step.

$$o^i_{range} = \sqrt{(R^i_x - P^k_x)^2 + (R^i_y - P^k_y)^2 + (R^i_z - P_z)^2} \tag{5.26}$$

The $\{P^k_x, P^k_y\}$ terms are from the sigma point's predicted position information and the P_z is a constant value denoting the pedestrian's height. This calculation is the only observation used when there are two or more radio observations.

When there is one or no radio observations, more information is needed to make a stable observation update. Equation 5.26 is used on any radio observations, and is supplemented by observing the velocity using the model in Equation 5.27

$$o_{velocity} = \frac{\sqrt{(P^k_x - P^{k-1}_x)^2 + (P^k_y - P^{k-1}_y)^2}}{\Delta t} \tag{5.27}$$

where the filter's last estimated position, $\{P^{k-1}_x, P^{k-1}_y\}$, is used along with the step's elapsed time (Δt) to approximate the velocity of the sigma point. This is compared with the observed velocity from the pedometry sensor.

5.2.4.3 Racking Intersection Models

The racking intersection models operate over the transition and observation models described in Section 5.2.4.1 and Section 5.2.4.2 respectively. These models only affect the normal operation when sigma points leave the bounds of the warehouse, or are found to be within a rack. As currently implemented the models only support simple rectangular rack shapes, arranged either horizontally or vertically.

A visual representation of these models is presented in Figure 5.4. The sigma points are represented as various colours of points with a red line indicating their orientation and velocity. The 2 dimensional position covariance is displayed as a light blue ellipse and the racking is represented as a grey box. Figure 5.4d shows the mean of the estimated position as purple point, and the radio ranges are projected into the graph as pink arcs.

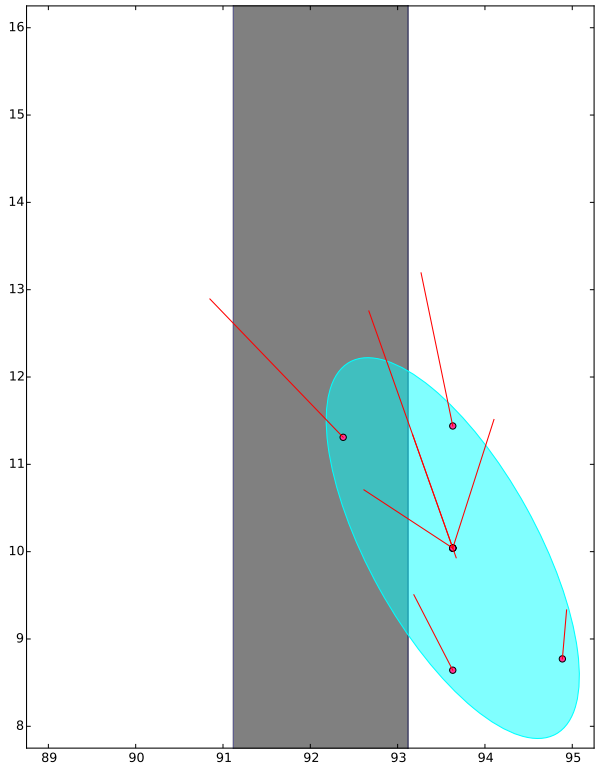

(a) Sigma Points From Covariance

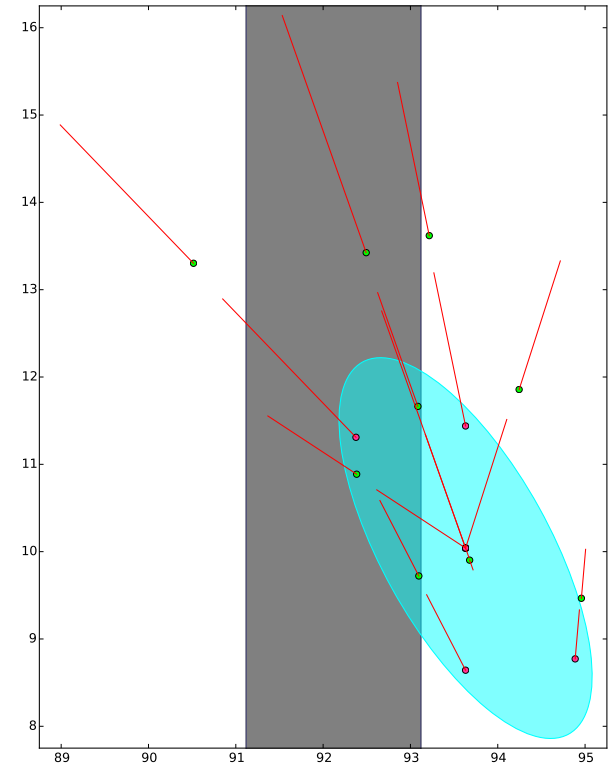

(b) Dead Reckoning Transition Model

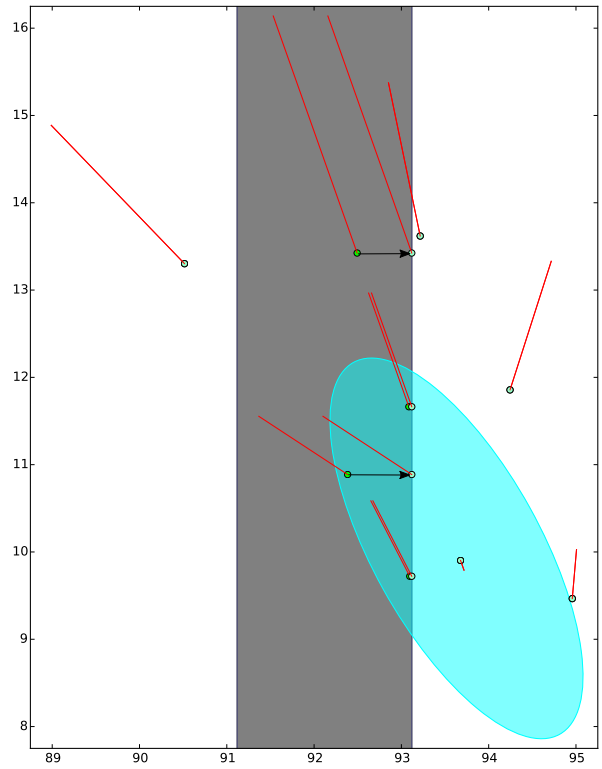

(c) Racking Intersection Transition Model

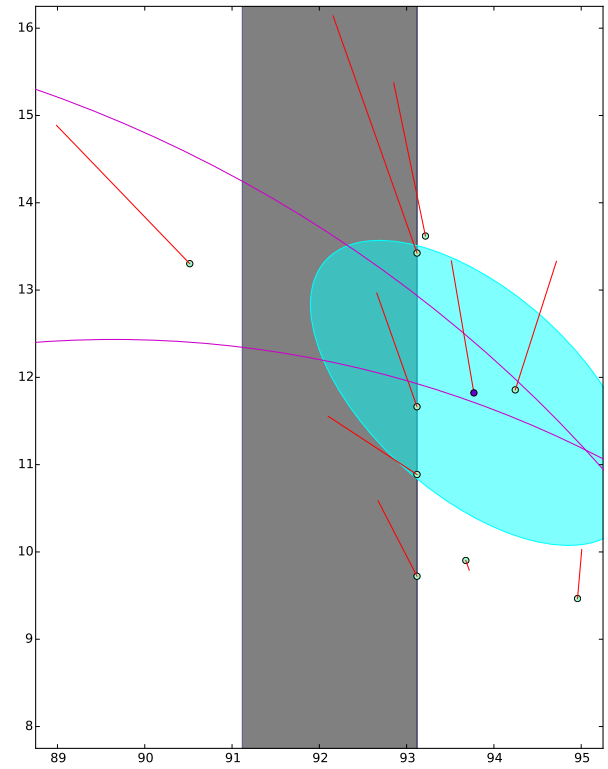

(d) Observation and Resulting Mean And Covariance

Figure 5.4: UKF Transition and Update

5.2.4.4 Racking Intersection Transition Model

The racking intersection transition model's changes the x and y position of any sigma point that is within a rack or outside the warehouse bounds to the nearest valid edge, shown in Figure 5.4c. The current implementation selects four candidate points relating to the four edges of the bounding box of the rack. The distance to each candidate point is calculated, and the candidate with the smallest distance is used as the new sigma point's x and y position.

5.2.4.5 Racking Intersection Observation Model

The observational model for racking intersection relies on a mock sensor observation (herein referred to a virtual observation) of how far the sigma point is from the 'correct' aisle. The aisles can be mapped out similar to the racking, or in the case of the implemented algorithm, inferred from the racking structure. The 'correct' aisle is determined as the first aisle a pedestrian enters. This is based on the presumption that the localisation is most accurate when entering and exiting the aisle. Radio coverage estimations presented in Figure 4.3 show the areas most covered by radios is the area outside the racking.

The first racking intersection observation model (used in the performance analysis in Section 5.2.5) used a much simpler racking intersection virtual sensor. When the sigma particles are found inside the racking, the sensor read a value of 1.0 instead of 0.0. This proved to not be effective in the real-time prototype testing, as the sigma particles would 'jump' the aisle and be stuck in adjacent aisles during periods of no radio contact.

5.2.5 Simulation Performance

The UKF performed well under simulation, shown in Figure 5.5 and Figure 5.6. The location error was 1.63 metres at 95% confidence. The UKF had a shorter execution time than the particle filter, and was easier to implement using pykalman libraries.

5.3 Conclusion

The UKF showed a clear performance and implementation advantage to the particle filter. On accuracy, filter stability, and execution efficiency the implemented UKF algorithm outperformed the particle filter. As such, this algorithm was used for the remainder of the thesis project.

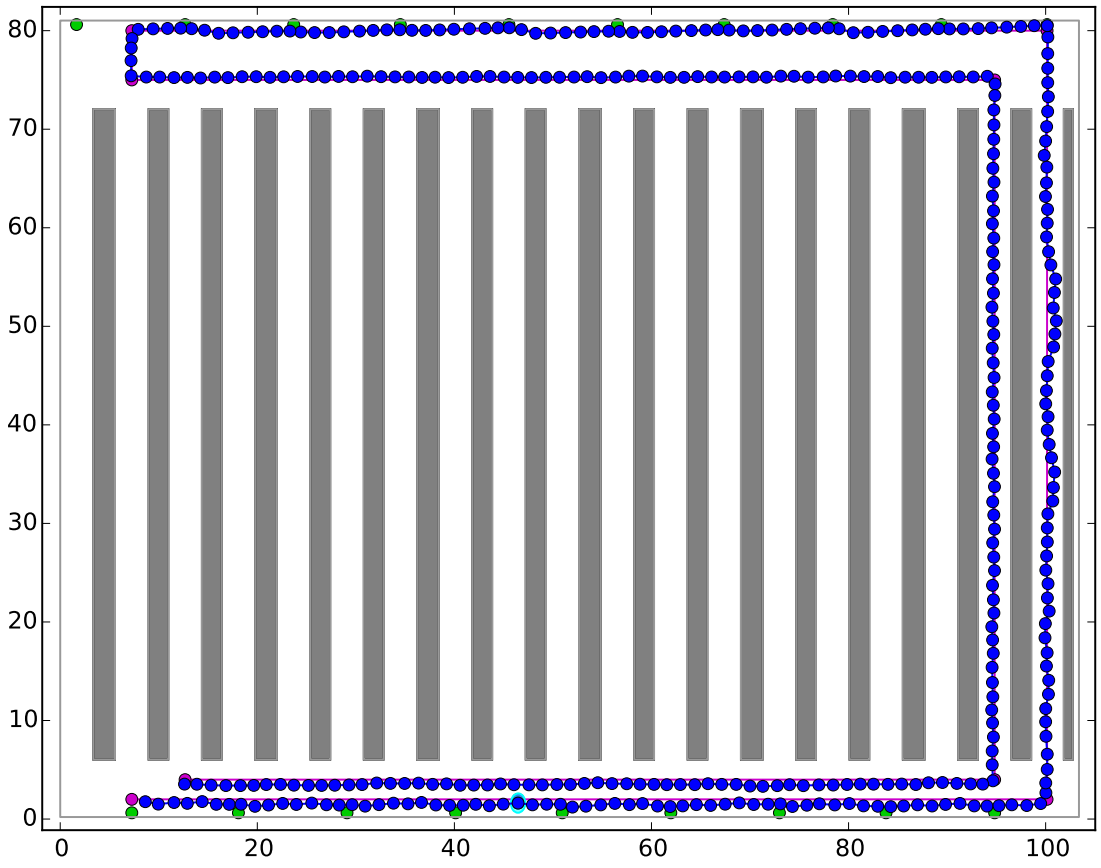

Figure 5.5: Simulated Unscented Kalman Filter Pedestrian Tracking

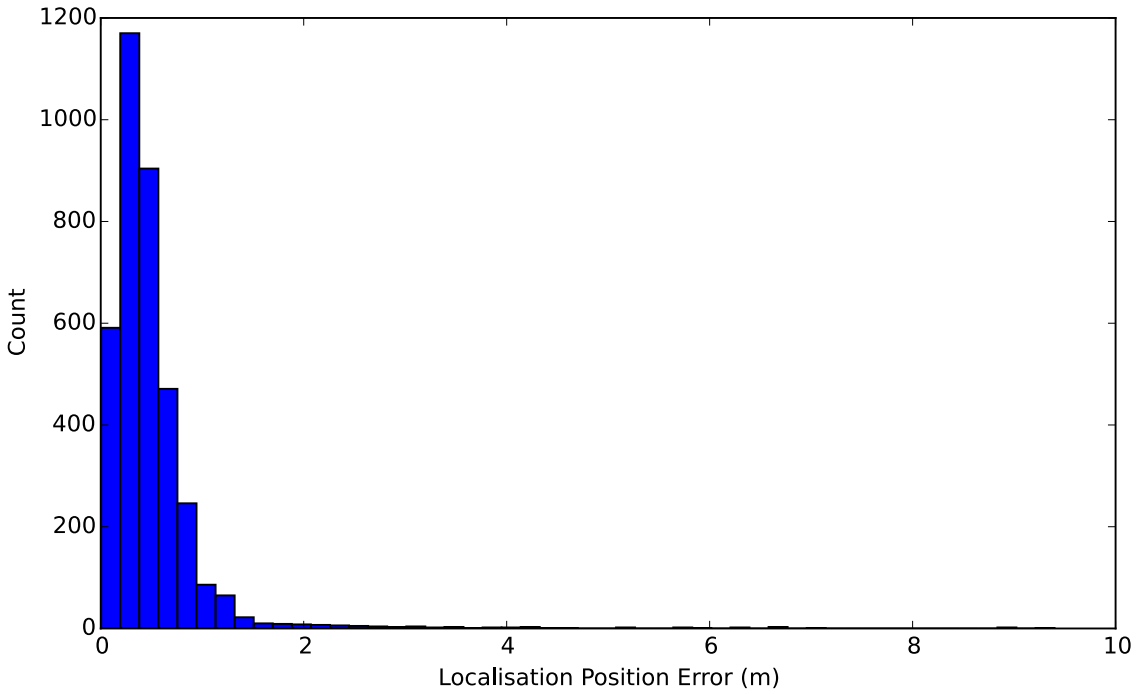

Figure 5.6: Simulated Unscented Kalman Filter Performance Over 10 Runs

Chapter 6

Real-Time Localisation System Prototype

The previous chapter described the UKF algorithm designed in a simulated environment. The next step is to build the hardware and design the software to implement the Real-Time Localisation System (RTLS) prototype. Section 6.1 gives an overview of the construction of the RTLS prototype and its constituent hardware. The software developed for the prototype is summarised in Section 6.3, with more detail on the pedometry tracking in Section 6.4. The chapter concludes with an analysis of how well the prototype hardware achieves the original goals of the project in Section 6.5.

6.1 Pedestrian Hardware

The pedestrian carries the bulk of the custom build hardware for the real-time localisation prototype, shown in Figure 6.1. The electronics were mounted on a high visibility vest, as it is required safety protocol on the warehouse floor. The main bulk of the electronics are mounted on a back-plate (Figure 6.2) with the UWB radio mounted on a separate plate on the left shoulder (Figure 6.3).

6.1.1 Embedded System

The embedded processor used in the real-time prototype was the STM32F4 Discovery Board[79]. The board uses a STM32F407 ARM Cortex-M4 with a floating point unit, 192 KB of RAM, and 1MB of Flash[80]. The STMicroelectronics chipset was selected primarily to reuse the sample code supplied by DecaWave for the STM32F105 processor on-board the EVB1000[81] used in the testing described in Chapter 3. The

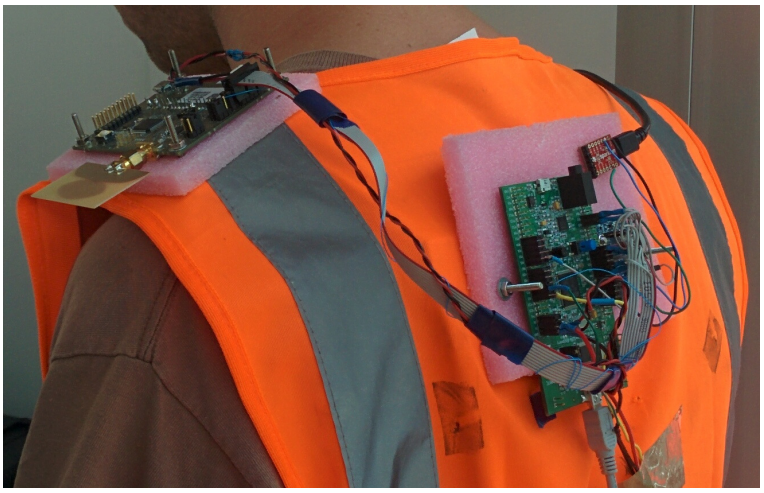

Figure 6.1: Real-Time Localisation System Prototype

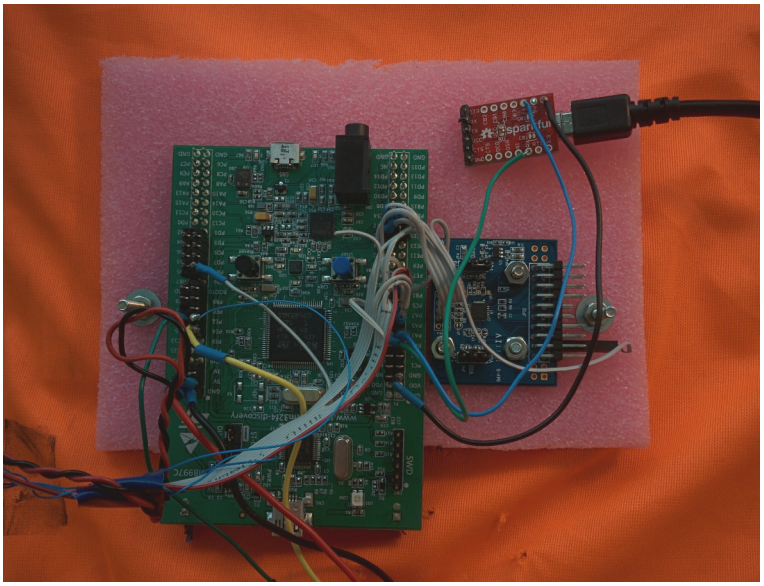

Figure 6.2: Real-Time Localisation System Back-plate

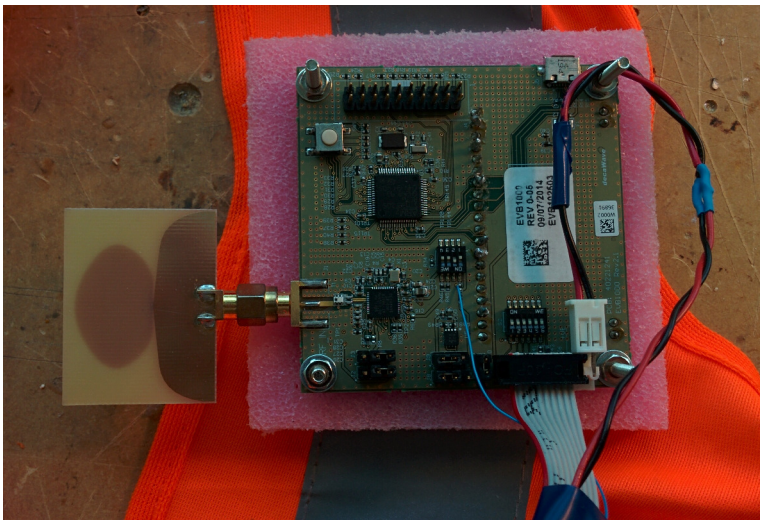

Figure 6.3: Real-Time Localisation System UWB Radio

STM32F407 processor was selected due to the large amount of RAM and Flash, as the goal was to implementing a UKF on the embedded hardware. The discovery board made development easier, with an on-board programmer and a large number of pins routed to standard headers.

6.1.2 Inertial Motion Unit (IMU)

A MPU-9150[82] on a break-out board was used to measure pedometry and pedestrian orientation. The InvenSense line of IMU's were selected for their Digital Motion Processor, discussed in greater detail in Section 6.4.1. The MPU-9150 was used because the Wireless Research Centre at the University of Canterbury already had the breakout board, and the newer MPU-9250 has no additional features that the application required[83]. The board is mounted on the back-plate of the vest, near the centre of the pedestrian's back, and close to the embedded controller so the I^2C communication lines are as short as possible.

6.1.3 Ultra-Wide Band Radio

The UWB radio section uses the same EVB1000 boards used in Chapter 3. The on-board processor is not used; instead the DW1000's SPI bus is connected to the STM32F4 Discovery Board through the J6 SPI header[67] on the EVB1000. The EVB1000 is also powered using the discovery board's 5V rail. An additional wire was soldered to the DW1000's reset pin, not available through the J6 header.

The EVB1000 is mounted on a separate foam plate on the pedestrian's left shoulder, as shown in Figure 6.1. The radio was mounted on the shoulder to avoid the pedestrian's body blocking the signal (discovered in Section 3.5). The ribbon cable carrying the SPI bus runs down the back to the embedded microcontroller.

6.1.4 Surveying Wheel

The surveying wheel, shown in Figure 6.4, was added to provide real-time ground-truth data for the performance analysis in Chapter 7. The wheel was modified to contain a hall effect sensor to electronically detect the 6 spokes on the 1m circumference wheel, which was read and timestamped by the embedded system on the pedestrian mounted hardware. Assuming the surveying wheel followed the pedestrian's path exactly with no wheel slip, the device should have a maximum error of 0.33 metres due to the unmeasured distance between spokes.

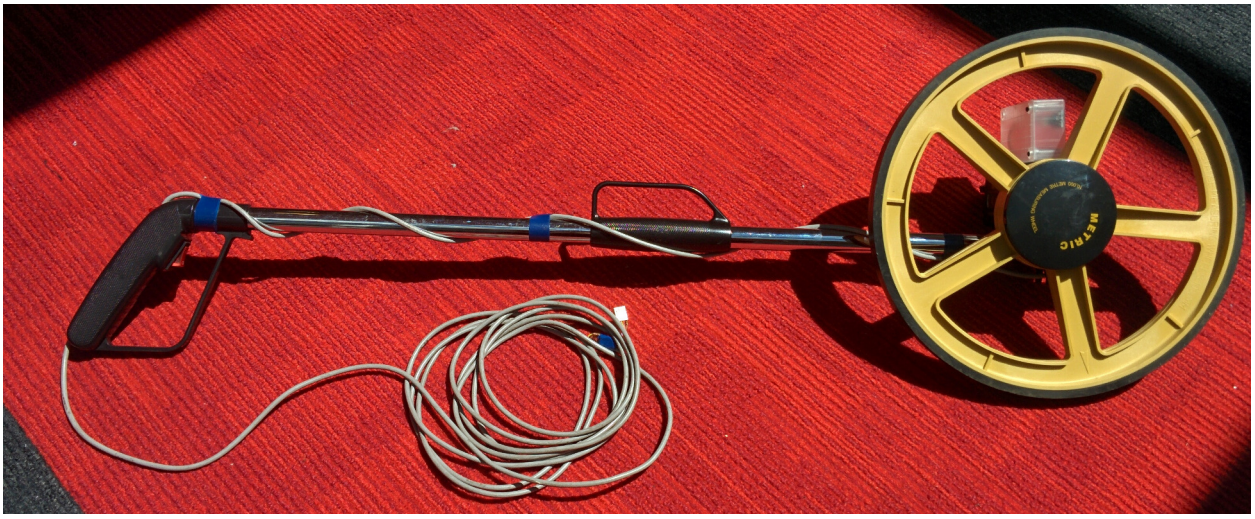

Figure 6.4: Survey Wheel With Hall Effect Sensor

6.2 Infrastructure Hardware

The UWB radios used in the infrastructure (herein referred to as the anchor radios) use the EVB1000 hardware and on-board microcontroller. The radio is powered by a 8000mAh lithium ion battery for long life and easy placement while testing in the warehouse. The radios were mounted to the walls upside down, as shown in Figure 6.5 so the PCB did not block the signal directly under the radio.

6.3 Software Architecture

The software used in the real-time prototype is segmented into three main domains. The PC system has the localisation software UKF using data collected and timestamped by the pedestrian embedded software. The pedestrian embedded software handles gathering data from the IMU, UWB radio, and the wheel counter; timestamping all the measurements with a common clock. The anchor radios run a simple software stack re-purposed from the DecaRanging application.

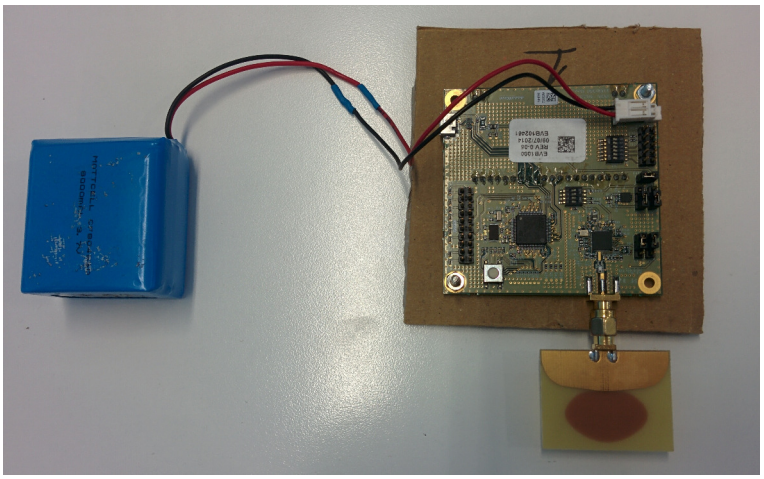

Figure 6.5: Anchor Radio and Battery

6.3.1 PC System Architecture

The PC localisation system runs a python application in real-time on a laptop connected to the embedded hardware. The software was developed as a modification of the offline simulation code first presented in Chapter 4. The application drives the entire system and contains the UKF localisation algorithms and the mapped anchor and racking positions. The PC communicates to the embedded system via a virtual serial port driven by a Sparkfun FTDI[84] breakout board.

Once a second, the PC software sends a packet to the embedded software with three anchor addresses to attempt ranging. The radios that are selected are the closest three radios (to the currently localised position) that should be within radio communication range (as calculated from the radio attenuation model developed in Section 4.1.1). The PC application then waits for the embedded system to return all the IMU observations gathered up to that point, and the radio ranges. Once the observations are gathered, the observations are used in the UKF algorithm described in Section 5.2.4 to continue the location tracking.

The initial design called to implement the UKF and other subsystems on the embedded system, eliminating the PC based application. This was not implemented due to time constraints, and for ease of development. The embedded system was chosen for power performance, and was not capable of running the python code natively. The python based UKF provided a better platform to modify the algorithm, and provided a convenient way to record and replay observations from trials. The PC implementation also eliminated the development time required to reimplement all the features already developed in the simulation.

6.3.2 Pedestrian Embedded System Architecture

The pedestrian embedded system gathers the timestamped observations required by the UKF localisation algorithm. The embedded system continually waits for a list of anchor addresses to be sent from the PC via

the UART while it records IMU observations as described in Section 6.4. Once the addresses are received, the embedded system begins ranging to each radio in turn recording the range and timestamp of each measurement. After all measurements are taken; the radio, pedometry, and orientation observations are sent to the PC software via the UART.

6.3.3 Anchor Software

The anchor radios software uses a modified version of the DecaRanging example software by DecaWave. Each anchor is assigned a static address through hardware switches on the front of the board. During operation, the anchor waits for a poll message from the pedestrian's tag. Once the poll message is received, the anchor and tag conduct the double sided two way ranging (discussed in Section 2.1.1.3) as implemented in the DecaRanging software[85].

6.4 Pedometry and Inertial Motion

The pedometry and orientation tracking are implemented using two different algorithms due to the limitations of the Digital Motion Processor included in the MPU-9150. The main purpose of the subsystem is to detect footfalls using the accelerometer, and extrapolate the pedestrian's forward velocity from the observations.

6.4.1 Invensense Digital Motion Processor (DMP)

The DMP is a proprietary Invensense feature which offloads motion processing algorithms to the IMU itself[82]. The DMP samples the sensors in the MPU-9150 at the maximum speed of 200Hz, freeing up the general purpose CPU for other tasks. The Invensense provided Embedded Motion Driver (EMD) is the only available algorithm suite that can be run on the DMP due to the proprietary and undocumented hardware.

The EMD was mainly used for the 6 axis orientation fusion feature. The EMD takes the raw gyro and accelerometer measurements at 200Hz, and fuses them to a quaternion (a 4 dimensional number that encapsulates the roll, pitch and yaw of the sensor). Not only does this fusion give a more reliable orientation measurement than manual integration, but the EMD normalises the quaternion to the gravity vector (using the accelerometer data). This quaternion is then read by the embedded processor at a far lower speed, and sent to the PC application.

The EMD also has a step counting feature, but it had some flaws that made it difficult to use for real-time pedometry tracking. The EMD's step counting algorithm has a 7 step latency before updating the step count for calibration and false-detection minimization[86]. After an undocumented amount of time where a step is not detected (about 1.5 seconds in practice), the EMD resets the calibration. As a single step can lead to

almost a metre of traveled distance, missing 7 steps for multiple UKF updates led to an unstable filter. The manual detection algorithm described below was used to fill in the data for these first seven steps before the EMD based step counting began to publish data.

6.4.2 Manual Step Detection

The manual step detection algorithm was designed to stand in place of the EMD for the 7 step calibration period. The algorithm reads in the accelerometer data at 50Hz, and uses a system of circular buffers to detect the axis most affected by gravity. Figure 6.6 is an example of the single axis acceleration data once the gravity vector is removed. The step detection algorithm then records the time of the 2 zero-crossing points (the rising edge and falling edge) shown as t_{rising} and $t_{falling}$ in Figure 6.7. The maximum and minimum accelerometer values are also tracked (shown as a_{max} and a_{min}). Once $t_{falling}$ is recorded, the step is recorded if the v_{max} and v_{min} values are over their respective thresholds and the time between t_{rising} and $t_{falling}$ is longer than a minimum threshold of 0.2 seconds.

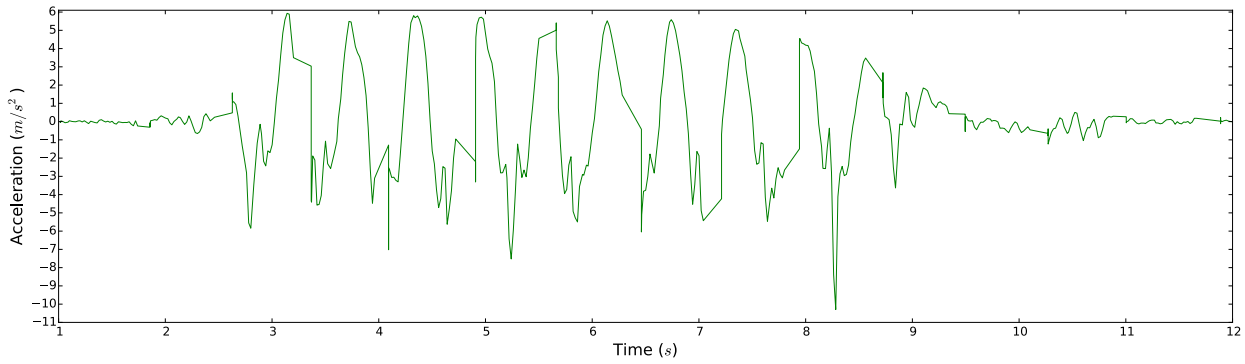

Figure 6.6: Gravity Compensated Accelerometer Measurements of Ten Steps

The performance and reliability of the manual step detection is not presented in this paper, as it was not rigorously measured. The algorithm did increase localisation performance once implemented. The current implementation's thresholds were calibrated specifically for a single pedestrian, but the thresholds can be adjusted online by matching the steps detected by the EMD pedometer. Any error the step detection introduced was a rapid change of velocity, which was counteracted by the UKF's constant velocity model.

6.5 Real-Time Localisation System Prototype Goals

The target of the masters thesis, as presented in Section 1.2 is a system that localises to 2.0 metres accuracy on an embedded platform with a 50 USD materials cost. Chapter 7 will analyze the accuracy of the prototype, while the section below details how the prototype meets the production targets.

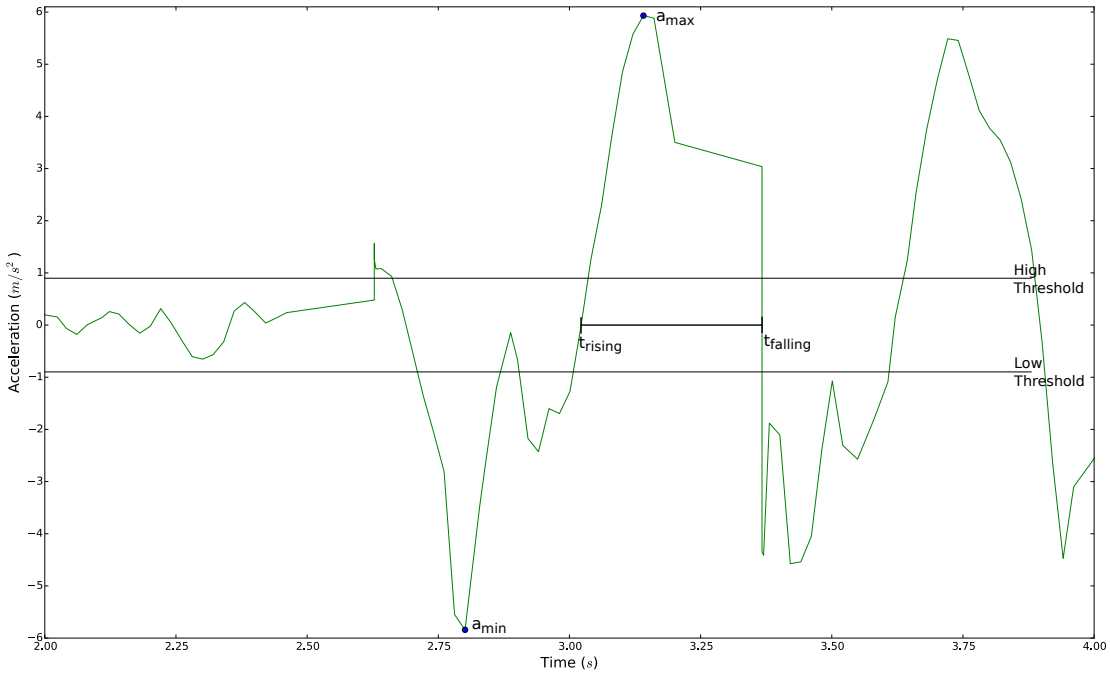

Figure 6.7: Manual Step Detection Parameters Annotated on Gravity Compensated Accelerometer Measurements

6.5.1 Localisation Algorithm Suitability for Embedded Environment

6.5.1.1 RAM and Flash Space

The current software for the embedded system takes around 87KB RAM[1], which is a little less than half the available 192KB of RAM on the processor. The embedded code was not optimised for memory, and as such its reasonable to assume the embedded system would have enough memory to run the UKF along with the other algorithms. The map information for the PC application was stored in an XML file which is only 8KB for the 10,000m^2 warehouse section. Storing the map in a binary format would significantly decrease the size. If more memory must be freed up, only a small portion of the map can be loaded from flash at any given time.

6.5.1.2 Execution Time

The major limitation of execution time in the embedded system is going to be the UKF algorithm. The RTLS prototype updates the UKF once a second, so the UKF update algorithm must be executed in less time than that. The UKF algorithm is currently implemented in python on the PC, so it can not be directly run on the embedded system to measure an accurate execution time. The execution time of the UKF update

[1] Just code and static variables, does not include stack and heap allocations at run-time

function on the Intel i7-2600 3.4 GHz AMD64 CPU is shown in Figure 6.8. The mean execution time on the PC is 33.3ms, with the longest execution time at 57ms.

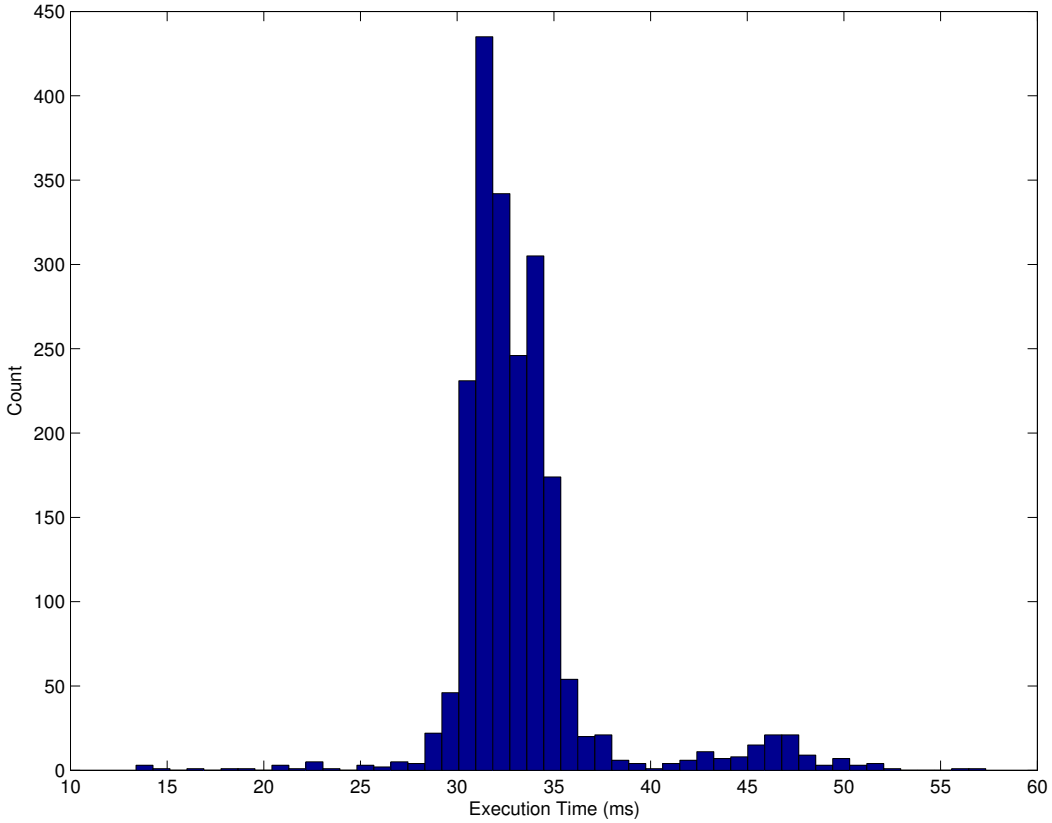

Figure 6.8: Execution Time of UKF Update Algorithm on PC

A rough approximation of the execution time on the embedded system can be obtained by scaling the execution time by a ratio of the clock speeds as done in Equation 6.1.

$$\frac{3400MHz}{168MHz} \approx 20.24 \tag{6.1a}$$

$$33.3ms * 20.24 = 674ms \tag{6.1b}$$

$$67.0ms * 20.24 = 1153ms \tag{6.1c}$$

This approximation gives a average execution time of 674ms with the longest update running in under 1.15s. This shows the algorithm is in the ballpark of running once a second, without too much optimisation required. No time was taken to optimise the python code, so it is reasonable to assume the UKF update can be executed in under a second when re-implemented and optimised on the embedded device.

6.5.2 Anticipated Power Requirements

6.5.2.1 Anchor Radio Power

The anchor radios are intended to be installed in fixed locations, powered by mains, and on at all times. The Figure 6.9 shows that the anchor radio reaches a steady state drop of a little under 1 volt on the 4 volt supply over the 4.9Ω current shunt resister.

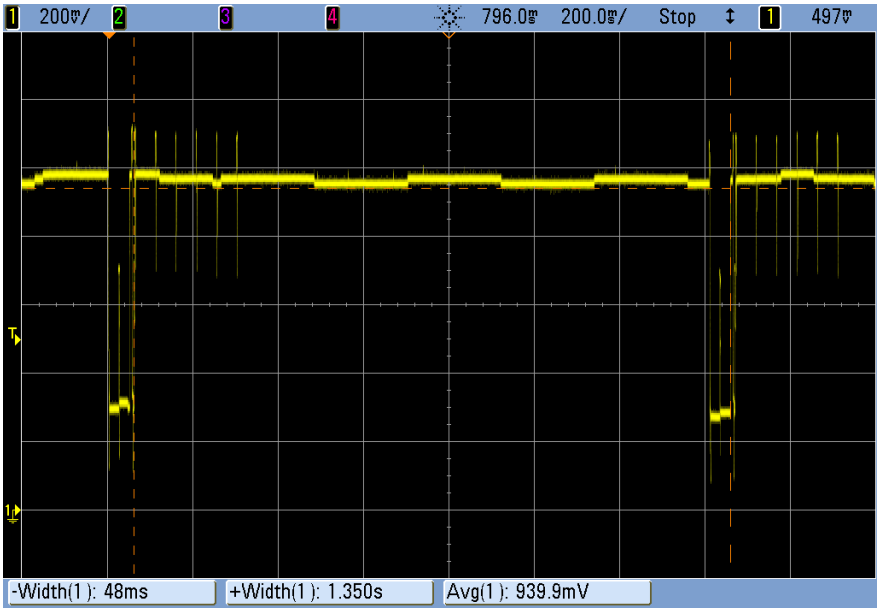

Figure 6.9: Anchor Radio's Measured Voltage Drop Over 4.9Ω Current Shunt Resister

This leads to a power consumption of approximately 0.6 watts, as calculated in Equation 6.2.

$$\frac{1.0V}{4.9\Omega} \approx 0.204A \tag{6.2a}$$

$$0.204A \times 3.0V \approx 0.612W \tag{6.2b}$$

6.5.2.2 Pedestrian Hardware Power

The pedestrian mounted hardware is more sensitive to power consumption, as the hardware must be powered by a battery. Figure 6.10 gives the voltage drop over the 4.9Ω current shunt resister on the 5V USB supply for the hardware pedestrian mounted hardware. The UWB radio's power draw can be seen as the seven spikes in voltage, shown in more resolution in Figure 6.11. The pattern is shown to repeat every 1.2s (shown as ΔX in Figure 6.10) which matches the observed 200ms radio communication time, plus 1.0s sleep between

each update. The steady state power consumption is calculated in Equation 6.3 to be 0.8 watts.

$$\frac{0.975V}{4.9\Omega} \approx 0.199A \tag{6.3a}$$

$$0.199A \times 4.025V \approx 0.8W \tag{6.3b}$$

The power consumption while the radio is operating is calculated in Equation 6.4 to be 1.1 watts.

$$\frac{1.608V}{4.9\Omega} \approx 0.328A \tag{6.4a}$$

$$0.328A \times 3.392V \approx 1.11W \tag{6.4b}$$

This leads to Equation 6.5 which estimates 6.5Wh is required to power the RTLS prototype for an 8 hour workday. This would require at least a 1750mAh battery to supply the required power for the full 8 hours.

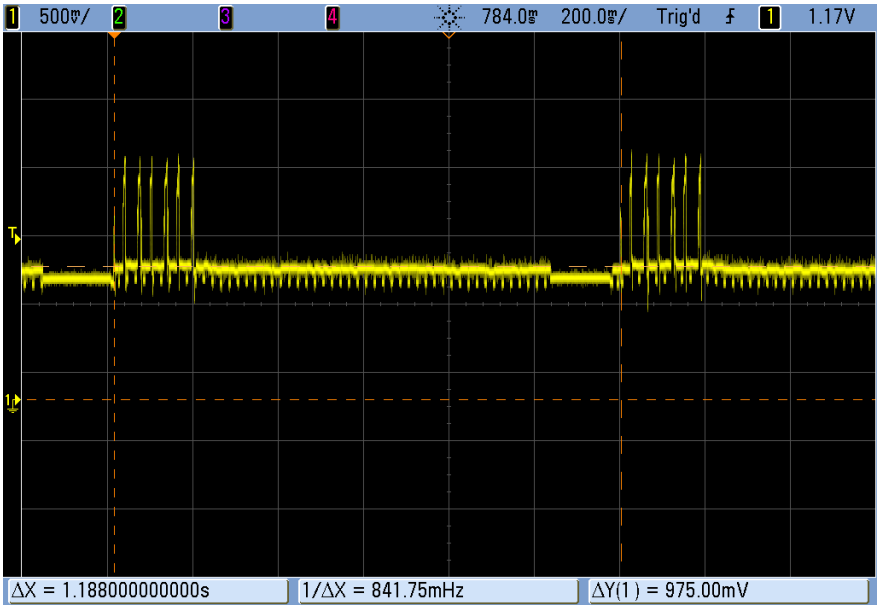

Figure 6.10: Pedestrian Mounted Hardware Voltage Over 4.9Ω Current Shunt Resister

$$\frac{39.2ms}{1180ms} \approx 3.32\% \tag{6.5a}$$

$$\frac{1180ms - 39.2ms}{1180ms} \approx 96.68\% \tag{6.5b}$$

$$0.0332 \times 1.1W + 0.9668 \times 0.8W \approx 0.81W \tag{6.5c}$$

$$0.81W \times 8.0h \approx 6.48Wh \tag{6.5d}$$

$$\frac{6.48W}{3.7V} = 1750mAh \tag{6.5e}$$

This is a surprisingly feasible power usage for a first generation prototype. The STM32F discovery board has multiple LED's, a built in programmer chip, and a USB peripheral that would not be drawing current

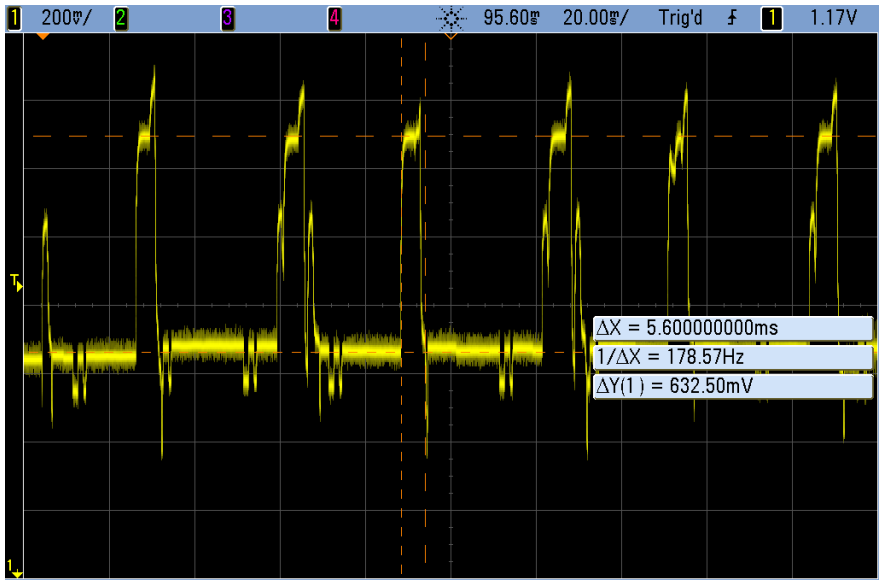

Figure 6.11: Radio Power Draw Analysis

on a consumer device. Likewise the code was not optimised for power draw at all, keeping the processor and UWB transceiver on at all times. As calculated in Equation 6.5b, the steady state is 97% of the total operation time, so massive gains can be made by optimising the sleep states of the hardware.

6.5.3 Anticipated Production Cost

The production cost of the prototype as a consumer product is hard to estimate with the state of the prototype. Table 6.1 is the best approximation of the price of critical components of the device at current market price. The total does not include the PCB production costs, passive circuit components, battery charging chips and circuitry, and an enclosure.

Subsystem	Item Name	Single Source	1000 Unit Cost (USD)
UWB Radio	DWM1000 Transceiver Module	Yes	17.59
Embedded Processor	STM32F407VET6	No[1]	6.36
Gyro and Accelerometer	Invensense MPU-6000	No[1]	5.85
Battery	LiPo 2500mAh 3.7V	No	10.00[2]
Sum			29.80

[1] Not a drop in replacement, would require change to code

[2] No direct quote, estimated from current market price with high error margin

Table 6.1: Real-Time Localisation System Components Cost Breakdown

Chapter 7

Real-Time Prototype Performance

The Real-Time Localisation System (RTLS) prototype developed in the previous chapter was tested in the existing warehouse section of the Foodstuffs Hornby Distribution Centre. The tests were conducted over two consecutive days, with changes in anchor placement over the days. During the tests the DC was quite congested, using floor space around the walls for temporary storage. This meant a great deal of wall space was inaccessible, and the anchors could not be evenly distributed according to the plan as laid out in Figure 4.2. On the second day (when the tests in Section 7.4 and Section 7.5 were conducted), the anchors on the lower wall (wall near 0m in the y axis) were surrounded by product as shown in Figure 7.1.

Figure 7.1: Placement of an Anchor Radio on Day Two of Testing

7.1 Path Planning and Ground Truth

The ground truth data was gathered using the surveying wheel, the implementation of which is described in Section 6.1.4. The planned paths were mapped out beforehand as a series of line segments, whose vertices were at known positions and marked with tape. When the path was walked, the pedestrian was followed by an assistant who kept the surveying wheel in line with the pedestrian's feet. At a vertex, the assistant clicked a button on the surveying wheel which logged the event and calculated the error between the ground truth wheel and the expected position of the vertex. To minimise any interaction with the radio, the assistant walked alongside the pedestrian's right side. This system allowed the measurement of the real-time performance of the localisation system, not just the performance while standing still.

7.1.1 Observed Ground Truth Error

Each vertex was measured and marked with more accurate tape measure before the trials. Figure 7.2 shows the distribution of the observed ground truth error accumulated by the wheel while traveling to each vertex in all tests. The average error is 0.4 metres with a 95% confidence at 1.0 metres. The magnitude of the observed error is slightly surprising. Due to the wheel counter measuring only five points on the metre circumference wheel, an error of up to 0.4 metres was expected[1]. The source of the remaining error is unknown.

7.2 Down Aisle Test

The first test of the RTLS prototype is the path shown in Figure 7.3 where the pedestrian walks up and then back down a single aisle. The path was selected because the simulations conducted in Section 5.2 show the best performance should be within the racking. The goal of this test is to confirm the simulation's predictive accuracy and measure the best case accuracy of the prototype RTLS.

Figure 7.4 shows the path from the five trials which were conducted. The RTLS prototype was localised and tracked the pedestrian throughout the path, even when 27.4% of the updates had no UWB radio contact. Figure 7.5 is the histogram of the localisation error over all trials. The average position has 1.0 metres of error, with 2.18 metres of error at 95% confidence.

7.3 Outside Aisle Test

The second test was conducted to demonstrate a more realistic short path with sections both inside and outside the aisles. The test was originally planned as a circular loop, but the temporary obstacles described

[1] $\frac{1}{5}m + \frac{1}{5}m = \frac{2}{5}m \quad or \quad 0.4m$

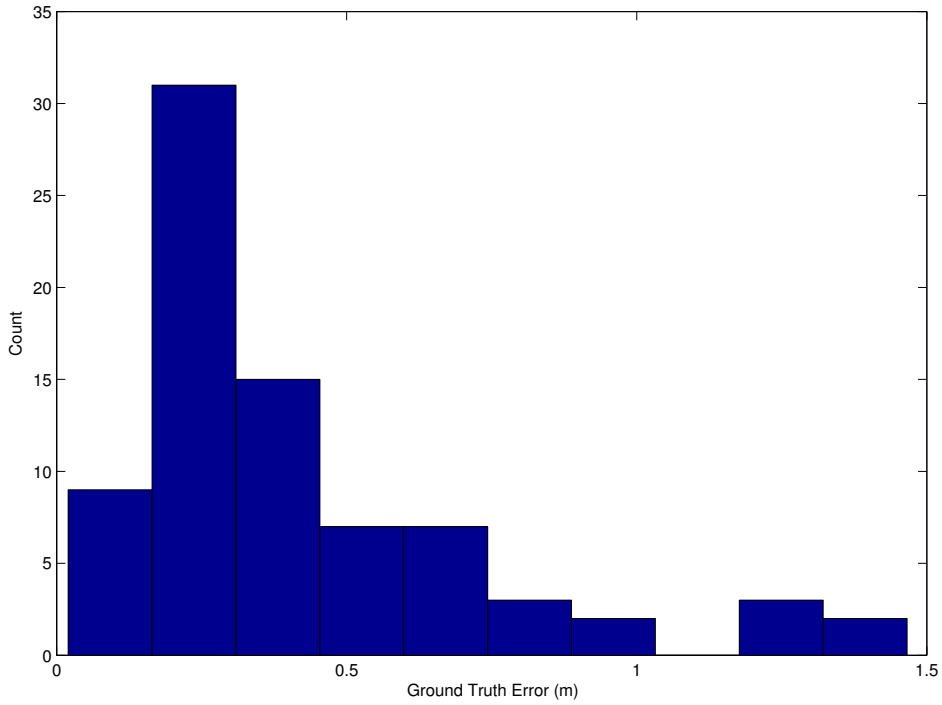

Figure 7.2: Ground Truth Error Distribution Over All Tests

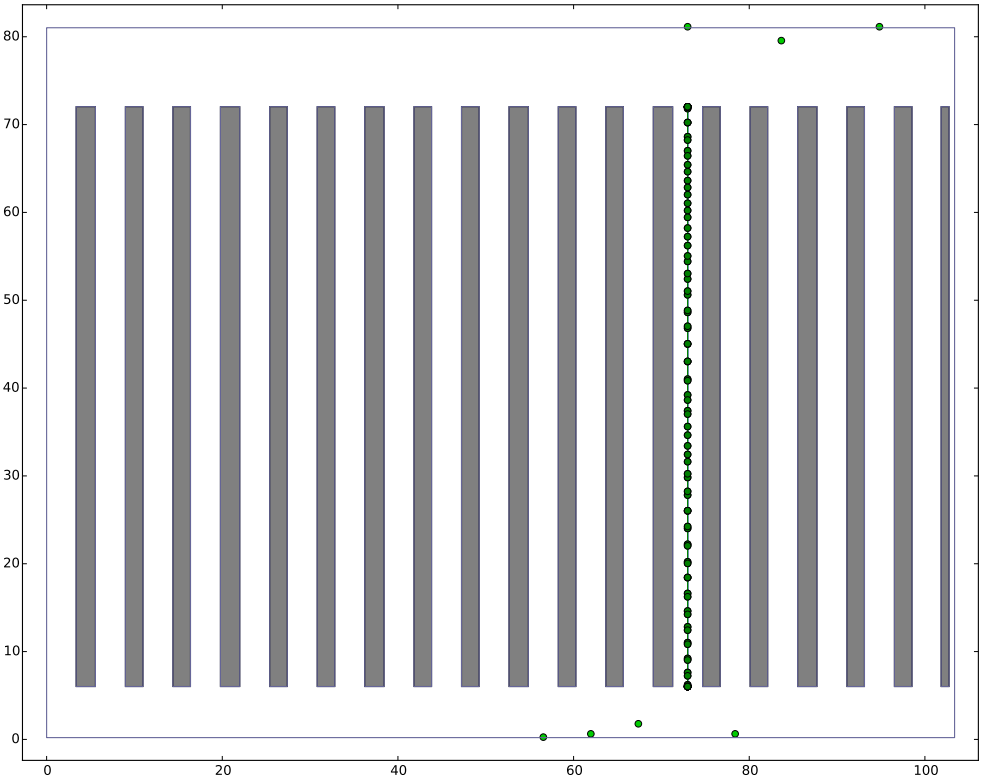

Figure 7.3: Down Aisle Test Path

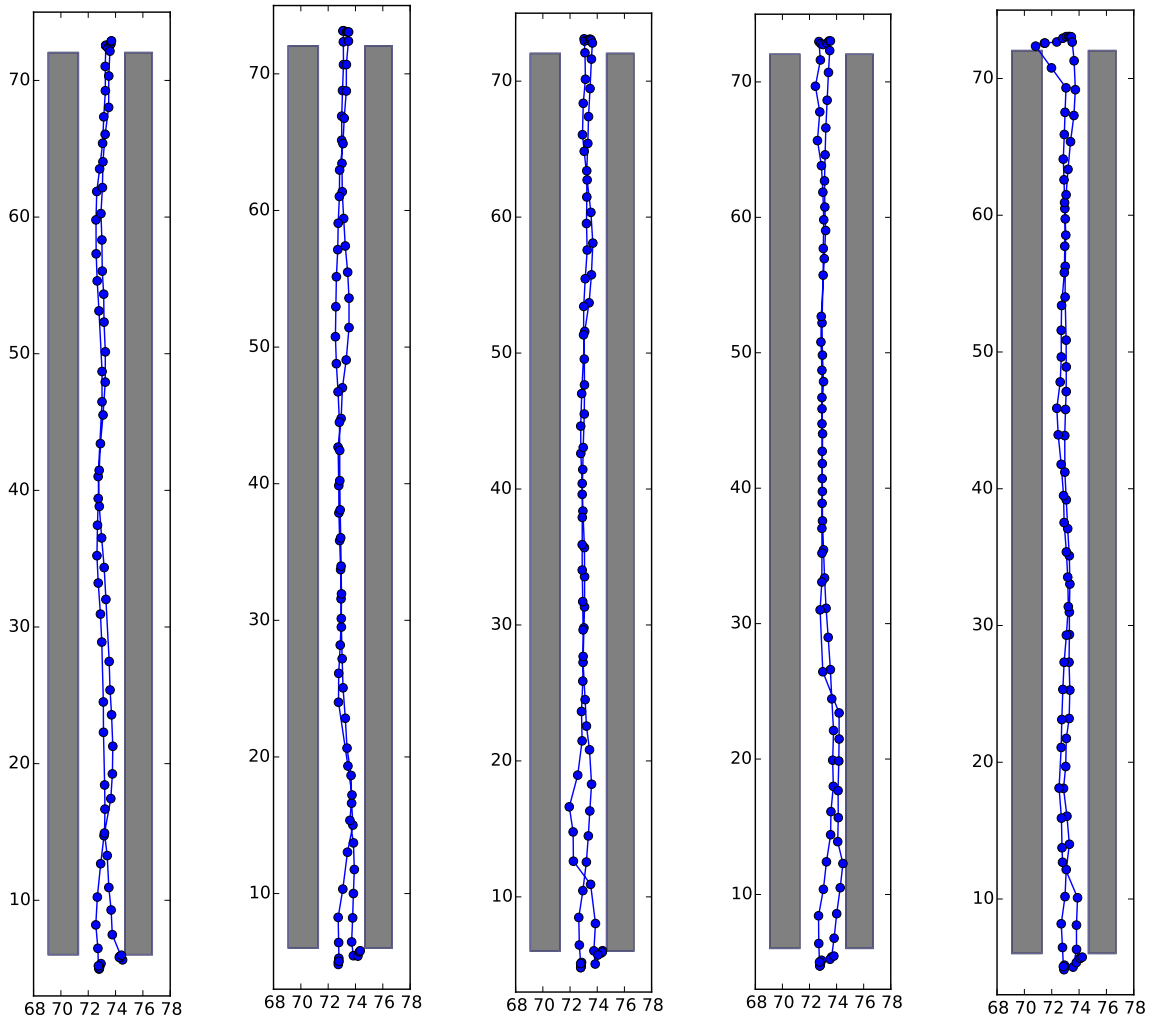

(a) (b) (c) (d) (e)

Figure 7.4: Mean Position During Down Aisle Real-Time Localisation Trials

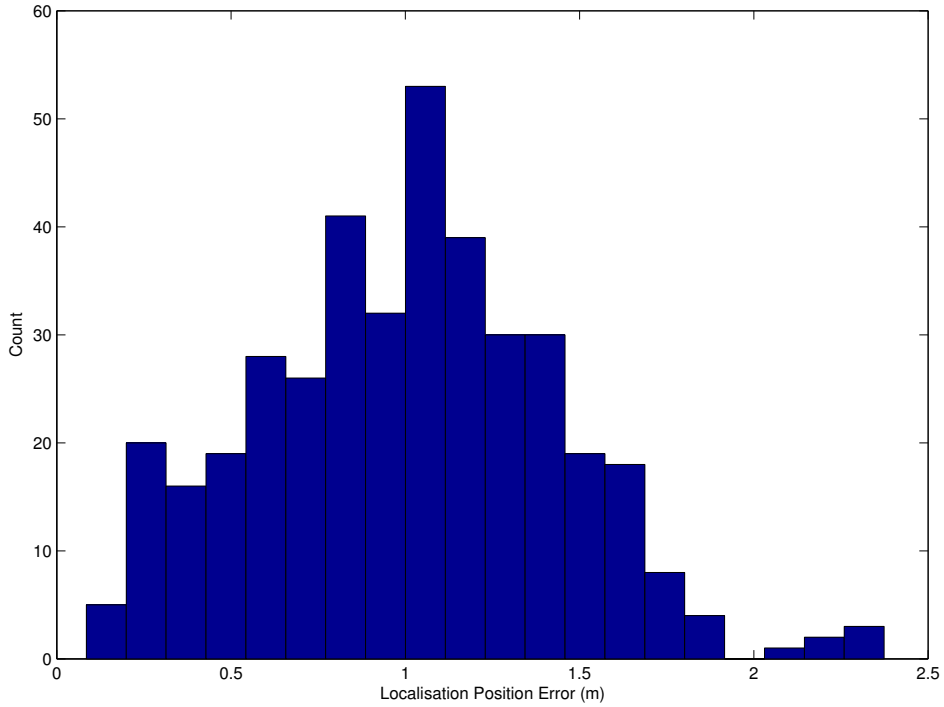

Figure 7.5: Down Aisle Localisation Error Over Five Trials

earlier limited the placement of the anchor radios. Figure 7.6 shows the modified test path; where the pedestrian starts at the bottom left and proceeds to walk the path down and back.

Figure 7.7 shows the RTLS prototype's results from the five trials conducted, with Figure 7.8 showing the localisation error distribution. The localisation tracking in the outside aisle test clearly performs worse than the test conducted in Section 7.2, with a average localisation error of 1.44 metres, and 4.0 metres at 95% confidence. In two trials (Figure 7.7c and Figure 7.7e) the ending position is stably localised in error greater than 4 metres. Figure 7.7d shows a similar ending error, but the position is trending back to the correct position.

7.4 Slalom Path Test

The next test is a long path that tests the localisation stability over longer tests and demonstrates the steady state accuracy. The path, shown in Figure 7.9, starts at the bottom right and ends at the top left, snaking though all the aisles covered by anchor radios. As in the test in Section 7.3, the anchors could not be uniformly distributed due to temporary obstacles in the warehouse.

Figure 7.10 shows the results from the three trials. The localisation is successful in tracking the pedestrian's general position. Figure 7.11 shows the distribution of the localisation error. The average error is 1.26 metres

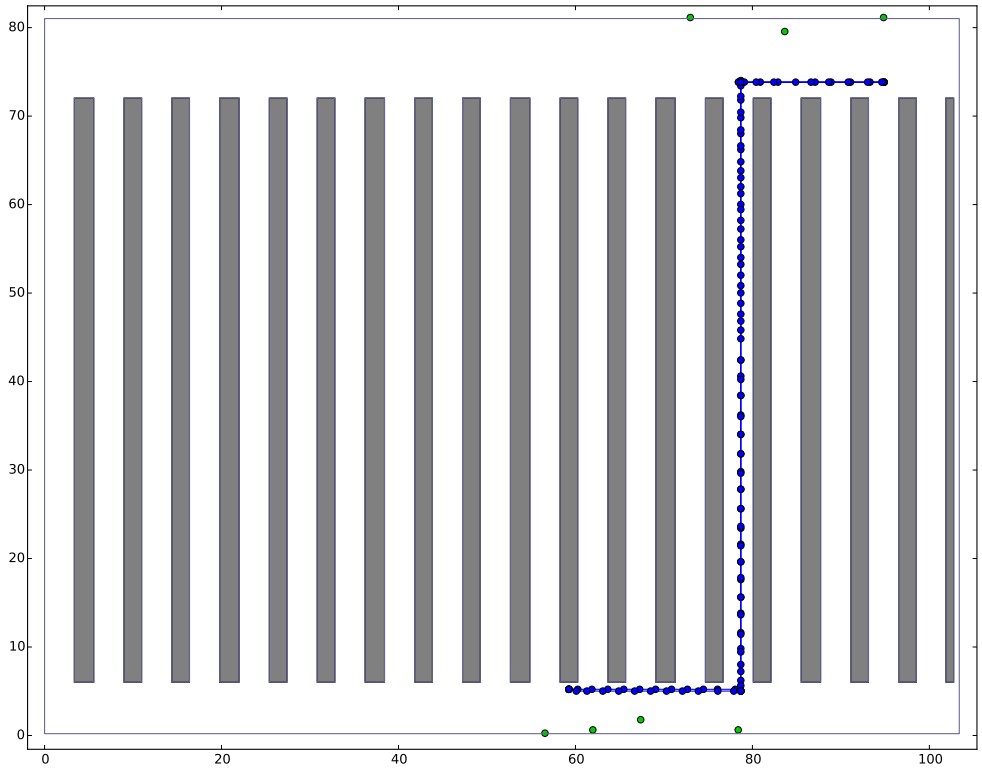

Figure 7.6: Outside Aisle Test Path

and a 95% confidence at 3.1 metres.

7.5 Arbitrary Missions Test

The last test of the RTLS prototype was designed to simulate a real-world situation of picking from arbitrary slots within the racking structure. The pedestrian started at the bottom right, and began picking from a randomly chosen slot (selected via a python script). When the pedestrian arrives at the spot the pedestrian would pace around the selected slot for at least 10 seconds before moving to the next target. The surveying wheel was not used for this test because of the unknown nature of the path taken in each trial. The wheel also required a second pause to re-align on 90° turns, leading to unnatural starts and stops while traversing between aisles.

Figure 7.12 gives the RTLS prototype's output for the five trials. The prototype remains localised throughout the test and returns to the starting position at the end of each trial. Figure 7.12b, Figure 7.12c, and Figure 7.12e show instances where the pedestrian remained in a single aisle for two slot interactions without ill effect to the localisation. In the mission for Figure 7.12c the slots were right next to each other, yet two distinct clusters can be seen.

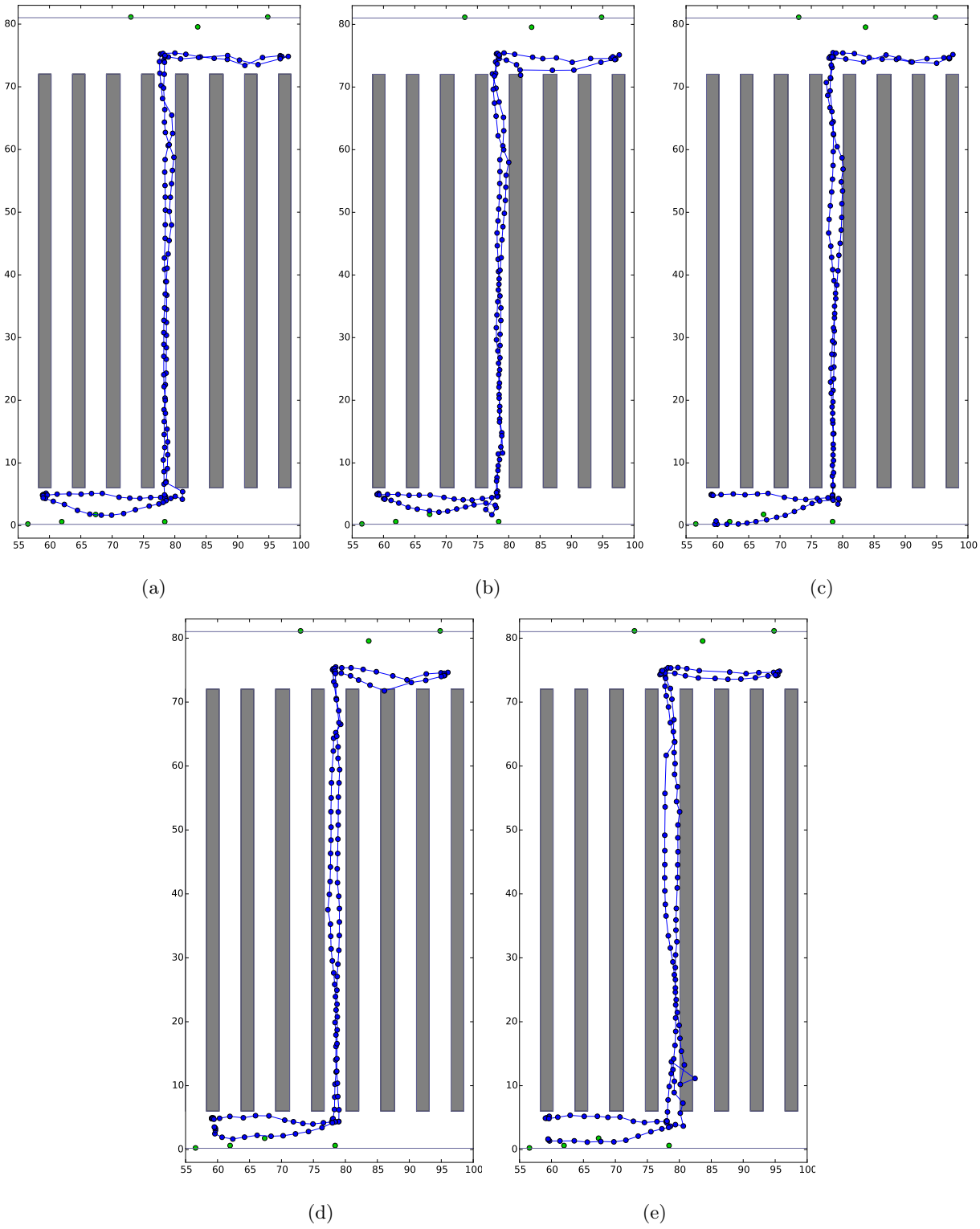

Figure 7.7: Mean Position In the Outside Aisle Localisation Trials

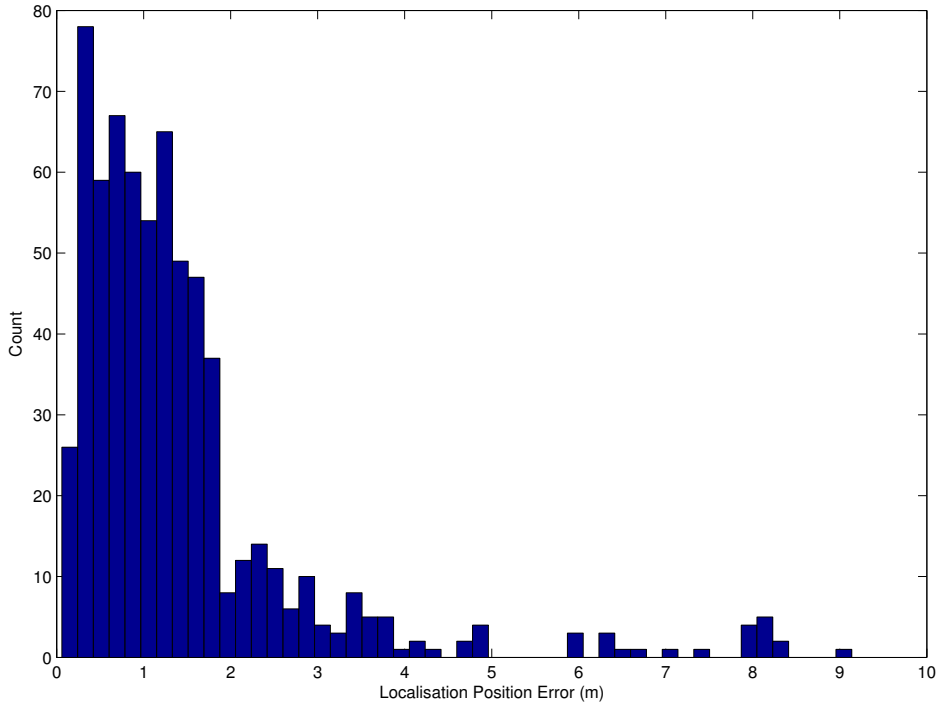

Figure 7.8: Outside Aisle Localisation Error Over Five Trials

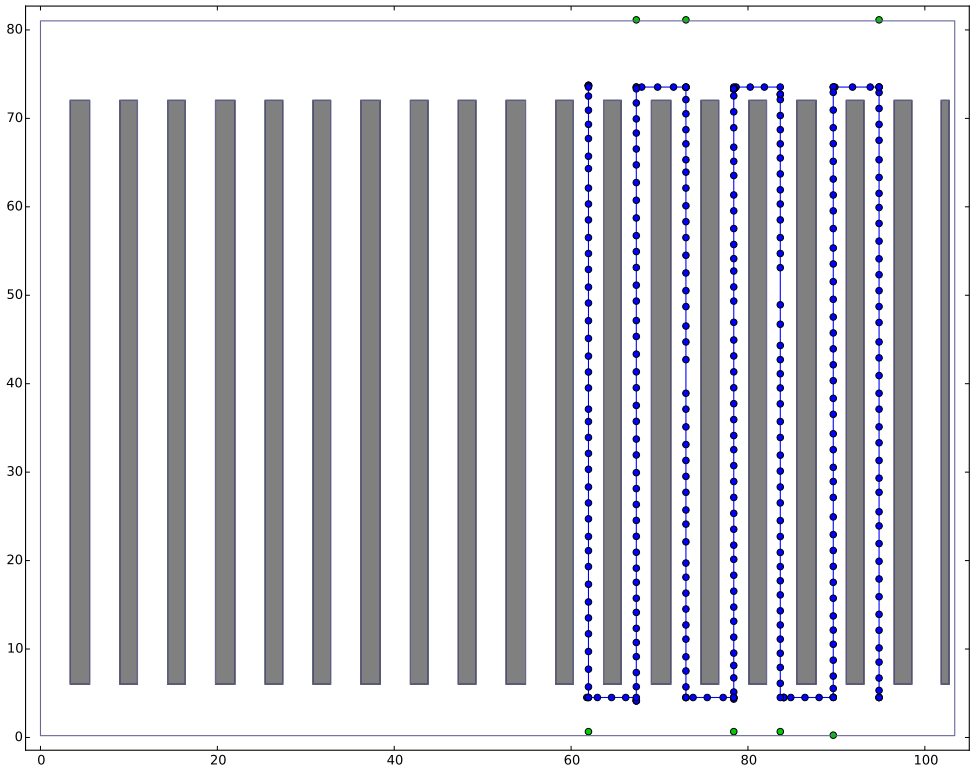

Figure 7.9: Slalom Test Path

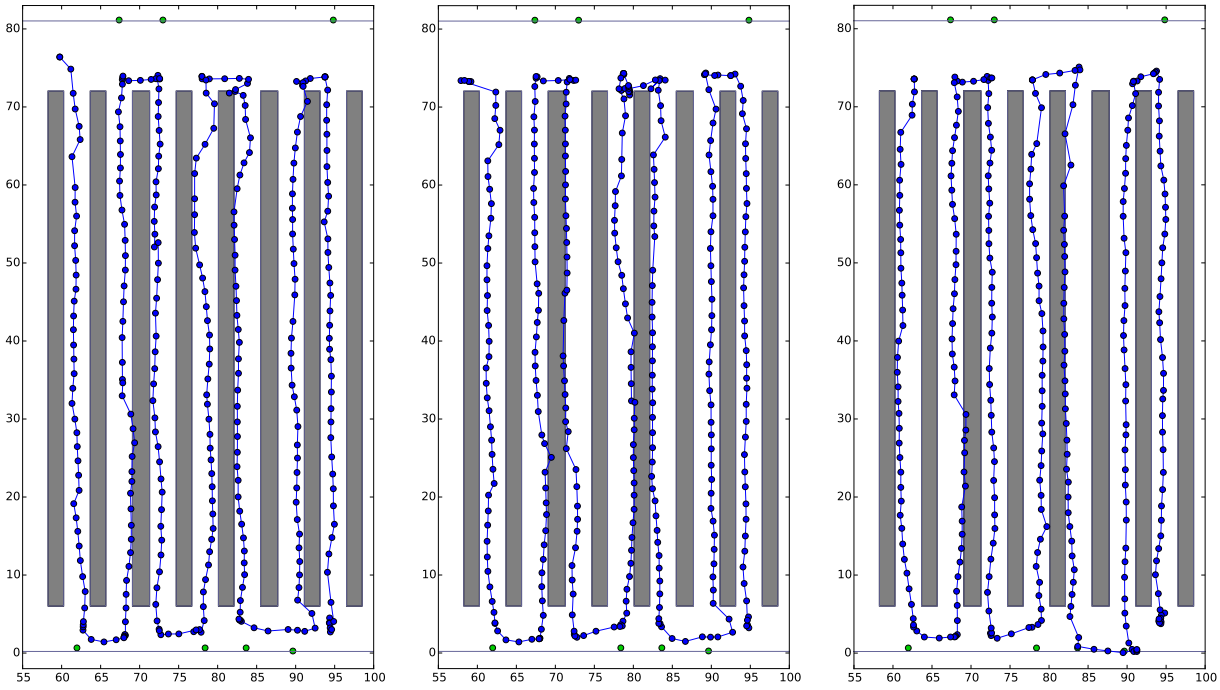

Figure 7.10: Mean Positions In The Slalom Localisation Trials

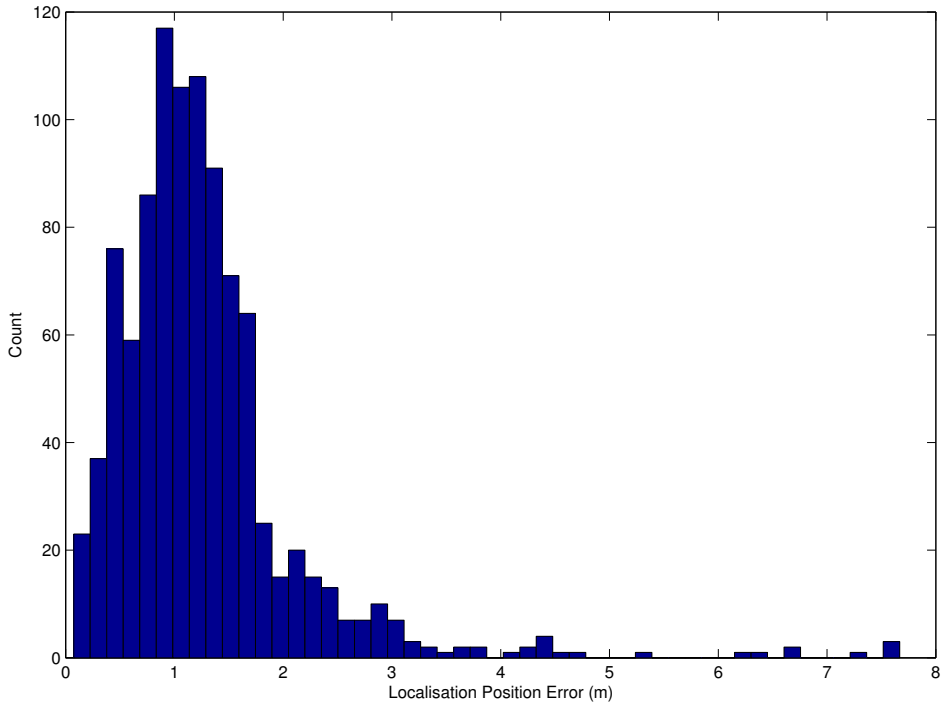

Figure 7.11: Slalom Localisation Error Over Three Trials

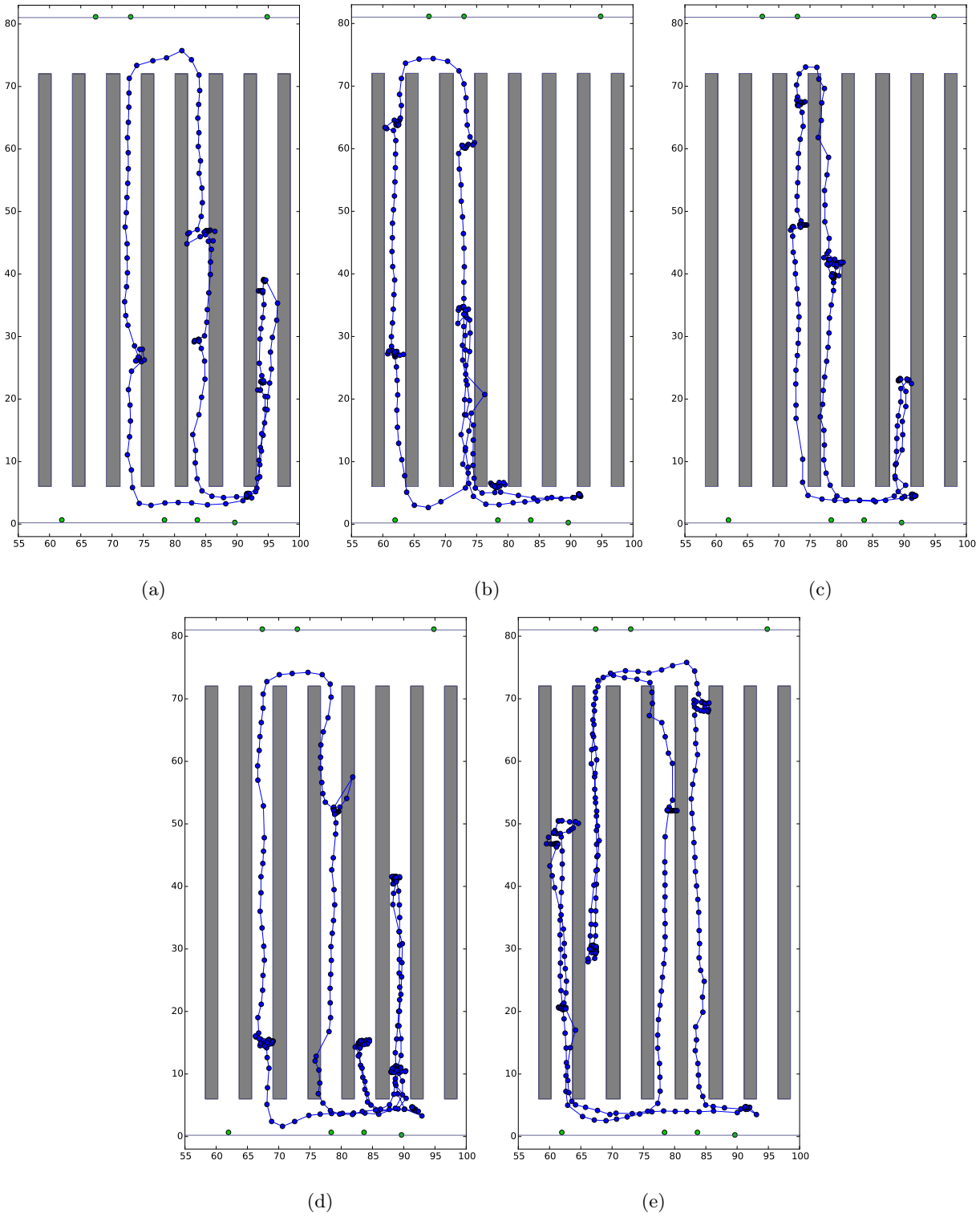

Figure 7.12: Mean Position In The Arbitrary Missions Localisation Trials

7.6 Discussion

Section	Test Name	Average Error (m)	Error at 95% Confidence (m)
Section 7.2	Down Aisle	1.0	2.18
Section 7.3	Outside Aisle	1.44	4.0
Section 7.4	Slalom	1.26	3.1

Table 7.1: Summary of Real-Time Localisation System's Tests

7.6.1 UWB Radio Coverage

The UWB radio coverage was significantly worse in the warehouse than predicted from simulation. Figure 7.13 was generated from nearest neighbor interpolation from the slalom tests, to be compared with the simulated radio coverage displayed in Figure 4.3.

The first observation is the simulation predicted areas outside the aisle would be covered by three radios at all times. Three radio coverage was spotty in the warehouse testing, occurring most often in the region at the bottom of the warehouse where three anchor radios were next to each other.

Figure 7.13 also reveals regions within the racking that have no radio coverage at all. Testing conducted in Section 3.6 and Section 3.10.2 concluded that a UWB radio had more than enough effective range to cover the length of the aisle. The pedestrian's head blocking the signal would not be the primary cause because the pedestrian is walking straight down the aisle.

The author's theory on the reduced effective range of the UWB communications is due to the antenna orientation. The planer omnidirectional antenna used on the prototype has regions where the gain is almost zero[87]. During range and performance testing, all the radios were oriented face on, giving only the best-case effective range. When testing the RTLS, as the pedestrian got further from the walls, the pedestrian's antenna trended to being edge on to the anchor radios' face. This would have resulted in a lower gain from the antenna, and a lower effective range for the UWB signals.

7.6.2 Racking Intersection Performance

The racking intersection algorithm performed well in maintaining the localisation with far fewer radio measurements than first expected. As seen in the simulation, the covariance of the UKF fills up the width of the rack. An example shown in Figure 7.14, step 66 of the slalom test in Figure 7.10a. The pink line shows the radio observation's mean, with the 2 sigma variance of the radio measurement denoted by the green lines.

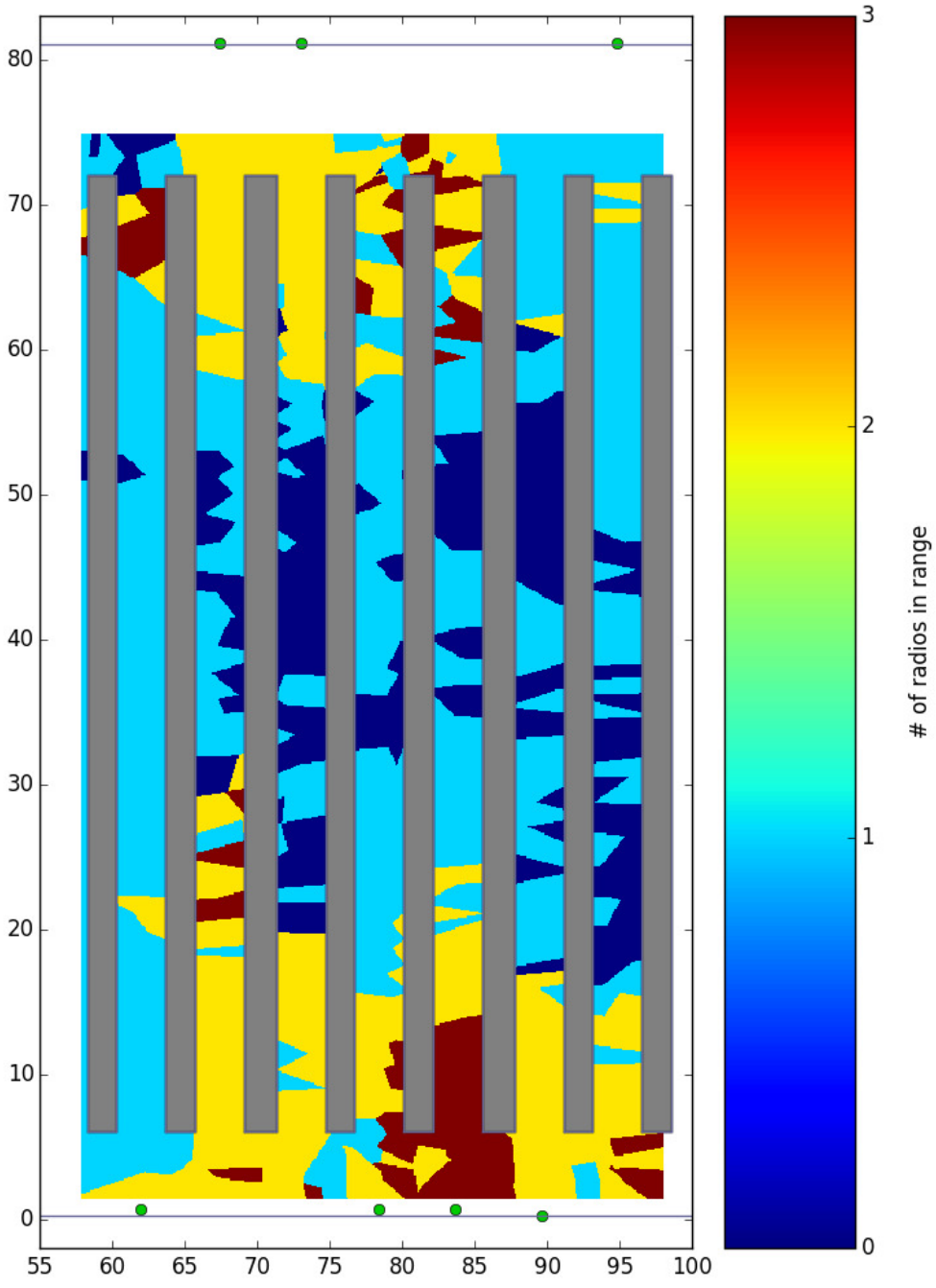

Figure 7.13: Slalom Test Radio Coverage

The localised position is shown as the purple point, with the red line denoting the velocity and orientation. The 2 sigma covariance of the position is shown as the light blue ellipsis, and fills the width of the aisle.

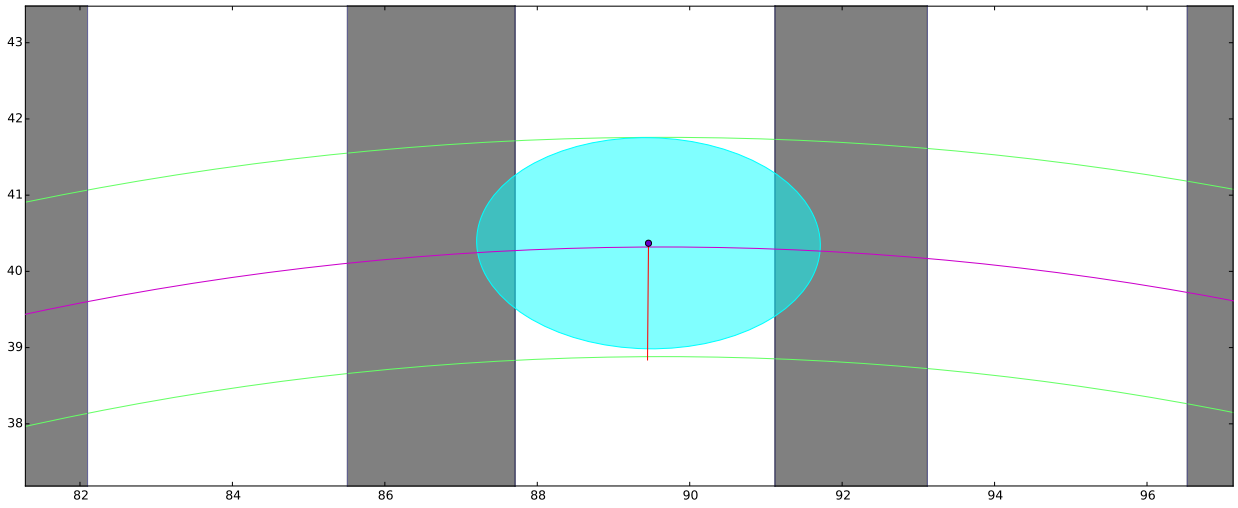

Figure 7.14: UKF Mean And Covariance Example In Racking

The position covariance shows the limits of the tracking accuracy within the aisles. Due to low resolution on the pedestrians position on the x axis, the covariance is constrained by the racking.

7.6.2.1 Wall Sliding

A common occurrence in the slalom test is the mean being 'stuck' on the face of a rack. Figure 7.15 shows the details of the UKF at step 220 on the third aisle from the left in Figure 7.10b. The sigma points at the observation phase of the UKF are shown as teal points with red velocity and orientation markers. Most of the sigma points are at the edge of the rack, having been moved there by the racking intersection translation model as described in Section 5.2.4.4. The concentration of the sigma points with a similar x value leads to a estimation with a mean with the same x value. This is compounded by the radio measurements having little accuracy in that dimension, so no correction is applied during the observation phase.

The orientation error keeps the localisation algorithm on the aisle's edge. The error is principally generated by the racking intersection translation algorithm moving all the sigma points to the edge of the rack. Sigma points with orientation error pointing towards the racking have their position error in the x dimension set the same as the other sigma points during the racking intersection translation. This results in a bias towards the racking.

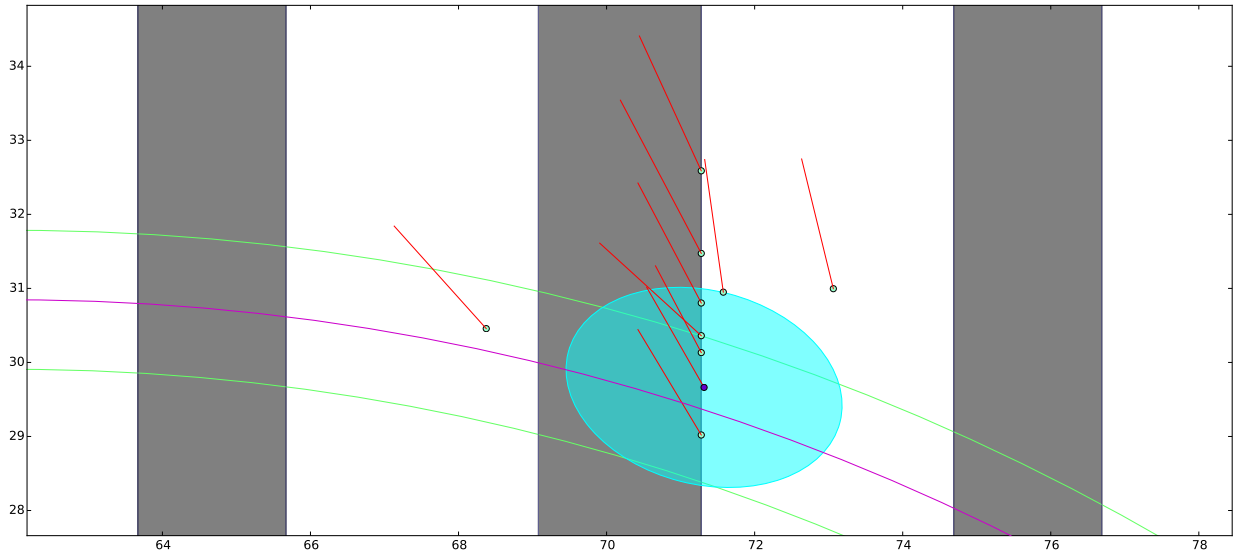

Figure 7.15: Detailed UKF Breakdown During Wall Sliding

7.6.3 Anchor Radio Four Outliers

The phenomenon discovered in Section 3.11 was witnessed in a single radio and aisle during the course of the test. Anchor radio four was positioned on aisle 405 on both days, and on both days (see Figure 7.16) gave measurements that were more than 10 metres short of the ground truth. No other radios over the two days of testing gave any measurements with this magnitude of error.

It is still unknown what causes the outlying measurements. Anchor radio four was not the same radio used in gathering data for Section 3.11. The aisle, shown in Figure 7.17, had a similar mix of product to other aisle in the test.

The outliers were filtered out of the UKF observations by a 7 metre threshold. Any observations that were more than 7 metres away from the predicted position were ignored. This filter operated separately from the UKF because erroneous measurements could lead to a magnification of linearisation errors, as demonstrated by Figure 7.18 (step 197 in Figure 7.12d).

There is no ground truth data for the test, but the tight grouping of blue historical mean positions show a reasonably good prediction of the pedestrian's current location. The update step produces a very bad estimation of the current position, moving the estimation approximately 6 metres and into the racking. It takes three more updates with good radio observations to return to a reasonable location estimation.

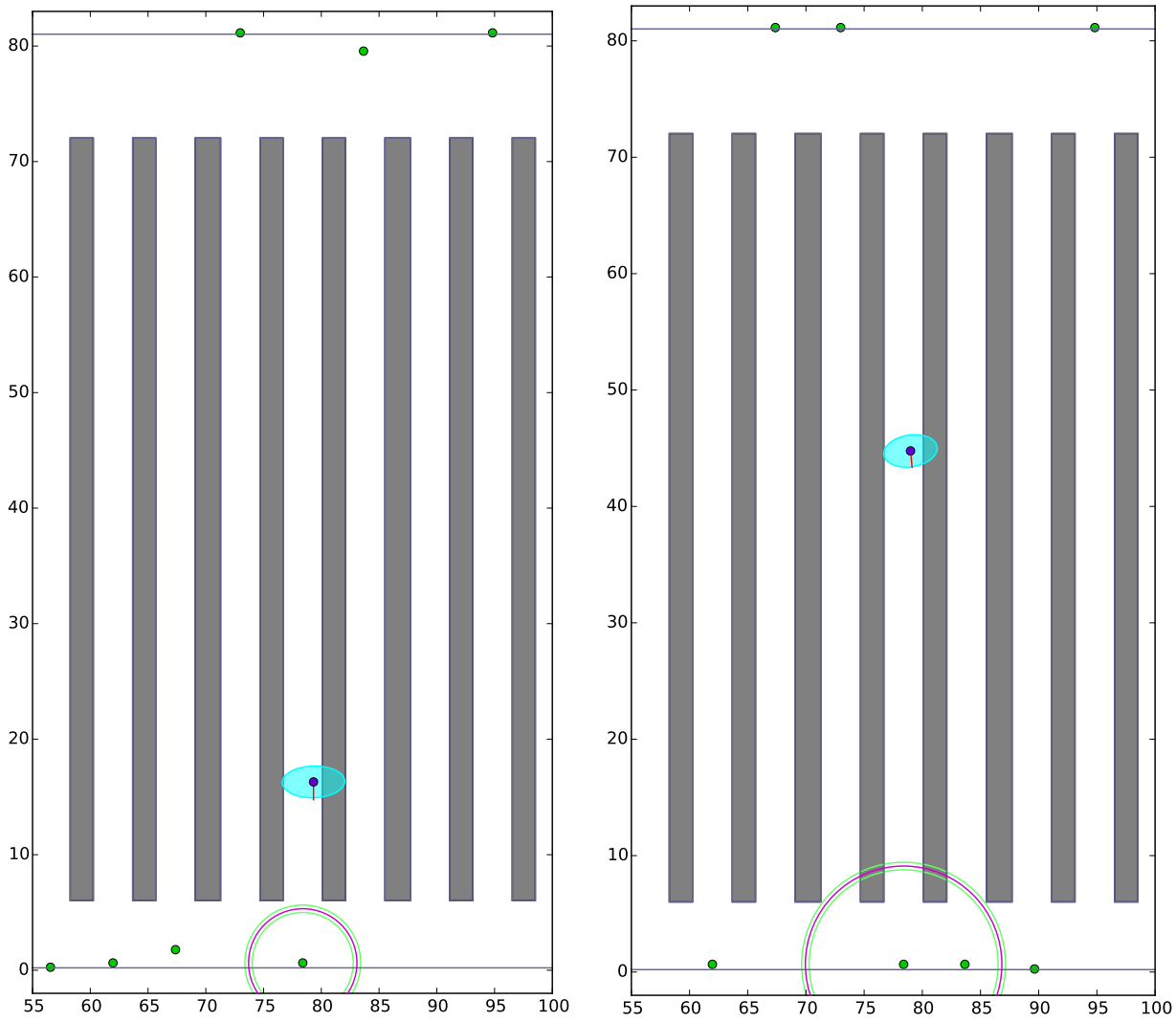

(a) Outside Aisle Test

(b) Slalom Test

Figure 7.16: Examples Of UWB Ranging Measurement Outliers

Figure 7.17: Aisle 405 In The Foodstuffs' Hornby Distribution Centre

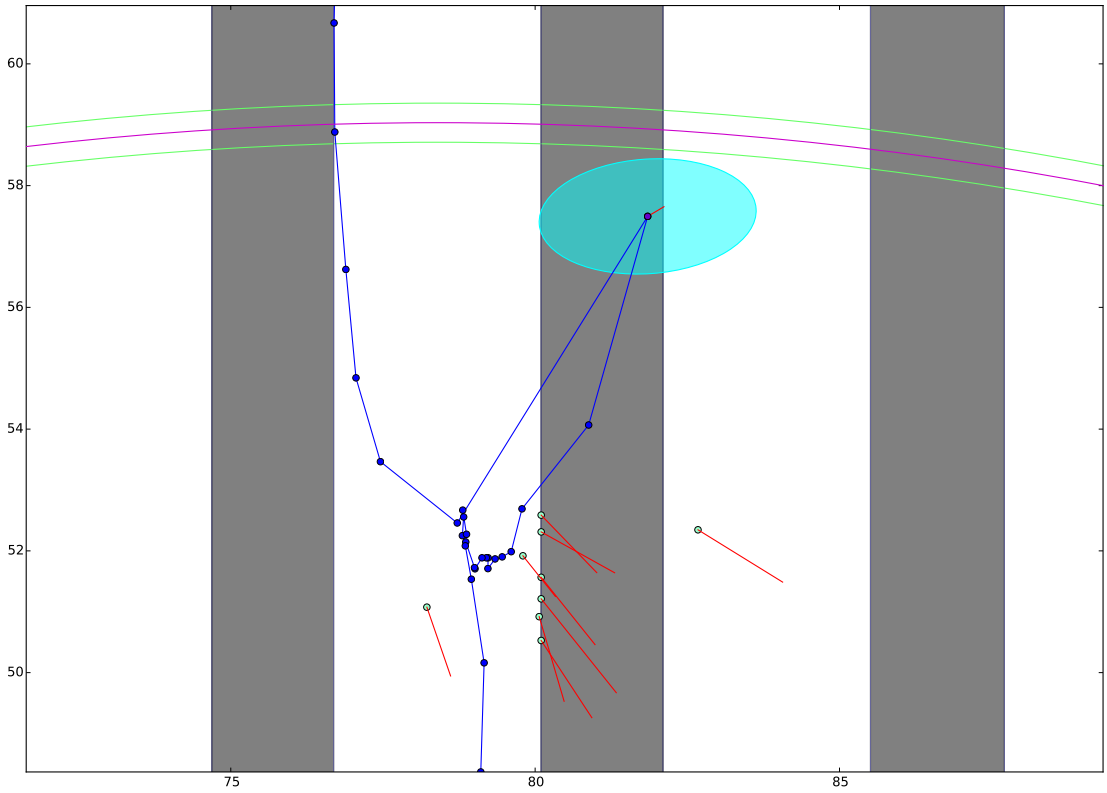

Figure 7.18: Erroneous Ranging Errors Magnifying Linearisation Error

7.7 Conclusion

This chapter presented the results of the Real-Time Localisation System Prototype hardware's performance in a warehouse environment. The system achieved the overall project goal of tracking the location of the pedestrians in all conducted tests, with an average accuracy a little better than 1.5 metres to ground truth. The RTLS was not as precise as the original target, ranging from 2m to 4m at 95% confidence.

Chapter 8

Future Work

This chapter proposes additional work to conduct based on the findings of this thesis. Improvements to the hardware in a second prototype are discussed in Section 8.1 and changes to the software are discussed in Section 8.2.

8.1 Hardware Improvements

8.1.1 Custom Printed Circuit Board (PCB)

The next step in prototyping this RTLS is to design and build the custom PCBs based on the hardware in the existing prototype. The major benefit of the PCB would be the increase in signal integrity when the microprocessor is communicating to the IMU and UWB radio transceiver. The maximum communication speed with the MPU-9150 IMU was a major bottleneck in the current prototype. The I^2C bus was only able to run at 175 kHz, where the maximum should be 400 kHz[82]. Replacing the IMU with the MPU-6000 would allow access to a 20MHz SPI bus for reading sensor information[72], allowing more information to be gathered for the pedometry algorithms.

A custom PCB would also permit a more realistic measure of the power requirements for the system. The current prototype has multiple systems that are drawing power without a function. The PCB with the embedded code improvements proposed in Section 8.2.1 will give an accurate prediction of the production hardware's power requirements.

8.1.2 UWB Antenna Design for Pedestrian and Anchors

It was decided early on in the project to use the omnidirectional antennas provided with DecaWave's EVB1000 development kit. As discussed in Section 7.6.1, the omnidirectional antennas did not provide a uniform gain in the RTLS testing. It will be valuable to select a new antenna that provides a more uniform gain when the pedestrian is walking down the aisles. Improvements could also be made in a more focused antenna on the anchor nodes, as they do not need to radiate energy into the outside walls of the warehouse.

8.1.3 Real-Time Ground Truth

The real-time ground truth recording, as discussed in Section 7.1.1, was not as accurate as first anticipated. The surveying wheel also limited the measurement to a single dimension at any given time. If the RTLS prototype's precision needs to be measured more accurately, a new real-time ground truth will have to be devised.

8.2 Software Improvements

8.2.1 Embedded Implementation of UKF

On the software side, implementation of the entire system on the embedded microcontroller is the next major step in the prototype. 60% of the microcontroller's time was spent sending the data over the UART bus to the PC application, which would be eliminated in the rewrite. During the rewrite, the power saving sleep modes on the UWB transceiver and microcontroller should leveraged for maximum power conservation.

8.2.2 Multiple User Spectrum Scheduling

Additional improvements can be done to manage the DW1000 transceivers more effectively. The current implementation uses long waits and timeouts to be compatible with the DecaWave's DecaRanging implementation. Additional work should be done to eliminate the long retransmission delays, powering off the transmitter more quickly.

8.2.3 Pedometry Algorithm Improvement

The course of designing the prototype has shown the EMD provided by Invensense are not sufficient to provide real-time velocity sensing based on pedometry. Improvements can be made on the accuracy of the

pedometry sensing by increasing the sample rate of the accelerometer (see Section 8.1.1) and doing the full pedometry tracking on the embedded system.

Reimplementing the pedometry on the embedded system will also allow for a more intelligent algorithm than the EMD provides. The prototype currently only counts the number of steps, and extrapolates velocity via the pedestrian's stride length. It is known that the stride length changes as the pedestrian walks faster[88], and the effect should be taken into account. The current algorithm also assumes that all velocity is in the direction the pedestrian is currently facing. Using the accelerometer's other axes, it should be possible to identify the direction of the steps.

8.2.4 Automatic Calibration of Pedestrian Characteristics

The RTLS prototype described in this thesis uses the pedestrian's height and stride length calibrated for a single person. In a commercial product, these parameters must be calculated on the fly. When standing still, three radio ranging measurements can be used to measure the pedestrian's height. Stride length is dependant to the length of the pedestrian's legs, which can be approximated from the height[89]. From this starting point additional algorithms relying on good UWB measurements can be used to further approximate the stride length.

Chapter 9

Conclusion

The goal of the project thesis is to develop a real-time localisation system that functions within a warehouse environment that can be practically produced. The prototype developed as part of the project achieved the basic performance requirements of the project of localising the pedestrian within an aisle. The prototype achieved localisation within an average of 1.4 metres with 95% confidence under 4.0 metres. This fell outside the initial goal of 2.0 metres at 95% confidence, but the localisation system was still stably tracking the pedestrian with that precision. The electronic hardware of the prototype would cost approximately 30 USD to manufacture in production. This leaves 20 USD for the packaging of the electronics into a robust wearable device. The installation cost is minimised to a single radio per covered aisle.

During the course of selecting the most viable radio technology, a novel investigation of three commercially available ranging technologies was conducted in the warehouse environment. To the authors best knowledge, the performance of UWB ranging and RIPS in this type of environment has not been analysed.

The prototype implemented in this project presents a system that can localise a pedestrian in a warehouse environment for under 50 USD. The testing conducted on the prototype shows the limits of the current design and the performance of the technology in a realistic setting. The future work, as proposed by this thesis, outlines the next steps to developing this prototype into a system that is commercially viable. As presented in this thesis, there is no observed reason to assume that the 2 metre accuracy goal at 95% confidence is unfeasible given improvements in the hardware and software of the prototype.

Appendix A

Glossary

AMD Advanced Micro Devices. Semiconductor company.

AoA Angle of Arrival. A localisation technique using triangulation.

AP Access Point. Usually referring to a WLAN Access Point.

ARM Advanced RISC Machine. Computer architecture commonly found in low power microprocessors.

COTS Commercial Of The Shelf. A commercially available product.

CPU Central Processing Unit.

CSS Chirp Spread Spectrum. A radio communication technique.

DC Distribution Centre.

DMP Digital Motion Processor. Specialised signal processing hardware in Invensense IMU chipsets.

DQF Distance Quality Factor. A factor used in Atmel's Ranging Tool Box to quantify the quality of the measurement.

DRIPS Dual-tone RIPS. A radio based localisation system.

DS-TWR Double-Sided Two Way Ranging. A ranging technique for radio signals.

DW1000 DecaWave UWB transceiver.

EKF Extended Kalman Filter.

EMD Embedded Motion Driver. Invensense supplied software for the DMP.

EVB1000 EValuation Board for the DW1000 UWB transceiver.

FCC Federal Communications Commission. U.S.A. government agency that regulates radio communications.

FM Frequency Modulated. Usually referring commercial VHF broadcasting between 87.5 MHz to 108.0 MHz.

FMCW Frequency Modulated Continuous-Wave. Radar technology.

FTDI Future Technology Devices International. A semiconductor company.

GNSS Global Navigation Satellite System.

GPS Global Positioning System. A U.S.A GNSS system.

I^2C Inter-Integrated Circuit. Short range serial communication bus commonly used in embedded systems.

IEEE Institute of Electrical and Electronics Engineers.

IMU Inertial Motion Unit. A sensor suite containing accelerometers and gyroscopes capable of measuring physical motion.

ISM Band Portion of the radio spectrum reserved for use in Industrial, Scientific and Medical applications.

KF Kalman Filter.

LDC Low Duty Cycle. A mode of operation for UWB radios that minimises interference with narrowband communication.

LED Light Emitting Diode.

MPU Motion Processing Unit. Invensense nomenclature for IMU with an integrated DMP.

NFER Near Field Electromagnetic Ranging.

NLoS Non-Line-of-Sight.

NZ New Zealand.

PC Personal Computer. Typically referring to any non ARM computer.

PCB Printed Circuit Board.

PMU Phase difference Measurement Unit. Hardware on the AT86RF233 to measure the phase delay of a received signal.

RAM Random Access Memory.

RF Radio Frequency.

RIPS Radio Interferometric Based Positioning System.

RSSI Received Signal Strength Indicator. Common measurement of a radio signal's strength.

RT-ToF Round-Trip Time-of-Flight. A ranging technique for radio signals.

RTB Ranging Tool Box. Atmel sample ranging code for the REB233SMAD Evaluation Kit.

RTLS Real-Time Localisation System.

SIS Sequential Importance Sampling. A common particle filter algorithm.

SPI Serial Peripheral Interface. A serial bus commonly used in embedded systems for short distance communication.

TDoF Time Difference of Flight. A radio based localisation technique.

ToF Time-of-Flight. A ranging technique for radio signals.

UART Universal Asynchronous Receiver/Transmitter. Hardware used in microcontrollers to drive a serial communication bus.

UKF Unscented Kalman filter.

USB Universal Serial Bus.

USD United States Dollar.

UT Unscented Transform.

UWB Ultra Wide-Band. Radio technology that utilises a bandwidth at least 500 MHz wide.

VHF Band Very High Frequency. Radio band from 30MHz to 300 MHz.

WLAN Wireless Local Area Network. Wireless communication technology in the 2.4GHz ISM band.

XML Extensible Markup Language. Commonly used for storing structured data.

Bibliography

[1] N. D. Pham, "The economic benefits of global navigation satellite system and its commercial and non-commercial applications," ndp|analytics, Tech. Rep., 2013.

[2] K. Ozsoy, A. Bozkurt, and I. Tekin, "Indoor positioning based on global positioning system signals," *Microwave and Optical Technology Letters*, vol. 55, no. 5, pp. 1091–1097, 2013.

[3] E. Jacobson, T. Lee, C. Popeck, M. Martorana, and S. Sokolowski, "Suo/sas geolocation: land navigation using multiple integrated sensors," in *Military Communications Conference, 2003. MILCOM'03. 2003 IEEE*, vol. 1. IEEE, 2003, pp. 186–191.

[4] P. Bahl and V. N. Padmanabhan, "Radar: An in-building rf-based user location and tracking system," in *INFOCOM 2000. Nineteenth Annual Joint Conference of the IEEE Computer and Communications Societies. Proceedings. IEEE*, vol. 2. Ieee, 2000, pp. 775–784.

[5] D. L. Hall and J. Llinas, "An introduction to multisensor data fusion," *Proceedings of the IEEE*, vol. 85, no. 1, pp. 6–23, 1997.

[6] R.-B. Zhang, J.-G. Guo, F.-H. Chu, and Y.-C. Zhang, "Environmental-adaptive indoor radio path loss model for wireless sensor networks localization," *AEU-International Journal of Electronics and Communications*, vol. 65, no. 12, pp. 1023–1031, 2011.

[7] T. Horberry, I. Johnston, T. Larsson, B. Corben, and J. Lambert, "An integrated approach to forklift safety," in *Proceedings 3rd International Conference on Traffic and Transportation Psychology*, 2004, pp. 5–9.

[8] V. Rakesh and G. K. Adil, "Layout optimization of a three dimensional order picking warehouse," *IFAC-PapersOnLine*, vol. 48, no. 3, pp. 1155–1160, 2015.

[9] Z. Farid, R. Nordin, and M. Ismail, "Recent advances in wireless indoor localization techniques and system," *Journal of Computer Networks and Communications*, vol. 2013, 2013.

[10] H. Liu, H. Darabi, P. Banerjee, and J. Liu, "Survey of wireless indoor positioning techniques and systems," *Systems, Man, and Cybernetics, Part C: Applications and Reviews, IEEE Transactions on*, vol. 37, no. 6, pp. 1067–1080, 2007.

[11] C. Rohrig and S. Spieker, "Tracking of transport vehicles for warehouse management using a wireless sensor network," in *Intelligent Robots and Systems, 2008. IROS 2008. IEEE/RSJ International Conference on.* IEEE, 2008, pp. 3260–3265.

[12] (2013) Product information: Dw1000. DecaWave Ltd. [Online]. Available: http://www.decawave.com/sites/default/files/product-pdf/dw1000-product-brief.pdf

[13] S. J. Julier and J. K. Uhlmann, "New extension of the kalman filter to nonlinear systems," in *AeroSense'97.* International Society for Optics and Photonics, 1997, pp. 182–193.

[14] E. Wan, R. Van Der Merwe *et al.*, "The unscented kalman filter for nonlinear estimation," in *Adaptive Systems for Signal Processing, Communications, and Control Symposium 2000. AS-SPCC. The IEEE 2000.* IEEE, 2000, pp. 153–158.

[15] D. Duckworth. (2012) Pykalman 0.9.2 documentation. [Online]. Available: https://pykalman.github.io/

[16] D. R. Lide, *CRC handbook of chemistry and physics.* CRC press, 2004.

[17] B. T. Fang, "Simple solutions for hyperbolic and related position fixes," *Aerospace and Electronic Systems, IEEE Transactions on*, vol. 26, no. 5, pp. 748–753, 1990.

[18] Z. Sahinoglu and S. Gezici, "Ranging in the ieee 802.15.4a standard," in *Wireless and Microwave Technology Conference*, 2006, pp. 1–5.

[19] Y. Jiang and V. Leung, "An asymmetric double sided two-way ranging for crystal offset," in *Signals, Systems and Electronics, 2007. ISSSE'07. International Symposium on.* IEEE, 2007, pp. 525–528.

[20] C. Wong, R. Klukas, and G. Messier, "Using wlan infrastructure for angle-of-arrival indoor user location," in *Vehicular Technology Conference, 2008. VTC 2008-Fall. IEEE 68th.* IEEE, 2008, pp. 1–5.

[21] E. A. Olsen, C.-W. PARK, and J. P. How, "3d formation flight using differential carrier-phase gps sensors," *Navigation*, vol. 46, no. 1, pp. 35–48, 1999.

[22] A. Vervisch-Picois and N. Samama, "Interference mitigation in a repeater and pseudolite indoor positioning system," *Selected Topics in Signal Processing, IEEE Journal of*, vol. 3, no. 5, pp. 810–820, 2009.

[23] P. H. Madhani, P. Axelrad, K. Krumvieda, and J. Thomas, "Application of successive interference cancellation to the gps pseudolite near-far problem," *Aerospace and Electronic Systems, IEEE Transactions on*, vol. 39, no. 2, pp. 481–488, 2003.

[24] N. Tahir and G. Brooker, "Recent developments and recommendations for improving harmonic radar tracking systems," in *Antennas and Propagation (EUCAP), Proceedings of the 5th European Conference on.* IEEE, 2011, pp. 1531–1535.

[25] M. Vossiek and P. Gulden, "The switched injection-locked oscillator: A novel versatile concept for wireless transponder and localization systems," *Microwave Theory and Techniques, IEEE Transactions on*, vol. 56, no. 4, pp. 859–866, 2008.

[26] S. Wehrli, R. Gierlich, J. Hüttner, D. Barras, F. Ellinger, and H. Jäckel, "Integrated active pulsed reflector for an indoor local positioning system," *Microwave Theory and Techniques, IEEE Transactions on*, vol. 58, no. 2, pp. 267–276, 2010.

[27] A. Resch, R. Pfeil, M. Wegener, and A. Stelzer, "Review of the lpm local positioning measurement system," in *Localization and GNSS (ICL-GNSS), 2012 International Conference on*. IEEE, 2012, pp. 1–5.

[28] A. Stelzer, K. Pourvoyeur, and A. Fischer, "Concept and application of lpm-a novel 3-d local position measurement system," *Microwave Theory and Techniques, IEEE Transactions on*, vol. 52, no. 12, pp. 2664–2669, 2004.

[29] (2002, April) Fcc 02-48: Revision of part 15 of the commission's rules regarding ultra-wide-band transmission systems. FCC. [Online]. Available: https://transition.fcc.gov/Bureaus/Engineering_Technology/Orders/2002/fcc02048.pdf

[30] *Radio communications regulations (general user radio licence for ultra wide band devices) notice 2015*, Ministry of Business, Innovation and Employment Std., 3 2015. [Online]. Available: https://www.gazette.govt.nz/assets/pdf-cache/2015/2015-go1512.pdf

[31] (2015, January) Brief specification of ir-uwb module um100 2.2. BESPOON. [Online]. Available: http://spoonphone.com/en/home/12-uposition-ir-uwb-module-basic.html

[32] M. Z. Win, G. Chrisikos, and A. F. Molisch, "Wideband diversity in multipath channels with nonuniform power dispersion profiles," *Wireless Communications, IEEE Transactions on*, vol. 5, no. 5, pp. 1014–1022, 2006.

[33] J.-Y. Lee, R. Scholtz *et al.*, "Ranging in a dense multipath environment using an uwb radio link," *Selected Areas in Communications, IEEE Journal on*, vol. 20, no. 9, pp. 1677–1683, 2002.

[34] S. Marano, W. M. Gifford, H. Wymeersch, and M. Z. Win, "Nlos identification and mitigation for localization based on uwb experimental data," *Selected Areas in Communications, IEEE Journal on*, vol. 28, no. 7, pp. 1026–1035, 2010.

[35] E. Karapistoli, F.-N. Pavlidou, I. Gragopoulos, and I. Tsetsinas, "An overview of the ieee 802.15.4a standard," *Communications Magazine, IEEE*, vol. 48, no. 1, pp. 47–53, 2010.

[36] J. Wang, Q. Gao, Y. Yu, H. Wang, and M. Jin, "Toward robust indoor localization based on bayesian filter using chirp-spread-spectrum ranging," *Industrial Electronics, IEEE Transactions on*, vol. 59, no. 3, pp. 1622–1629, 2012.

[37] *nanoPAN 5375 RF Module Factsheet*, Nanotron Technologies GmbH, 9 2009. [Online]. Available: http://www.nanotron.com/EN/pdf/Factsheet_nanoPAN_5375_RF_Module.pdf

[38] (2015, November) Lorawan, iot & synchronization. Semtech Corporation. [Online]. Available: http://www.slideshare.net/zahidtg/lorawan-iot-synchronization

[39] M. Maróti, P. Völgyesi, S. Dóra, B. Kusỳ, A. Nádas, Á. Lédeczi, G. Balogh, and K. Molnár, "Radio interferometric geolocation," in *Proceedings of the 3rd international conference on Embedded networked sensor systems.* ACM, 2005, pp. 1–12.

[40] B. Kusy, J. Sallai, G. Balogh, A. Ledeczi, V. Protopopescu, J. Tolliver, F. DeNap, and M. Parang, "Radio interferometric tracking of mobile wireless nodes," in *Proceedings of the 5th international conference on Mobile systems, applications and services.* ACM, 2007, pp. 139–151.

[41] C. Wang, Q. Yin, and W. Wang, "An efficient ranging method based on chinese remainder theorem for rips measurement," *Science China Information Sciences*, vol. 53, no. 6, pp. 1233–1241, 2010.

[42] *Atmel AVR2152: RTB Evaluation Application Software User's Guide*, Atmel Corporation, 2 2013, rev. 8443A-AVR-02/2013. [Online]. Available: http://www.atmel.com/Images/Atmel-8443-RTB-Evaluation-Application-Software-Users-Guide_Application-Note_AVR2152.pdf

[43] Y. Wang, L. Li, X. Ma, M. Shinotsuka, C. Chen, and X. Guan, "Dual-tone radio interferometric positioning systems using undersampling techniques," *Signal Processing Letters, IEEE*, vol. 21, no. 11, pp. 1311–1315, 2014.

[44] Y. Wang, X. Ma, C. Chen, and X. Guan, "Designing dual-tone radio interferometric positioning systems," *Signal Processing, IEEE Transactions on*, vol. 63, no. 6, pp. 1351–1365, 2015.

[45] B. Dil and P. J. Havinga, "Stochastic radio interferometric positioning in the 2.4 ghz range." in *SenSys*, 2011, pp. 108–120.

[46] H. G. Schantz, "Near field phase behavior," in *IEEE ANTENNAS AND PROPAGATION SOCIETY INTERNATIONAL SYMPOSIUM*, vol. 3. IEEE; 1999, 2005, p. 134.

[47] ——, "A near field propagation law & a novel fundamental limit to antenna gain versus size," in *IEEE Antennas and Propagation Society International Symposium*, vol. 3. IEEE; 1999, 2005, p. 237.

[48] H. G. Schantz and R. E. DePierre, "System and method for near-field electromagnetic ranging," US Patent US6 963 301 B2, 11 8, 2005.

[49] A. J. Compston, J. D. Fluhler, and H. G. Schantz, "A fundamental limit on antenna gain for electrically small antennas," in *Sarnoff Symposium, IEEE*, 2008, pp. 1–5.

[50] F. Vanheel, J. Verhaevert, E. Laermans, I. Moerman, and P. Demeester, "Automated linear regression tools improve rssi wsn localization in multipath indoor environment," *EURASIP Journal on Wireless Communications and Networking*, vol. 2011, no. 1, pp. 1–27, 2011.

[51] K. Kaemarungsi and P. Krishnamurthy, "Properties of indoor received signal strength for wlan location fingerprinting," in *Mobile and Ubiquitous Systems: Networking and Services, 2004. MOBIQUITOUS 2004. The First Annual International Conference on.* IEEE, 2004, pp. 14–23.

[52] Y. Gao, J. Niu, R. Zhou, and G. Xing, "Zifind: Exploiting cross-technology interference signatures for energy-efficient indoor localization," in *INFOCOM, 2013 Proceedings IEEE.* IEEE, 2013, pp. 2940–2948.

[53] P. Ibach, V. Stantchev, F. Lederer, A. Weiß, T. Herbst, and T. Kunze, "Wlan-based asset tracking for warehouse management," in *IADIS International Conference e-Commerce, Porto, Portugal*, 2005.

[54] Y. Chen, D. Lymberopoulos, J. Liu, and B. Priyantha, "Fm-based indoor localization," in *Proceedings of the 10th international conference on Mobile systems, applications, and services.* ACM, 2012, pp. 169–182.

[55] *Low Power Broadcast Radio Stations*, Federal Communications Commission. [Online]. Available: https://www.fcc.gov/guides/low-power-broadcast-radio-stations#UNLICENSED

[56] A. Matic, A. Popleteev, V. Osmani, and O. Mayora-Ibarra, "Fm radio for indoor localization with spontaneous recalibration," *Pervasive and Mobile Computing*, vol. 6, no. 6, pp. 642–656, 2010.

[57] *Atmel AVR2160: REB233SMAD Evaluation Kit - Quick Start Guide*, Atmel Corporation, 4 2012, rev. 42000B-AVR-04/12. [Online]. Available: http://www.atmel.com/images/doc42000.pdf

[58] *MCU Wireless AT86RF233 Preliminary Datasheet*, Atmel Corporation, 7 2014, rev. Atmel-8351E-MCU_Wireless-AT86RF233_Datasheet_072014. [Online]. Available: http://www.atmel.com/Images/Atmel-8351-MCU_Wireless-AT86RF233_Datasheet.pdf

[59] *Atmel AVR2150: RTB Evaluation Application – User's Guide*, Atmel Corporation, 2 2013, rev. 8441A-AVR-02/2013. [Online]. Available: http://www.atmel.com/Images/Atmel-8441-RTB-Evaluation-Application-Users-Guide_Application-Note_AVR2150.pdf

[60] *Si4712/13 Datasheet*, Silicon Laboratories, 2 2008, rev. 1.1. [Online]. Available: http://www.silabs.com/Support%20Documents/TechnicalDocs/Si4712-13-B30.pdf

[61] *Adafruit Si4713 FM Radio Transmitter with RDS/RDBS Support*, Adafruit Industries, LLC, 7 2014. [Online]. Available: https://learn.adafruit.com/downloads/pdf/adafruit-si4713-fm-radio-transmitter-with-rds-rdbs-support.pdf

[62] *Getting Started with Eleven*, Freetronics Pty Ltd., version 1.0. [Online]. Available: http://www.practicalarduino.com/freetronics/Eleven_Getting_Started_v1_0.pdf

[63] L. Fried. Adafruit si4713 library. GitHub. Adafruit Industries, LLC. [Online]. Available: https://github.com/adafruit/Adafruit-Si4713-Library

[64] *Si4702/03 Data Sheet*, Silicon Laboratories, 7 2009, rev. 1.1. [Online]. Available: https://www.silabs.com/Support%20Documents/TechnicalDocs/Si4702-03-C19.pdf

[65] S. Monk. Sparkfun si4703 arduino library. GitHub. SparkFun Electronics. [Online]. Available: https://github.com/sparkfun/SparkFun_Si4703_Arduino_Library

[66] *DW1000 User Manual*, DecaWave Ltd., 2015, version 2.05.

[67] *EVK1000 User Manual*, DecaWave Ltd., 2014, version 1.07. [Online]. Available: http://www.decawave.com/sites/default/files/product-pdf/evk1000_user_manual_v107.pdf

[68] V. Sipal, M. John, D. Neirynck, M. McLaughlin, and M. Ammann, "Advent of practical uwb localization: (r)evolution in uwb antenna research," in *Antennas and Propagation (EuCAP), 2014 8th European Conference on*. IEEE, 2014, pp. 1561–1565.

[69] *RX-800i Series Laser Rangefinders Complete Operation Manual*, Leupold and Stevens Inc., 2012. [Online]. Available: https://www.leupold.com/wp-content/uploads/2012/07/NEW_RX-800i_RngFndr_InstMan_03_20_2012.pdf

[70] P. Goyal, V. J. Ribeiro, H. Saran, and A. Kumar, "Strap-down pedestrian dead-reckoning system," in *Indoor Positioning and Indoor Navigation (IPIN), 2011 International Conference on*. IEEE, 2011, pp. 1–7.

[71] O. J. Woodman, "An introduction to inertial navigation," *University of Cambridge, Computer Laboratory, Tech. Rep. UCAMCL-TR-696*, vol. 14, p. 15, 2007.

[72] *MPU-6000/MPU-6050 Product Specification*, InvenSense Inc., 5 2012, revision: 3.3.

[73] *ADIS16334 Data Sheet*, Analog Devices Inc., 5 2013, rev. B. [Online]. Available: http://www.analog.com/media/en/technical-documentation/data-sheets/ADIS16334.pdf

[74] N. J. Gordon, D. J. Salmond, and A. F. Smith, "Novel approach to nonlinear/non-gaussian bayesian state estimation," in *IEE Proceedings F (Radar and Signal Processing)*, vol. 140, no. 2. IET, 1993, pp. 107–113.

[75] F. Gustafsson, "Particle filter theory and practice with positioning applications," *Aerospace and Electronic Systems Magazine, IEEE*, vol. 25, no. 7, pp. 53–82, 2010.

[76] M. S. Arulampalam, S. Maskell, N. Gordon, and T. Clapp, "A tutorial on particle filters for online nonlinear/non-gaussian bayesian tracking," *Signal Processing, IEEE Transactions on*, vol. 50, no. 2, pp. 174–188, 2002.

[77] R. E. Kalman, "A new approach to linear filtering and prediction problems," *Journal of Fluids Engineering*, vol. 82, no. 1, pp. 35–45, 1960.

[78] J. K. Uhlmann, "Algorithms for multiple-target tracking," *American Scientist*, pp. 128–141, 1992.

[79] *UM1472 User manual, Discovery kit for STM32F407/417 lines*, STMicroelectronics, 1 2014, rev 4. [Online]. Available: http://www.st.com/st-web-ui/static/active/en/resource/technical/document/user_manual/DM00039084.pdf

[80] *STM32F405xx and STM32F407xx Datasheet*, STMicroelectronics, 10 2015, rev 6. [Online]. Available: http://www.st.com/web/en/resource/technical/document/datasheet/DM00037051.pdf

[81] *Product Information: EVB 1000*, DecaWave Ltd., 2013.

[82] *MPU-9150 Product Specification*, InvenSense Inc., 6 2013, revision: 4.3. [Online]. Available: http://43zrtwysvxb2gf29r5o0athu.wpengine.netdna-cdn.com/wp-content/uploads/2015/02/MPU-9150-Datasheet.pdf

[83] *MPU-9250 Product Specification*, InvenSense Inc., 1 2014, revision: 1.0. [Online]. Available: http://43zrtwysvxb2gf29r5o0athu.wpengine.netdna-cdn.com/wp-content/uploads/2015/02/MPU-9250-Datasheet.pdf

[84] *T231X USB TO FULL HANDSHAKE UART IC Datasheet*, Future Technology Devices International Limited, 2013, version 1.2. [Online]. Available: http://cdn.sparkfun.com/datasheets/Components/General%20IC/DS_FT231X.pdf

[85] *DecaRanging Source Code Guide*, DecaWave Ltd., 2014, version 1.7.

[86] *Embedded Motion Driver 5.1.1 Tutorial*, InvenSense Inc., 12 2013, revision: 1.0.

[87] M. John and M. Ammann, "Antenna optimization with a computationally efficient multiobjective evolutionary algorithm." *Articles*, p. 24, 2009.

[88] Q. Ladetto, "On foot navigation: continuous step calibration using both complementary recursive prediction and adaptive kalman filtering," in *Proceedings of ION GPS*, vol. 2000, 2000, pp. 1735–1740.

[89] V. Renaudin, M. Susi, and G. Lachapelle, "Step length estimation using handheld inertial sensors," *Sensors*, vol. 12, no. 7, pp. 8507–8525, 2012.